Dynamics of the Top Quark Beyond the Standard Model

by

Sung Hoon Jung

A dissertation submitted in partial fulfillment
of the requirements for the degree of
Doctor of Philosophy
(Physics)
in The University of Michigan
2011

Doctoral Committee:

Professor James D. Wells, Chair
Professor Ratindranath Akhoury
Professor Duncan G. Steel
Professor Bing Zhou
Assistant Professor Aaron T. Pierce

To my parents, Hee-Sang Jung and Tae-Sook Kim, who always supported my choices.

ACKNOWLEDGEMENTS

It is a pleasure to acknowledge those people who have helped me get through all sorts of challenges during my graduate study, and helped me grow into the person I am today. First of all, I appreciate my advisor James Wells for all of support he provided to me. I admire his insights, and I learned a lot from his thoughtful guidance and his encouragement into researches that looked hard at first but turned out to be very exciting and important. I also appreciate Aaron Pierce for lots of valuable discussions that we had. His passion always made our collaborations exciting. It was also a valuable experience to work with my other collaborators, Shrihari Gopalakrishna, Hitoshi Murayama and Giulia Zanderighi. I am also grateful to Ratindranath Akhoury, Dante Amidei, Kiwoon Choi, Eung Jin Chun, Gian Giudice, Gordon Kane, Chul Kim, Aaron Leanhardt, Hyun-Min Lee, Jianming Qian, Riccardo Rattazzi, Tom Schwarz, Duncan Steel, Krzysztof Turzynski, Andrew Weiler and Bing Zhou for conversations we had. I warmheartedly thank my colleagues with whom I spent time chatting about everyday lives of physicists; Yanou Cui, Jason Evans, Sandeepan Gupta, Kentaro Hanaki, Jeongwon Lee, Javi Serra, Jing Shao and Philip Szepietowski. I express special appreciation to Jieun Lee who always enjoyed listening to me about what I am working on, where I am stuck in, and what I am excited about. Finally, this thesis would not have been possible if it were not for my family and my other beloved friends.

TABLE OF CONTENTS

LIST OF FIGURES

CHAPTER I

Introduction

The Standard Model (SM) of modern particle physics can describe all phenomena that have been observed so far at high energy experiments. However, the SM is not a complete theory of nature as will be discussed in this chapter. Thus, various physics models that can extend or replace the SM at some high energy scale have been proposed in the last few decades. To broaden our view of the universe, it is crucial to discover (or exclude) such new physics beyond the SM. In this introduction, we review the successes and mysteries of the SM, and motivate the search for new physics utilizing the top quark.

1.1 Description of the Standard Model

The SM describes dynamics of elementary matter particles which feel electromagnetic, weak and strong nuclear forces. The forces are described by the Yang-Mills gauge theory of quantum field theory. The description of forces using gauge theory was successfully confirmed when, among many candidate theories of forces, the gauge theory's unique predictions of Bjorken scaling violation and asymptotic freedom were observed in the 1970's.

The SM is based on the gauge group $U(1)_Y \times SU(2)_L \times SU(3)_C$. Once the representations of fermions have been specified, the gauge theory fixes the form of interactions between gauge bosons mediating the force and matter fermions. Because of their importance, the representations of leptons and quarks are shown in the Table 1.1. Interestingly,

	$L = (\nu_L, e_L)$	e_R	$Q = (u_L, d_L)$	u_R	d_R	h
$U(1)_Y$	-1/2	-1	1/6	2/3	-1/3	1/2
$SU(2)_L$	□	.	□	.	.	□
$SU(3)_C$	.	.	□	□	□	.

Table 1.1: SM particle contents and quantum number assignments under gauge symmetries. □ and a small dot imply fundamental and singlet representations.

the assignment in Table 1.1 cancels all gauge anomalies only when the lepton and quark contributions are added, hence supporting such nontrivial assignments. The consequent chiral interactions of $SU(2)_L$ are experimentally well confirmed. The number of colors is well measured to be $N_c = 3$ when the hadronic cross sections are precisely measured. Exchange of the Z boson gives rise to observed neutral currents. The great success of the SM culminated when all the gauge bosons of the SM were discovered at CERN, undoubtedly confirming the gauge symmetry content of the SM.

The Higgs mechanism is a hypothetical method incorporated in the SM to generate masses of particles. A gauge symmetry does not allow mass terms of gauge bosons. But the condensation of a scalar particle can consistently hide the apparent gauge symmetry and allow massive gauge bosons after all. The Higgs boson is just such a hypothetical scalar particle which condenses and spontaneously breaks $SU(2)_L \times U(1)_Y \to U(1)_{em}$. Moreover, fermions must resort to the Higgs mechanism because the chiral nature of $SU(2)_L$ prohibits any chiral fermion mass terms to appear. Since the chiral $SU(2)_L$ is broken by Higgs condensation, fermions can be massive only through the Higgs mechanism. Masses of the gauge bosons and fermions are then proportional to the products of the Higgs vacuum expectation value (vev) and their couplings to the Higgs scalar. The agreement of the ratio of W and Z boson masses between the SM and the measurement is another success of the SM Higgs mechanism. The ratio, in the SM, is given by a ratio of $U(1)_Y$ and $SU(2)_L$ gauge couplings. However, this is not generally true, but is true when the Higgs is in a doublet representation of $SU(2)_L$ as assumed in the SM.

Leptons and quarks come in three generations in the SM. In other words, there are three nearly identical copies of up and down quarks, the electron and neutrino. Only the masses of leptons and quarks in different generations are different. Although having three generations looks redundant, all twelve kinds of leptons and quarks were indeed observed (the last one, the top quark, was discovered in 1995 at the Tevatron). It was also found by Kobayashi and Maskawa that at least three generations of quarks are needed to incorporate enough parameters to describe all observed CP violation phenomena. When particles carrying the same quantum numbers from each generation mix, flavor-changing phenomena is predicted. Flavor-changing physics of mesons observed in low-energy collider experiments and the observed transmutation of solar neutrinos are mostly in agreement with the descriptions within the SM. However, flavor-changing neutral currents (FCNC) are not observed (at high precision) nor predicted by the SM, which further support for the SM.

1.2   Shortcomings of the Standard Model

Despite of the great success of the SM, there are various reasons to think of new physics beyond the SM. The SM is not likely a complete theory of nature which is valid all the way up to the Planck scale. First of all, gravity is not incorporated into the SM. Gravity cannot be described by a renormalizable 4-dimensional field theory action. Nevertheless, since there are other types of candidate gravitational theories which are influential only at some high energy scale, we put this issue aside in this work.

The Higgs mass parameter is often used to discuss the possible incompleteness of the SM. In the SM, the Higgs mass sets the scale of the masses of W and Z bosons, i.e. the electroweak scale. However, the Higgs mass is quadratically sensitive to the upper scale at which the SM is valid. This is because the path integral includes virtual particle loop corrections to the Higgs mass which gives a factor of momentum squared, which should be

evaluated at the highest possible energy scale where the SM is valid. If the SM is valid up to the Planck scale, the Higgs mass would be about the order of the Planck scale. A large hierarchy of the Planck scale and the electroweak scale can only be possible if Planck-scale numbers are somehow added and subtracted to produce a much smaller weak-scale number. This unlikely fine-tuned situation is one reason to hesitate calling the SM complete.

The Higgs scalar is also expected to play an important role in restoring unitarity. Unitarity violation is most dramatic in scatterings of longitudinal electroweak gauge bosons because the longitudinal polarization vector grows with scattering energy. Adding the exchange of the Higgs scalar calms down the growing behavior of the amplitude. The remaining terms of the amplitude at high energy are proportional to the Higgs mass squared. Thus the criteria that the SM is unitary at an arbitrarily high energy leads to an upper bound of the Higgs mass of about a TeV. The resulting restoration is easily understandable from the Goldstone equivalence theorem since the emissions of scalars do not suffer from the growing behavior, and the self interaction is proportional to the Higgs mass. This argument leads to consideration of new physics scenarios influential at TeV-energy scale.

Observed pattern of SM fermion masses is not well understood in the SM. Masses of SM fermions are measured to be in a wide range of energy scales of a few order of the magnitude. The electron is 10^6 times lighter than the top quark, and the top quark is as heavy as W and Z bosons. The very lightness of the electron may not be a theoretical problem because a chiral symmetry prohibits fermion masses. However, there is no compelling or necessary reason to believe such a wide range of masses realized in nature. This question can be somewhat resolved if a much smaller variations of theory parameters can lead to a wide range of masses. In the SM, however, Higgs Yukawa coupling and fermion masses are directly proportional and Yukawa inherits the pattern of fermion masses.

Another shortcoming of the SM that is somewhat relevant to this thesis is the lack

of CP violation required for baryogenesis. Baryogenesis is a hypothetical mechanism of generating the particle-antiparticle asymmetry observed in nature by utilizing new sources of CP violation that might have occurred before or during a phase transition of the early universe. The amount of CP violation that a baryogenesis mechanism requires is not accommodated by the CKM matrix of the SM. Thus additional sources of CP violation is often looked for in new physics models.

Given the various aspects discussed above regarding deficiencies of the SM, it is not likely a complete theory. Various new physics scenarios of electroweak symmetry breaking (EWSB) have been proposed in the last few decades. Due to the preference for a sub-TeV Higgs boson by various theoretical and experimental arguments, the new physics is expected to be influential around a TeV energy scale. This is the energy regime that the Tevatron partially explored and the LHC will be thoroughly probing. In the next section, we discuss and motivate why the top quark can be (directly or indirectly) relevant to search of new physics at such hadron colliders.

1.3   The top quark and electroweak symmetry breaking

In many new physics theories, the top quark is treated somewhat specially. The top quark is more closely tied to EWSB mechanism than other fermions or it can provide important discovery modes. In this section, we discuss important roles that the top quark actually plays in various promising new physics theories. This discussion will motivate topics studied in the rest of this thesis.

In one type of new physics models, the electroweak scale (i.e., the Higgs mass) can be stabilized under quantum corrections by invoking additional symmetries. Typical examples are supersymmetry (see for example [1]) and the Little Higgs models (see for example [2]). To complete representations under the new invoked symmetry, new particles associated with each SM particle are introduced. In general, the strong top Yukawa coupling makes

the one-loop corrections from the top quark and its partner top quark important. For example, the little hierarchy of supersymmetry is basically determined by the masses of superpartners of the top quark – the stop. The stop is also often RG driven to be the lightest strongly coupled scalar superpartner by the strong top Yukawa. Decay chains of supersymmetry is then likely to involve stops, and consequently top quarks.

Another category of new physics achieves the EWSB via the condensation of fermion pairs. Since there is no fundamental scalar degree of freedom, such models are free from the Higgs mass quadratic divergence issue discussed above. The top-color model and the (top-color-assisted) technicolor model (see for example [3]) are typical examples of this category. In these models, the top quark condenses by itself and breaks the electroweak symmetry, determining the majority of the electroweak scale and its mass. The advantage is that the large top mass is directly generated while light masses are indirectly generated. It is possible because the mass of the top quark is similar to the electroweak scale. Knowing the dynamics of the top quark beyond the SM is thus very important.

Lastly, even in a warped extra dimension scenario (see for example [4]), where a hierarchy M_{Pl}/M_{EW} is exponentially warped down to $\ln(M_{Pl}/M_{EW}) \sim \mathcal{O}(10)$, the top quark is treated differently among quarks. In general, the top quark has to localize around the UV brane in such a way that it overlaps strongly with the Higgs boson, making it the heaviest SM fermion. Consequently, the top quark couples strongly to Kaluza-Klein particles residing around the UV brane. Therefore, the top quark is a main target for the discovery of such models.

Thus, in these major categories of new models of EWSB, the top quark is a very important particle that can reveal important hints of models. Its heaviness makes it special, requiring it to interact strongly and directly with the EWSB sector. It it thus well motivated to study the top quark in search of new physics.

1.4 Topics of the thesis

In the rest of this thesis, three important phenomenologies of the top quark, or new physics which puts special emphasis on the top quark, are discussed. These are based on three papers [5, 6, 7].

Firstly, the forward-backward asymmetry of the top quark is discussed, as it is measured at the Tevatron to be $2 \sim 3.5\sigma$ larger than the Standard Model prediction. It is argued that if the deviation is the effect of new physics, t-channel physics is promising physics responsible for it. Model building based on a new abelian gauge symmetry is detailed. These physics ideas can be discovered at hadron colliders through precise measurements of the top pair cross section, especially in the high invariant mass region, as well as the production of like-sign top pairs, which can be observed as events containing like-sign dileptons.

Second, it is argued that the most important discovery mode of a warped extra dimension can be production of four top quarks. This is especially true if the bulk profiles of light quarks are almost flat allowing a relatively light Kaluza-Klein scale. This ansatz is motivated from the results of electroweak precision tests and flavor physics. Depending on Kaluza-Klein gluon couplings to third generation fermions, the like-sign dilepton or the single lepton topology of four top quarks can be the best collider signature.

Finally, in supersymmetric theories, the superpartner of the top quark – the stop – is often the lightest scalar super-partner. Heavy scalars of the first two generations suppress several generically large contributions to well-measured observables including the electric dipole moment. Given the possibility of the LHC improving its probing sensitivity, the discovery reach of the LHC and precision measurements of dipole moments are compared within supersymmetry frameworks having light stops. Although dipole moments are better probes within the near future, the LHC can provide another interesting independent

opportunity for discovery.

CHAPTER II

The Forward-Backward Asymmetry of the Top Quark

2.1 Measurements at Tevatron

Recently the CDF collaboration published an observation of a forward backward asymmetry in top quark production [8, 9]. Focusing on the high-energy region where new physics effects might be most influential, CDF measured

$$A_{FB}^+ = 0.475 \pm 0.114, \tag{II.1}$$

where A_{FB}^+ is the rest frame asymmetry in top production restricted to $m_{t\bar{t}} > 450$ GeV. For comparison, the SM predicts $A_{FB}^+ = 0.088 \pm 0.013$. The inclusive measurements are also made in the semi-leptonic decay mode, and are given by

$$A_{FB}^t = 0.15 \pm 0.055 \quad \text{(lab frame)}, \qquad A_{FB}^t = 0.158 \pm 0.074 \quad \text{(rest frame)}. \tag{II.2}$$

This measurement builds on previous intriguing measurements of the foward backward asymmetry, [10, 11, 12], that consistently yielded large values. The Standard Model (SM) prediction [13, 14, 15] is dominated by $\mathcal{O}(\alpha_S^3)$ QCD interference effects and is $A_{FB}^t = 0.038 \pm 0.006$ and 0.058 ± 0.009 in the lab and the rest frame, respectively [8]. The theory prediction is further studied by resuming threshold soft gluon contributions, and the result implies that the current theory predictions might not be subject to large unaccounted higher order corrections [16]. Asymmetry is different in the lab and the rest frame because

a boost between two reference frames can flip the direction of top quarks, hence always diluting asymmetry measured in the rest frame.

The rest frame inclusive asymmetry is also independently measured in the dilepton decay channel [9]. Reconstructing $t\bar{t}$ rest frame, the asymmetry is measured as

$$A_{FB}^{ll} = 0.42 \pm 0.16 \tag{II.3}$$

which can be compared with the SM prediction $A_{FB}^{ll} = 0.06 \pm 0.01$. Interestingly, the asymmetry is also indirectly measured using only the well-measured relative angles of two charged leptons without reconstructing any top quark momenta, hence reducing jet energy scale uncertainties. This observable, of course, is not exactly the same as top quark asymmetry because there is no 100% correlation of directions of top quarks and their leptons. However, it can provide another consistency check of a large asymmetry. This measurement has not been fully unfolded to the parton level value which can be directly compared with field theory calculation of new physics contribution. However, the result is in agreement with another intermediate result leading to the parton level values quoted in eq.(II.3).

At present, all these (some are independent) results consistently yield $2-3.5\sigma$ deviations from the Standard Model predictions. This motivates study of new physics explanation of a large asymmetry. In this chapter, we discuss t-channel exchange of a gauge boson as a promising explanation. We first thoroughly discuss features of t-channel physics phenomena and present best model of a new abelian gauge symmetry. We also prove some theoretical consistencies of the abelian gauge model. Possible extensions with invisible decay modes of the gauge boson will be discussed at the end, and future prospect of a non-Abelian gauge symmetry is briefly discussed.
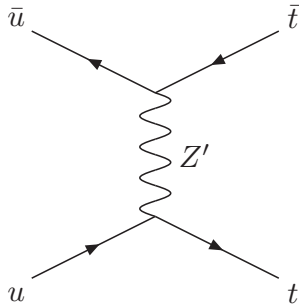
Figure 2.1: t-channel diagram of the Z' that mediates $t\bar{t}$ production.

2.2 Phenomenology of Abelian t-channel physics

Brief description of t-channel exchange phenomena. We study the physics with an extra abelian gauge symmetry. Color singlet Z' couples only to right-handed up-type quarks with a coupling constant $\alpha_X = g_X^2/4\pi$. In terms of mass eigenstates, the Z' interaction Lagrangian is given by

$$\mathcal{L}_{Z'} = g_X \, \bar{u} \, \gamma^\mu P_R \, t \, Z'_\mu + \epsilon_U g_X \, \bar{u}_i \, \gamma^\mu P_R \, u_i \, Z'_\mu + h.c. \tag{II.4}$$

where right-handed projection $P_R = (1 + \gamma_5)/2$ and generation index i. In addition to flavor-changing interaction of the first term in eq.(II.4), we also allow a small flavor-diagonal interaction given by ϵ_U. The flavor-changing interaction will be responsible for the t-channel exchange of Z' that generates a large asymmetry. Relevant t-channel process is shown in Fig. 2.1. We discuss the necessity of $\epsilon_U \neq 0$ in next subsection, but we discuss general features of t-channel physics induced by flavor-changing interaction in this subsection.

There are several advantages of the t-channel physics in point of view of the forward-backward asymmetry. First, the t-channel physics has the Rutherford enhancement in forward scattering. This enhancement originates from the t-channel boson propagator which diverges (up to finite decay width of a boson) when all initial, final states and internal boson become massless, and scattering angle between initial and final states $\cos \theta \to 1$. The
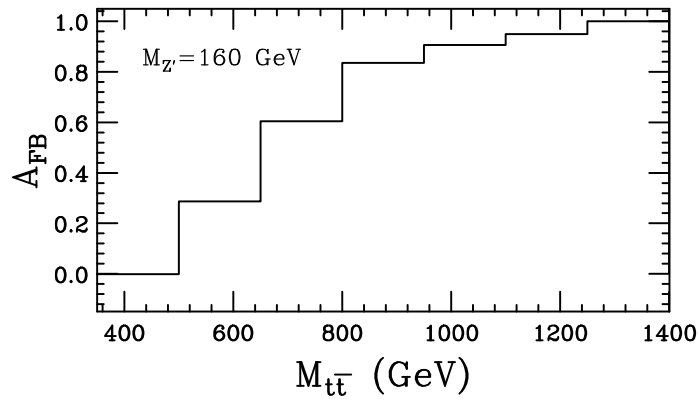
Figure 2.2: The forward-backward asymmetry A_{FB} of top quarks in the $p\bar{p} \to t\bar{t}$ process are shown as a function of invariant mass $m_{t\bar{t}}$ for SM and the t-channel physics with $M_{Z'} = 160\,\mathrm{GeV}$.

Rutherford enhancement is softened in case of the $t\bar{t}$ asymmetry not only because of finite masses of the top quark and the Z', but also because detectors cannot detect particles scattered along the beam line ($\cos\theta = 1$). However, the remnants of the enhancement are large enough to make the t-channel physics interesting. The forward-backward asymmetry as a function of the invariant mass of top anti-top is shown in Fig. 2.2, where it can be seen that the t-channel physics prefers forward scattering, especially in the high energy limit. This is because finite masses of top quark and Z' are less important in the high energy limit. This phenomena is very analogous to physics in the Rutherford scattering of electrons off nucleus, or in the QED Coulomb scattering $e^-\mu^- \to e^-\mu^-$.

Secondly, t-channel Z' does not require initial quark anti-quark pairs to be in color singlet combination. Consequently, the t-channel physics can interfere with QCD. Small coupling α_X can have large effects of order $\alpha_X\alpha_S$ through the interference. Interference effect can also be negative which makes t-channel physics nontrivial.

Thirdly, t-channel physics does not show up as a resonance peak. This allows relatively light Z' while avoiding resonance search limits. However, there will be a large enhancement of $t\bar{t}$ invariant mass distribution (not as a peak feature) in the high-energy region. This is another manifestation of the Rutherford enhancement which was similarly seen as a large

asymmetry in the high-energy region in Fig. 2.2.

Despite of these good aspects, the (unsuppressed) flavor-changing interaction in eq.(II.4) looks challenging at first. However, constraints on the flavor changing interactions of right-handed top quark is relatively weak. This is first because the Cabibbo-Kobayashi-Maskawa(CKM) matrix depends only on diagonalization of left-handed quarks, hence constraining only left-handed flavor changing physics. Secondly, flavor-changing phenomena is better measured in terms of mesons composed of down-type quarks and charm quarks, but not top quarks. If interaction eq.(II.4) had involved charm quarks, it would have been constrained by measurements of charm mesons. In Section 2.3, we prove that realizing the proper flavor-changing interactions in eq.(II.4) can always be theoretically possible (although origin of such interaction is not our main concern here).

Another possible issues of interactions eq.(II.4) regarding gauge anomaly cancellation and generation of SM Yukawa couplings will be discussed in Section 2.3 in more detail.

Asymmetry and cross sections.

A challenge for any model wishing to generate a large A_{FB}^t is avoiding a too large modification of the $t\bar{t}$ production cross section. The current measurement from 2.8 fb^{-1} at CDF [19] is $\sigma(t\bar{t}) = 7.0 \pm 0.3$ (stat) ± 0.4 (syst) ± 0.4 (lumi) pb for $m_t = 175$ GeV, in good agreement with the SM prediction of $\sigma(t\bar{t})_{SM} = 6.73 - 6.90$ pb [20], and is consistent with measurements from D0 [21] that use smaller data sets.

A typical color singlet Z' with flavor diagonal couplings does not interfere with the dominant (color-octet) QCD production process. Thus, it is difficult to avoid a large shift of the $t\bar{t}$ production cross section as well as the appearance of a resonance. On the other hand, the t-channel exchange of our Z' in $p\bar{p} \rightarrow t\bar{t}$ interferes with QCD. It is possible then to have smaller modifications to the cross section while having a large contribution to A_{FB}^t. There is no resonance present in the $M_{t\bar{t}}$ spectrum.
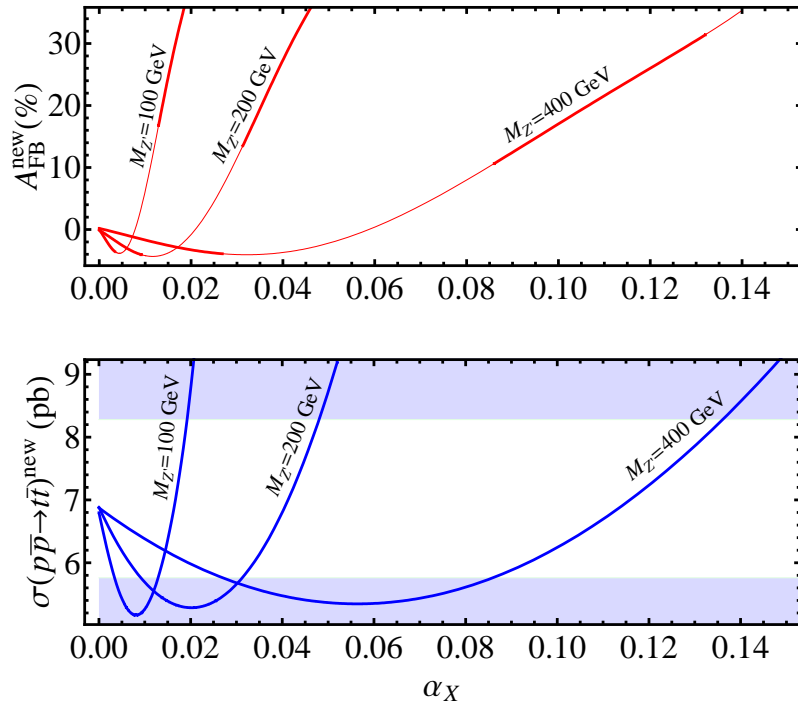
Figure 2.3: α_X versus A_{FB}^{new} and $\sigma(t\bar{t})$ for $M_{Z'} = 100, 200, 400$ GeV (from the left). In the lower panel, shaded regions deviate by more than 2σ from $\sigma(t\bar{t})^{new}$. Corresponding disfavored regions are shown as thinned lines in the upper plot. The superscript "new" emphasizes that only pure Z' and SM contributions are included (without fake processes).

We use MadGraph/MadEvent 4.4.17 [74] with CTEQ6.6M parton distribution function to generate event samples, and BRIDGE 2.0 [76] to decay unstable particles. We do not carry out parton showering or detailed detector simulation. We assume $m_t = 175$ GeV and fix renormalization and factorization scales at $\mu_R = \mu_F = m_t$. We apply an overall multiplicative $K = 1.31$ factor to the resulting cross section to match the SM prediction for $\sigma(t\bar{t})$ when $\alpha_X \to 0$. If we subsequently were to vary $\mu_{R,F}$ from $m_t/2$ to $2m_t$ we would get a $^{+3\%}_{-5\%}$ variation in the asymmetry rates quoted below.

We plot cross section and A_{FB}^{new} in Fig. 2.3 as a function of α_X for three Z' masses. A_{FB}^{new} indicates the A_{FB}^t induced only in the $t\bar{t}$ final state. The QCD interference contribution (5%) is not included. Similarly, the "new" in $\sigma(p\bar{p} \to t\bar{t})^{new}$ emphasizes that other (reducible) contributions that might enter the $t\bar{t}$ sample are not included. They are discussed below.

Comparing the two panels of Fig. 2.3 indicates a potential simultaneous fit to a large A_{FB}^t and the correct cross section. However, new physics can contribute to final states that fake the $t\bar{t}$ final state. This could pollute both the cross section and the A_{FB}^t measurement. Reducible backgrounds that contaminate the sample arise, e.g., from $tt/\bar{t}\bar{t}$, $tZ'/\bar{t}Z'$ events, and modify the results of Fig. 2.3 by $\delta A_{FB}^{fake}, \delta\sigma(t\bar{t})^{fake}$. If $M_{Z'} < m_t$, it is also important to include effects of exotic top decays $t \to uZ'$ which can take events away from the registered $t\bar{t}$ cross section. Assuming Z' decays are completely hadronic, they reduce the dilepton top cross section relative to the lepton+jets channel. At CDF and D0, $t\bar{t}$ production is defined by specific final state topologies with at least one b quark tag, several hard jets, and one ("$l + j$ sample") or two ("dilepton sample") charged leptons. CDF has measured $\sigma(t\bar{t}) = 7.2 \pm 0.75$ pb from the $l + j$ sample [22], and 6.7 ± 0.98 pb from the dilepton sample [23]. To avoid a too large discrepancy between these two channels, Fig. 2.4 shows that a light $Z'(M_{Z'} \lesssim 120$ GeV) is to be avoided.

For our "best point" (the red star in Fig. 2.4) we show comparisons with these cross sections in Table 2.1. Our simulation method is to construct event samples based on cuts detailed in [22, 23], and rescale the result by the inverse of the SM event selection efficiency (again using our simulation) to approximate their unfolding procedure.

For our best point, the total asymmetry is about 18%, see Table 2.1. This includes the SM α_s^3 contribution, the Z' tree contribution, and contributions due to δA_{FB}^{fake}. The last is negative largely due to anti-correlation of t direction with that of u in $gu \to tZ'$ production. We estimate $|\delta A_{FB}^{fake}|$ at a few percent, not quite canceling with the $+5\%$ SM contribution. There is a small uncertainty in this estimate, as the kinematics of these events differ from those analyzed in the $t\bar{t}$ events.

Table 2.1 shows the top quark asymmetry and the inferred $t\bar{t}$ cross section of our best point in the $l + j$ and dilepton channels. The asymmetry is high, and the cross sections
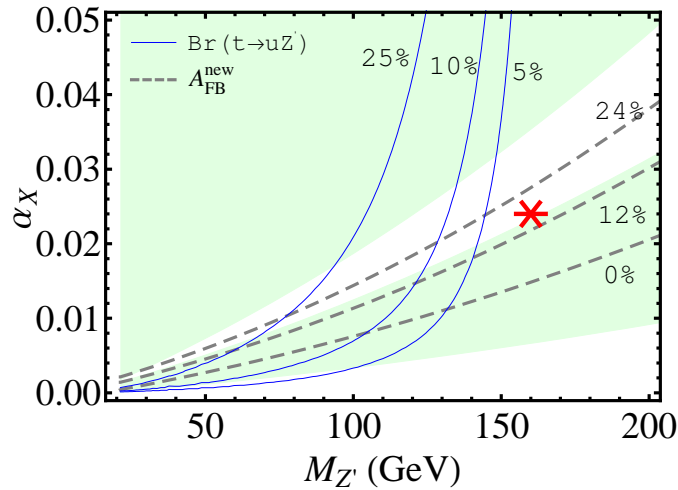
Figure 2.4: A contour plot of A_{FB}^{new} and $BR(t \rightarrow Z'u)$ in the α_X - $M_{Z'}$ plane. In colored regions, $\sigma(t\bar{t})^{new}$ deviates 2σ from of the measurement quoted in text. Parameter space around the red star is preferred. A much larger α_X gives too many like-sign top quarks, or a large distortion of the $M_{t\bar{t}}$ spectrum. Larger masses lead to larger distortions of the $M_{t\bar{t}}$ spectrum. Smaller masses give a large branching ratio for $t \rightarrow Z'u$, leading to tension between measurement of top cross sections in different channels.

	$l + j$ (pb)	dilepton (pb)	A_{FB}^{tot} %
$M_{Z'} = 160$ GeV, $\alpha_X = 0.024$	7.5	5.8	18
Measurements [22, 23, 10]	7.2 ± 0.8	6.7 ± 1.0	19 ± 7

Table 2.1: $t\bar{t}$ cross sections and total asymmetry for our best parameter point compared with measurements at CDF. There are measurements from D0 as well that use less data, and thus have larger error bars [21, 24]

are within errors of the measurements. A prediction is the inferred cross section from the dilepton sample should be less than from the $l + j$ sample: $tZ'/\bar{t}Z'$ events produce relatively more events in the $l + j$ sample than in the dilepton sample. In addition, events with exotic top decays ($t \rightarrow Z'u \rightarrow u\bar{u}u$) may contribute to the $l + j$ sample but not the dilepton sample.

Additional collider constraints. Our model yields no resonances, but new t-channel physics modifies the $M_{t\bar{t}}$ distribution – especially in the higher invariant mass bin due to the Rutherford enhancement. This distribution has been measured by the CDF experiment in the lepton + jet channel [25] and is shown in Fig. 2.5. We also show the apparent $M_{t\bar{t}}$ from this model, which includes contributions from fake processes. We observe that the
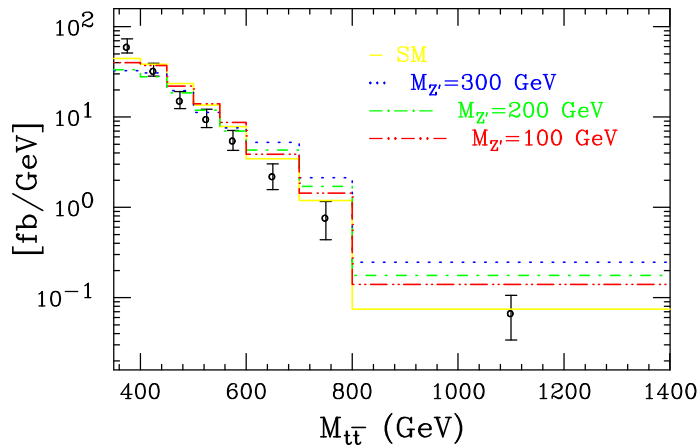
Figure 2.5: The $M_{t\bar{t}}$ invariant mass spectrum. Data from the CDF measurement [25] is shown along with our SM simulation. Also shown are $M_{Z'} = 100, 200, 300$ GeV, with $\alpha_X = 0.013, 0.03, 0.055$, respectively. Each $(\alpha_X, M_{Z'})$ pair would provide an $A_{FB}^{new} \simeq 10\%$.

heavier the Z', the more the last bin deviates from the measurement. This is because the Rutherford singularity (beneficial to the generation of the A_{FB}^t) is most effective at $M_{t\bar{t}} \gg M_{Z'}$. A higher mass Z' will thus need higher α_X because it cannot take full advantage of the singularity, leading to larger distortion of $M_{t\bar{t}}$. Thus, lighter Z' is favored.

The t-channel exchange of Z' can also produce like-sign top-quark events $uu(\bar{u}\bar{u}) \to tt(\bar{t}\bar{t})$, which have been discussed in a different context by [26]. Like-sign tops can be observed as like-sign dilepton events plus b tag(s). CDF has measured only 3 such events with 2 fb^{-1} of data [27]. The SM expectation is also small but with large error: 2.1 ± 1.8 events. Our best point model predicts 5–6 events. Higher Z' mass models produce too many such events from, e.g., $tZ' \to tt + \bar{u}$ if $Z \to u\bar{u}$ (i.e., ϵ_U) is not large enough. For very large ϵ_U, constraints on the Z' from the dijet channel [28, 29] become important. This is another reason why we desire $M_{Z'} < M_t$. This combination of constraints largely determines the location of the "best point" of Fig. 2.4.

There is another reason that $Z' \to t^{(*)}\bar{u}$ decays are potentially dangerous. CDF has measured after cuts the ratio 494/156 of $t\bar{t}+0$ jets to $t\bar{t}+n$ jets with 2.7 fb^{-1} of data, consistent with the SM value [25]. If the $Z' \to t^{(*)}\bar{u}$ decays are present, they will preferentially

contribute to the $t\bar{t}$+n jets, potentially at a dangerous level. A non-zero $\epsilon_U \gtrsim 0.05$ removes this conflict.

There are also potential contributions to the single-top sample. As discussed earlier, with $\epsilon_U \neq 0$, decays of the $Z' \to u\bar{u}$ dominate. Then the dominant contribution to the single-top sample comes from the process $ug \to tZ' \to tu\bar{u}$. This process (after multiplication by a K-factor of 1.3), gives a production cross section of 3 pb. This is comparable to the SM prediction for single-top production (2.9 pb). The measurement of single-top at D0 and CDF [30, 31] relies on a multivariate analysis using detailed kinematic information to extract the single-top events from a large background dominated by W+heavy flavored jets. These backgrounds are nearly an order of magnitude larger than the signal described here. It is not possible to say without such a detailed experimental analysis whether a constraint presently exists.

Flavor physics. One might wonder whether the novel flavor violation of this model is constrained by B meson decays. The structure of the theory wherein off-diagonal couplings are limited to the right-handed up-type quarks make this model particularly safe.

Box diagrams containing both intermediate W and Z' bosons communicate flavor violation to the B sector, giving operators of the form $\mathcal{O}_{d,s} = (\bar{b}\Gamma d_i)(\bar{u}\Gamma u)$, where $d_i = d, s$. However, these operators are only 0.3% (4%) for $d_i = d(s)$ of the SM tree level CKM-suppressed contributions to similar operators, and are of no concern. Moreover, even the CKM-suppressed $\mathcal{O}_s$ is negligible compared to the penguin contribution in processes like $B \to K\pi$, see, e.g., [32].

Flavor changing neutral currents of SM gauge bosons are also induced by one-loop penguin diagrams where Z' runs in the loop with one off-diagonal and one diagonal coupling. The $t \to ug$ measurement by CDF [33] gives the strongest bound. For $(M_{Z'}, \alpha_X)$ pair with $A_{FB}^{new} \simeq 10\%$, this measurement translates into a relatively weak bound $\epsilon_U \lesssim \mathcal{O}(1)$.

Structure of Couplings. As an existence proof, we note that we can reproduce the desired couplings by starting with $U(1)_X$ charges of the three right-handed up-type quarks of $\{-1+\epsilon_U,\ 0+\epsilon_U,\ 1+\epsilon_U\}$. To find the couplings in the mass basis, we perform the rotation on the right handed up quarks. For appropriate Yukawa couplings, there exists a unitary matrix, W_u^R, that transforms the diagonal couplings above into the desired predominantly off-diagonal couplings. The up-type Yukawa couplings are determined in terms of this W_u^R and the V_u^L, which enters the CKM matrix $V_{CKM} \equiv V_u^L V_d^{L\dagger}$. Refer to Section 2.3 for more detailed discussions.

A direction similar to the minimal $U(1)_{Z'}$ discussed here is to introduce an $SU(2)_{flavor}$ gauge symmetry under which the (t_R, u_R) form a doublet. The A_{FB}^t can then be explained through the t-channel exchange of the W' gauge bosons. Because the W' carries a conserved "top-charge", its production and exchange no longer contribute to like-sign top quark production. Avoiding a large (negative) contribution to the A_{FB}^t from, e.g., $ug \to W't$ requires the introduction of a small $W' - \bar{u} - u$ coupling. This can be engineered if the $SU(2)_{flavor}$ is broken by multiple Higgs fields, for example a triplet and a doublet. Searches for like-sign top will not be decisive in determining whether nature realizes this approach. The other phenomenology may be quite similar to that presented here: differences between the lepton+jet and the dilepton $\sigma_{t\bar{t}}$ cross sections will still be present. This model predicts additional contributions to the single top sample as well.

Discussion. The exchange of a t-channel Z' with a $Z' - u - t$ coupling can produce a large A_{FB}^t consistent with other top quark observables. Our best parameter point $M_{Z'} = 160$ GeV with $\alpha_X = 0.024$ generates $A_{FB}^{tot} \simeq 18\%$, about four times larger than the SM prediction. The most constraining collider observable is the search for like-sign top quarks events, which is ameliorated by the introduction of small flavor diagonal couplings. The diagonal couplings are essential also in $M_{t\bar{t}}$ distribution as well as for ensuring $\sigma(t\bar{t}+0$

jets)$/\sigma(t\bar{t} + n$ jets) is consistent with observation. More precise measurements of the top cross section and searches for like-sign tops at the Tevatron should be decisive for this model.

Although heavier Z' ($m_{Z'} > m_t$) suffers from a relatively large like-sign top signal and a disfavored $M_{t\bar{t}}$ distribution, narrow regions of the parameter space might remain. In this region, one is pushed to a large $\epsilon_U \approx 0.3$ (larger values are constrained by dijet searches). In this case, the maximum $A_{FB}^{tot} \lesssim 10\%$.

In summary, it has been shown how a large positive asymmetry arises from the t-channel physics while being consistent with other measurements. Given these successful phenomenologies, we further discuss if this model is theoretically consistent in next two sections.

2.3 Existence proof

In this section, we discuss various theoretical and phenomenological issues regarding a flavor-changing interaction between up and top quarks (mass eigenstates) in eq.(II.4). Specifically, we focus on following flavor-changing interaction in this section

$$\mathcal{L}_{Z'} = g_X \, \bar{u} \, \gamma^\mu P_R \, t \, Z'_\mu + h.c. \tag{II.5}$$

Can such flavor changing coupling be consistent with the CKM measurements and observed quark masses? Can gauge anomaly be cancelled? How can we obtain the SM Yukawa couplings which are not invariant under $U(1)_{Z'}$?

To address the first question, we set relevant notations. The mass eigenstates q and the gauge eigenstates $\tilde{q}$ are related by unitary matrices W and U

$$q_R = W_q \tilde{q}_R, \quad q_L = U_q \tilde{q}_L. \tag{II.6}$$

These matrices diagonalize the Yukawa matrices λ_q

$$U_q \lambda_q W_q^\dagger = D_q \tag{II.7}$$

where D_q are diagonal matrices whose diagonal elements are the mass eigenvalues of q-type quarks. The Yukawa matrices are complex matrices subject only to the measured CKM matrix $V_{CKM} = U_u U_d^\dagger$. Since we consider only up-type right-handed couplings, CKM matrix measurements do not restrict the form of W_u and U_u. The only constraints are unitarity of U_u and W_u.

Let Q_X be a Z' coupling matrix to up-type right-handed quarks in the gauge eigenstate basis. This matrix is diagonal in this basis, but not necessarily proportional to the identity matrix. Our coupling structure in eq.(II.5) is possible if there exists a solution W_u of the following characteristic equation of matrices

$$W_u^\dagger Q_X W_u = \begin{pmatrix} 0 & 0 & 1 \\ 0 & 0 & 0 \\ 1 & 0 & 0 \end{pmatrix}. \tag{II.8}$$

The solution W_u always exists because a symmetric matrix can be diagonalized by an orthogonal matrix. Diagonal elements of Q_X are $-1, 1, 0$.

Chiral coupling structure of eq.(II.5) may disturb gauge anomaly cancelation. Without additional fermions, $Z' - Z' - U(1)_Y$ mixed anomaly is not cancelled. However, we can easily make a theory anomaly free by additional heavy exotic fermions. Table 2.2 shows one example solution with two exotic (Dirac) fermion states $A^{1,2}$, We do not discuss this issue any more.

	A_L^1	A_R^1	A_L^2	A_R^2
Y	-2	-2	-2	-2
$U(1)_X$	0	1	0	-1
$SU(3)$	0	0	0	0
$SU(2)$	0	0	0	0

Table 2.2: Charges of additional fermion states to cancel anomalies.

As $U(1)_X$ charges giving rise to a proper flavor-changing interaction are flavor-dependent

(see eq.(II.8)), the SM Yukawa couplings of up-type quarks are not invariant under $U(1)_X$. Although radiative corrections or higher-dimensional operators may be fully responsible for Yukawa couplings, it is especially hard to imagine a top Yukawa coupling generated in this way is not suppressed and order one. One possible resolution is to take Z'-charge of right-handed top quark to be zero (recall that one eigenvalue of Z' coupling matrix in eq.(II.8) is zero). Alternatively, we can also take the Froggatt-Nielsen approach [17] (similarly Matrix model of Leurer-Nir-Seiberg [18]). We simply assume that there are enough numbers of heavy exotic fermions and proper charges of SM particles under a global symmetry so that the Froggatt-Nielsen mechanism can work.

This mechanism of effectively generating Yukawa interactions necessarily mixes SM particles with exotic particles. This mixing might seem dangerous at first to our existence proof shown above because Yukawa matrices and mixing matrices are not just given by SM ones. Suppose there is a $m \times n$ fermion mass matrix M. $m, n \geq 3$ since three generations of SM fermions are involved. $M^T M$ is a symmetric(hermitian) matrix, thus can be diagonalized by an orthogonal(unitary) matrix. Successive unitary rotations can be written as one unitary rotation. Thus, our existence proof above is still valid.

In summary, the desired flavor-changing coupling structure between right-handed up and top quarks is at least theoretically consistent. The origin of such interactions is beyond the scope of this thesis.

2.4 Gauge fixing independence

As an aside, we clarify how gauge fixing independence is achieved when the SM Yukawa couplings are effectively generated by higher-dimensional operators. Every physical quantity should be independent of gauge fixing terms, and this is necessarily true if a gauge theory description is valid. We begin by asking a few questions that one might have regarding this issue, and we prove the independence of gauge fixing terms. As will be discussed,

each diagram will be individually dependent on fixing terms, but physical quantities will not be.

SM fermions obtain masses from electroweak symmetry breaking, not just from Z' breaking. It may not be clear if the Goldstone boson eaten by Z' couples to SM fermions. Moreover it may not be clear if gauge fixing dependence is cancelled in Z' mediated processes. We study this issue in detail.

To clarify those questions, let us first consider a $2 \rightarrow 2$ fermion scattering process in an chiral abelian gauge symmetry with R_ξ gauge with one flavor. The gauge boson propagator is dependent on the gauge fixing parameter ξ, and this dependence should be cancelled by the Goldstone boson contribution which is also dependent on ξ. The ghost shows up at loop-level, thus it is irrelevant to this discussion. Gauge fixing dependent part of the gauge boson contribution

$$i\mathcal{M} \propto g_V^2 \frac{m_f^2}{m_V^2} \bar{u}\gamma^5 u \frac{-i}{q^2 - \xi m_V^2} \bar{u}\gamma^5 u \tag{II.9}$$

is cancelled by the Goldstone contribution

$$i\mathcal{M} \propto \lambda_f^2 \bar{u}\gamma^5 u \frac{i}{q^2 - \xi m_V^2} \bar{u}\gamma^5 u \tag{II.10}$$

after using the relation $m_f = \lambda_f m_V / g_V$. This simple field theory calculation raises a question; how does this cancellation occurs if hidden Higgs is not involved in generation of SM fermion masses and the above relation does not hold? Moreover, in mass eigenstate basis, how does diagonal Goldstone coupling cancel ξ dependence of possible off-diagonal Z' contribution?

The key observation needed to answer these questions is that $U(1)_X$ is a chiral theory. SM fermion masses are double protected by SM and $U(1)_X$ chiral gauge symmetries, in other words SM fermions can be massive only when both chiral symmetries are broken. After exotic fermions (needed to cancel anomaly) are integrated out, low energy effective

couplings between SM fermions and scalars can be written as

$$\mathcal{L} \ni \sum_i \left(\frac{\phi_X}{v_X}\right)^{n_{ij}} \overline{Q}_L^i \lambda_{ij} q_R^j \, \phi_{SM}. \tag{II.11}$$

where X-charge difference $n_{ij} = X[Q_L^i] - X[q_R^j]$ with a charge of a hidden Higgs ϕ_X is normalized to unity. i, j indices run over SM generations. SM fermions are massive only after both Higgses ϕ_{SM} and ϕ_X get vev. It is also clear that the Goldstone mode of ϕ_X couples to SM fermions. Does this hidden Goldstone coupling have correct structure to cancel gauge fixing dependence of gauge propagator?

To see how this can happen, let us begin with a simple toy model: a spontaneously broken chiral $U(1)$ with two flavors.

$$\mathcal{L} = \mathcal{L}_K + \overline{\psi}_R^i \begin{pmatrix} 1 & 0 \\ 0 & -1 \end{pmatrix}_{ij} \gamma_\mu \psi_R^j V^\mu + (\phi \overline{\psi}_L^i \lambda_i \psi_R^1 + \phi^* \overline{\psi}_L^i \lambda_i' \psi_R^2 + h.c.) \tag{II.12}$$

where $i, j = 1, 2$, and a charge of ϕ is normalized to unity. After Higgs gets vev, fermion mass matrix is

$$\mathcal{M} = v \begin{pmatrix} \lambda_1 & \lambda_1' \\ \lambda_2 & \lambda_2' \end{pmatrix}. \tag{II.13}$$

This matrix is diagonalized by two unitary matrices U and V

$$U \mathcal{M} V^\dagger = \mathcal{M}^D. \tag{II.14}$$

However, the Goldstone coupling (after substituting $\phi(x) = v + h(x) + ia(x)$)

$$\mathcal{L}_a = ia \, \overline{\psi}_L^i \, y_{ij} \, \psi_R^j + h.c. \tag{II.15}$$

where

$$y_{ij} = \begin{pmatrix} \lambda_1 & -\lambda_1' \\ \lambda_2 & -\lambda_2' \end{pmatrix}_{ij} = \frac{1}{v} \mathcal{M}_{ik} \begin{pmatrix} 1 & 0 \\ 0 & -1 \end{pmatrix}_{kj}. \tag{II.16}$$

We note that Goldstone coupling is *not* the same as Yukawa coupling. y_{ij} is not diagonalized by U and V, but becomes

$$(UyV^\dagger)_{ij} = \frac{1}{v}\mathcal{M}_i^D \left\{ V \begin{pmatrix} 1 & 0 \\ 0 & -1 \end{pmatrix} V^\dagger \right\}_{ij}. \tag{II.17}$$

This is exactly what is needed to cancel gauge fixing dependence because gauge coupling in the mass eigenstate basis is just the right-hand side without $\mathcal{M}^D/v$ factor! To see this, we write the Goldstone coupling in eq.(II.15) in terms of Dirac fermion notation as

$$\mathcal{L}_a = ia\overline{\psi}^i(m_i - m_j)\left(VQV^\dagger\right)_{ij}\psi^j + ia\overline{\psi}^i(m_i + m_j)\left(VQV^\dagger\right)_{ij}\gamma^5\psi^j. \tag{II.18}$$

where Z' coupling matrix $Q = \text{diag}(1, -1)$. We note that vectorial coupling is proportional to mass difference of two fermions which would vanish in case of flavor diagonal Z'. On the other hand, gauge fixing dependent part of gauge boson propagator gives

$$\overline{u}(p')^i\,(VQV^\dagger)_{ij}k^\mu\gamma_\mu(1 + \gamma^5)\,u(p)^j \Rightarrow (VQV^\dagger)_{ij}\,\overline{u}(p')^i\left\{(m_i - m_j) + (m_i + m_j)\gamma^5\right\}u(p)^j. \tag{II.19}$$

Cancellations of sort eq.(II.9) and eq.(II.10) indeed occur. The Goldstone boson coupling is not the same as Yukawa coupling. Indeed, it is not diagonal and becomes parallel to gauge boson coupling in the mass eigenstate basis.

This can be easily generalized to cases with several chiral gauge symmetries which independently protects fermion masses. For simplicity, we consider N chiral $U(1)$'s with N_F flavors and arbitrary charges. We assume that each gauge symmetry is spontaneously broken by their own Higgses. Each $U(1)_a$ has $N_F \times N_F$ diagonal coupling matrices C_L^a and C_R^a

$$C_L^a = -\text{diag}(n_1^a, \cdots, n_{N_F}^a), \quad C_R^a = -\text{diag}(m_1^a, \cdots, m_{N_F}^a). \tag{II.20}$$

Low energy effective couplings between fermions and scalars read

$$\sum_{i,j}\Pi_a\left(\frac{\phi_a}{v_a}\right)^{n_i^a - m_j^a}\overline{Q}_L^i\lambda_{ij}q_R^j. \tag{II.21}$$

For dimensionality, we can think of λ as usual dimensionless yukawa matrix multiplied by a scale which might be the lowest breaking scale. Mass matrix is diagonalized by U and V as usual. Goldstone boson a_a coupling eq.(II.15) read

$$
y_{ij} = \begin{pmatrix} x_{11}^a \lambda_{11} & \cdots & x_{1N_F}^a \lambda_{1N_F} \\ & \ddots & \\ x_{N_F 1}^a \lambda_{N_F 1} & \cdots & x_{N_F N_F}^a \lambda_{N_F N_F} \end{pmatrix}_{ij} = -(C_L^a \lambda)_{ij} + (\lambda C_R^a)_{ij} \qquad \text{(II.22)}
$$

where $x_{ij}^a = n_i^a - m_j^a$. Matrix addition is simply element by element. This coupling becomes in the mass eigenstate basis

$$
(UyV^\dagger)_{ij} = \frac{1}{v_a}\left\{ m_i(VC_R^a V^\dagger)_{ij} - (UC_L^a U^\dagger)_{ij}m_j \right\} \qquad \text{(II.23)}
$$

where relative sign difference reflects opposite eigenvalues of γ^5. No dummy index is assumed. As before, Goldstone coupling $\mathcal{L}_a$ can be rewritten in terms of Dirac fermion notation as

$$
\begin{aligned}
\mathcal{L}_a &= ia\overline{\psi}^i\left\{(UyV^\dagger)_{ij} - (VyU^\dagger)_{ij}\right\}\psi^j + ia\overline{\psi}^i\left\{(UyV^\dagger)_{ij} + (VyU^\dagger)_{ij}\right\}\gamma^5\psi^j \\
&= i\frac{a}{v_a}\overline{\psi}^i\left\{(m_i - m_j)(UC_L^a U^\dagger)_{ij} + (m_i - m_j)(VC_R^a V^\dagger)_{ij}\right\}\psi^j \\
&\quad + i\frac{a}{v_a}\overline{\psi}^i\left\{ - (m_i + m_j)(UC_L^a U^\dagger)_{ij} + (m_i + m_j)(VC_R^a V^\dagger)_{ij}\right\}\gamma^5\psi^j. \qquad \text{(II.24)}
\end{aligned}
$$

Parts in curled brackets in the last equation are exactly what we obtain, as in eq.(II.9) and eq.(II.18), by contracting $k^\mu k^\nu$ part of gauge boson propagator to external fermion lines. Gauge fixing dependence indeed cancels out.

In summary, as chiral symmetry prohibits fermion mass, massive fermions should somehow couple to Goldstone bosons of the symmetry. Being a phase degree of freedom, the Goldstone boson has interactions that are not identical to Higgs Yukawa couplings. Those interactions, however, indeed rotate in a proper way to cancel gauge fixing dependence of gauge boson contribution.

2.5 Phenomenology with the flavor-diagonal coupling varied

This section is complementary to Section 2.2. We detail phenomenology of the flavor-changing interactions of the Z' in the presence of the flavor-diagonal coupling ϵ_U. We study various cross section observables as a function of the strength of the flavor-diagonal coupling ϵ_U. By these detailed study, we end up with the best point presented in Section 2.2. To make this section somewhat self-contained, we sometimes repeat the same explanations or arguments in this section as already given in Section 2.2.

As seen in Section 2.2, many phenomenological difficulties of the flavor-changing physics arise from direct Z' productions. As Z' does not distinguish top and anti-top (Z' decays equally to $t\bar{u}$ and $\bar{t}u$), like-sign dilepton signal was induced. This measurement strongly constrained the model. In addition, direct Z' productions followed by $Z' \rightarrow tu$ decays can not only mimic $t\bar{t}$ productions, but also preferentially contribute to the cross section measured in semi-leptonic decay mode of $t\bar{t}$. Consequently, the cross section measured in dileptonic mode is somewhat small. Those faking contributions to $t\bar{t}$ involve extra light-quark jets, and thus it is potentially measurable or constrained by $t\bar{t} + j$ event samples.

These difficulties were somewhat alleviated by the flavor-diagonal coupling ϵ_U in eq.(II.4). No additional flavor changing physics is induced. Our proof of existence in Section 2.3 is still valid because Z' interaction matrix in the generation space (so, 3×3 matrix) is still a symmetric matrix. We detail how all those phenomena mentioned in the previous paragraph depend on the strength of the flavor-diagonal coupling. We also discuss many other phenomenological constraints induced by the flavor-diagonal coupling such as resonance searches and loop-induced flavor-changing interactions between SM particles.

The interaction Lagrangian that we consider in this section is the same as eq.(II.4), but we simply use a different notation for the flavor-diagonal couplings as given by

$$\mathcal{L} = g_X \bar{u}\gamma^\mu P_R t Z'_\mu \ + \ c g_X \, \bar{u}_i \gamma^\mu P_R u_i Z'_\mu \ + \ h.c. \tag{II.25}$$

where the second term is the flavor-diagonal right-handed couplings previously denoted by ϵ_U. The flavor diagonal coupling is now parmaterized by a (small) constant $0 \leq c \leq 1$.

Effects of flavor diagonal coupling is incorporated in the new decay channel of Z'. For Z' lighter than top quark, most(almost 100%) Z' would decay into light quark pairs. Then Z' production does not contribute to LSDL or cross section measurements in the dilepton channel because Z' decays do not accompany leptons. Moreover, Z' and $tt + \overline{tt}$ contributions to other measurements become less significant. For Z' heavier than top quark, $tt + \overline{tt}$ contribution does not change because top does not decay to Z'. Z' production contribution now depends on the branching ratio of new decay channel (in other words, c). We will estimate this dependence below.

Flavor diagonal coupling can produce $t\bar{t}$ pair via exchange of s-channel Z'. However, this contribution is negligible compared to QCD and the t-channel processes because s-channel propagator does not meet the pole for $M_{Z'} \lesssim 350\,\text{GeV}$, and coupling constant is small. So in this section, we will ignore this contribution by focusing on Z' lighter than $350\,\text{GeV}$ which is actually our favored parameter space.

We chose several benchmark points to study flavor diagonal couplings. For several masses of Z', coupling constant α_X are chosen to generate pure new physics contribution to asymmetry $A_{FB}^{new} \simeq 10\%$. This might be the borderline between large and small asymmetry. The benchmark points are following.

benchmark A	B	C	D	E	F
$100\,\text{GeV}, \alpha_X = 0.013$	$130, 0.016$	$160, 0.02$	$200, 0.03$	$250, 0.04$	$300, 0.055$

Table 2.3: Benchmark points ($M_{Z'}, \alpha_X$).

First of all, the most serious problem LSDL signal can be largely alleviated as shown in Fig. 2.6(a). For Z' lighter than top quark, most LSDL events come from $tt + \overline{tt}$ productions as expected. For Z' heavier than top, LSDL signal gets faded as diagonal coupling
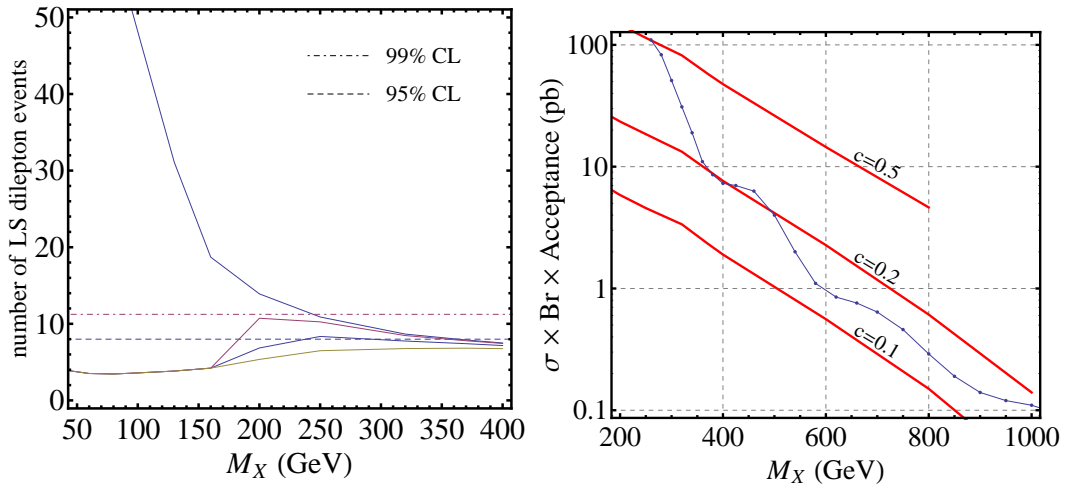
Figure 2.6: (left) Number of Like-Sign DiLepton events with event selections. From top, $c = 0, 0.2, 0.5, 1$. (right) Constraints on c from the resonance search in the dijet channel at Tevatron.

gets stronger. We can see that small diagonal coupling can make most parameter space consistent with 99% CL bound, and $c \gtrsim 0.5$ can make most parameter space consistent with 95% CL bound.

The most stringent bound on flavor diagonal coupling is from the resonance search in the dijet channel at Tevatron as shown in Fig. 2.6(b). Although this search put relatively weak bounds for light Z', $c \simeq 0.5$ is safe only for $Z'(M_X \lesssim 250\,\mathrm{GeV})$. Heavier $Z'(250\,\mathrm{GeV} \lesssim M_X \lesssim 350\,\mathrm{GeV})$ might need to have $c \lesssim 0.2$. Thus, heavy Z' can still have trouble with 95% CL bound on LSDL signal (99% bound can be fine for all ranges of M_X).

Other (weaker) pheno constraints on flavor diagonal couplings are summarized in Fig. 2.7. These include one-loop induced SM FCNC via Penguin diagrams, hadronic decay of Z boson and $\Upsilon(1S)$ via exchange of s-channel Z'.[1] With our benchmark points (α_X such that $A_{FB}^{new} \simeq 0.1$), diagonal coupling is weakly bounded $c \lesssim 1$ for $M_X \lesssim 350\,\mathrm{GeV}$.

Another effect of diagonal couplings is to increase forward-backward asymmetry as well as to decrease (would-have-been measured) cross sections. These are also because

---

[1] If Z' does not couple to bottom quark, there is no tree-level contribution to $\Upsilon(1S)$ decay. However, we show this constraint for completeness.
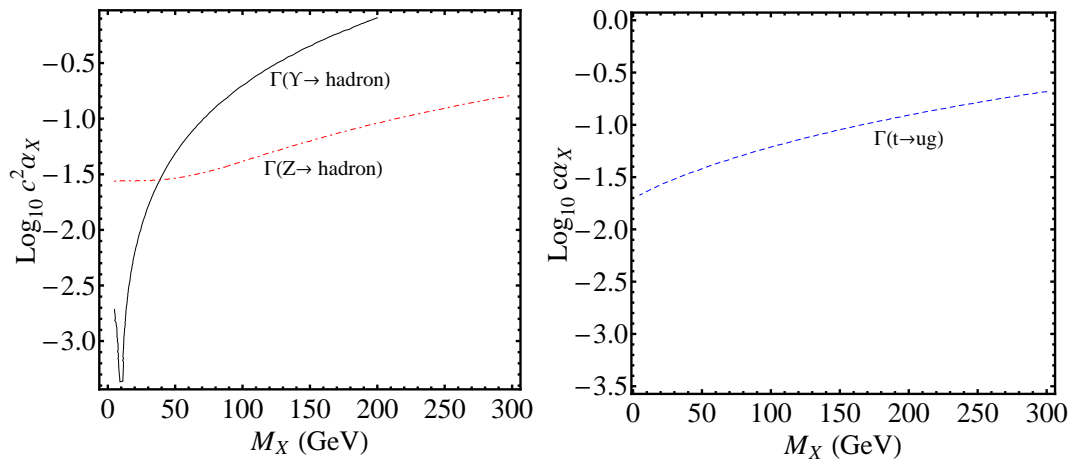
Figure 2.7: Several phenomenological constraints on M_X-α_X parameter space are shown. These include flavor changing coupling of gluon(blue dashed) which is proportional to c, and hadronic decay width of $\Upsilon(1S)$ (black solid) and Z boson (red dot-dashed) which are proportional to c^2. Regions above each line are excluded.

Z' now can decay to light quark pairs which has nothing to do with top and bottom quarks. Less events from direct Z' productions are accepted at the asymmetry, cross section measurements (recall that large negative asymmetry was measured from Z' productions). We estimate total asymmetry by

$$A_{FB}^{tot} = \frac{\sum_i A_{FB}^i \sigma_i \epsilon_i}{\sum_i \sigma_i \epsilon_i} \approx 5\% + \frac{A_{FB}^{new}\sigma_{new} + A_{FB}^{tt}\sigma_{tt} + A_{FB}^{Z'}\sigma_{Z'}\epsilon_{Z'}/\epsilon_{SM}}{\sigma_{new} + \sigma_{tt} + \sigma_{Z'}\epsilon_{Z'}/\epsilon_{SM}}. \qquad \text{(II.26)}$$

where ϵ is an acceptance factor. Here we used the result that acceptances are quite similar for several processes except for Z' productions, and total cross section were close to SM predictions. As shown in Fig. 2.8, the stronger diagonal couplings, the larger asymmetry and the smaller cross sections. $8 \sim 10\%$ (more conservatively, $\sim 12\%$ with stronger α_X coupling) asymmetry can be obtained. Results for light Z' is also shown in Table 2.4 (results are independent of value of c).

In Fig. 2.8, we estimate the dependence of c by assuming that $Z'Z'$ productions are negligible. We also assume that the branching ratio of $t \to uZ'$ is of order one percent (which is reasonable) so that fraction of single top plus Z' productions and fraction of $t\bar{t}+\overline{t\bar{t}}$ productions which become $Z'Z'$ events by top decays are very small. Then contributions of
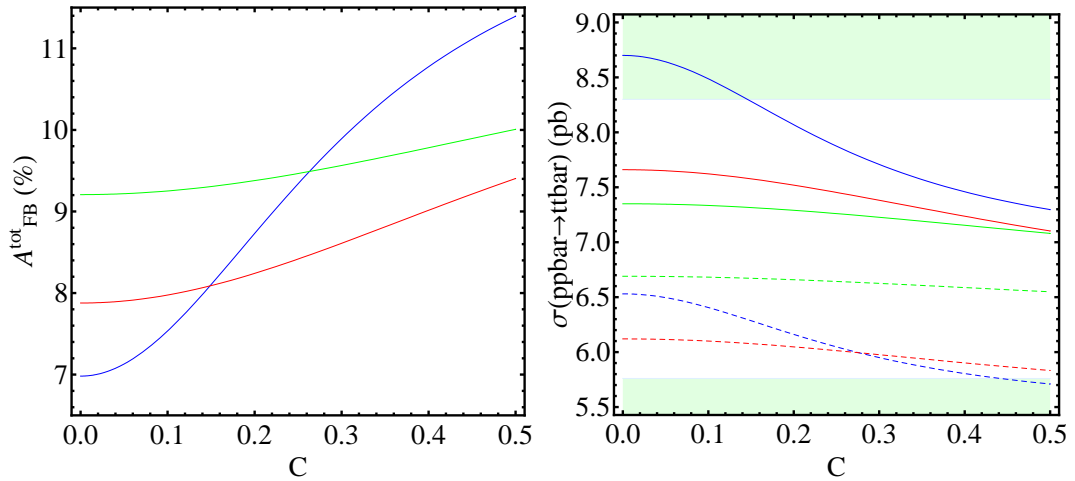
Figure 2.8: (left) Total asymmetry as a function of diagonal coupling, c, is plotted. Blue $200\,\text{GeV}$, red $250\,\text{GeV}$, green $300\,\text{GeV}$. (right) Total $t\bar{t}$ production cross section vs. diagonal coupling. Solid lines are l+j channel, dashed lines are dilepton channel. Colored region is excluded by 2σ bounds of overall measurements.

Z' productions scales proportional to branching ratio of $Z' \to t\bar{u}$. Acceptance as a function of c is then given by

$$A(c) = A_{u\bar{u}}(1-x) + A_{t\bar{u}} x \qquad \text{(II.27)}$$

where $x = Br(Z' \to t\bar{u}, \bar{t}u)$ which implicitly depends on c. $A_{ff'}$ is an acceptance factor assuming $Br(Z' \to ff') = 1$.

Mass	l+j $(c = 0)$	dilepton	l+j $(c > 0)$	dilepton	$A_{FB}^{tot}(c = 0)$	$A_{FB}^{tot}(c > 0)$
$160\,\text{GeV}$	8.59 pb	6.79	5.72	4.95	6%	14.5%
$130\,\text{GeV}$	9.41	6.13	6.42	4.02	$\sim 0\%$	12%
$100\,\text{GeV}$	9.69	6.03	7.59	3.35	2%	12.5%

Table 2.4: (would-have-been measured) cross sections in lepton plus jet(l+j) channel and the dilepton channel with diagonal couplings turned off($c = 0$) and on($c > 0$). Also, total asymmetry estimation is shown.

Direct Z' productions also complicated $t\bar{t}$ cross section measurements with only four jets $(t\bar{t} + 0)$ and with more than four jets $(t\bar{t} + j)$. This is because fake $t\bar{t}$ events from Z' productions involve several extra jets from Z' decays. The ratio of $t\bar{t} + 0$ and $t\bar{t} + j$ was measured to be close to QCD K-factor 1.31 since standard $t\bar{t}$ production processes can produce extra jets only through QCD radiations. However, this QCD K-factor was
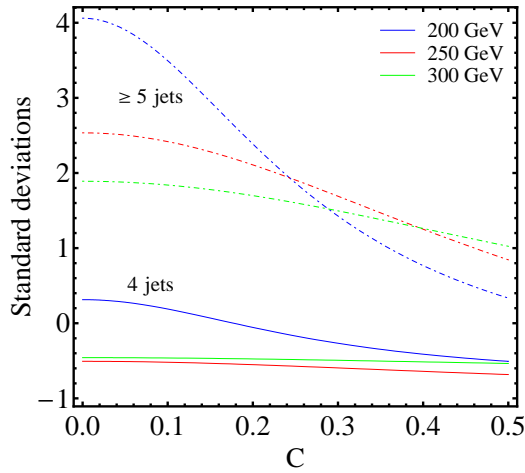
Figure 2.9: Standard deviations of $t\bar{t} + 0$ and $t\bar{t} + j$ number of events as a function of diagonal coupling c.

theoretically calculated, and was measured in other QCD processes as well. Thus, deviation from this ratio maybe another hint of the new physics. Table 2.5 and Fig. 2.9 show the results. Without diagonal couplings ($c = 0$), too much events with extra jets ($t\bar{t} + j$) were expected. However, this can not only be reduced, but also can be safe with 2σ deviations with diagonal couplings $c \gtrsim 0.2$ for most ranges of mass.

Mass	$t\bar{t} + 0(c = 0)$	$t\bar{t} + j(c = 0)$	$t\bar{t} + 0(c > 0)$	$t\bar{t} + j(c > 0)$
160 GeV	0.34 σ	4.39 σ	-1.15 σ	-1.16 σ
130 GeV	0.03 σ	9.31 σ	-1.08 σ	-1.09 σ
100 GeV	0.89 σ	10.62 σ	-2.07 σ	-0.18 σ

Table 2.5: Standard deviations of $t\bar{t} + 0$ and $t\bar{t} + j$ number of events with diagonal couplings turned off($c = 0$) and on($c > 0$).

We also look at invariant mass distributions again. We impose same event selection cuts as CDF used, and rescaled number of events in each bin by acceptances of Standard Model. This distribution was also distorted by Z' production contributions especially for very light $Z'(M_{Z'} \lesssim 150\,\text{GeV})$ because Z' were abundantly produced. As can be seen in Fig. 2.10, this distortion disappeared and invariant mass distributions are in quite good agreement for $M_{Z'} \lesssim 300\,\text{GeV}$.
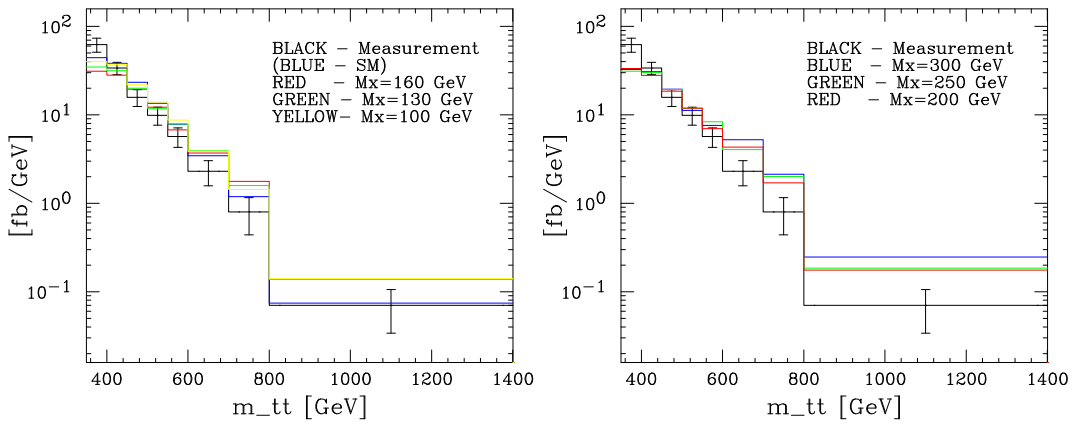
Figure 2.10: Invariant mass $m_{t\bar{t}}$ distributions for several values of $M_{Z'}$. $c = 1$ is used. Smaller c would cause a little up-shift in the right panel only due to larger Z' contributions, but is not significant.

Many processes from Z' physics can fake single top production which is successfully measured by CDF and D0 at Tevatron. As Z' would decay to light quark pairs, direct Z' productions with top quark can fake single top production. In addition, there are several processes producing single top with associated light quark jets. Among many of them, $u\bar{u} \to t\bar{u}$ and its charge conjugate are dominant. We ignored these contributions to $t\bar{t}$ productions. This is because either (1) these processes do not contain many enough jets (recall that most event selections require at least 3-4 jets with one b-taaging as well as one charged lepton and missing energy), or (2) cross sections are too small. We numerically checked that $t\bar{t}$ fake from single top plus jet productions is negligible. However, event selections for single top production measurement are less constraining than $t\bar{t}$. For example, they require less number of jets (sometimes without b-tagging requirement). So we study how much Z' physics can fake single top productions.

Single top production was measured by CDF and D0 by combining several results from different complicated techniques looking at kinematic distributions. We will rather estimate Z' physics contributions to number of selected events (before discriminating signal and backgrounds from kinematic distributions). Then we will ensure that selected events are not only small, but also their kinematic distributions are not significantly different

from many standard backgrounds of single top productions. Z' physics then might be easily buried under large backgrounds. We tabulate this numerical result in Table 2.6.

160 GeV , 0.024, $c > 0$	D0 (l+j)	CDF(l+j)
direct Z'	0.6 σ	0.4 σ
$tt + \bar{t}\bar{t}$	0.3 σ	0.1 σ
$tj, tjj, \bar{t}j, \bar{t}jj$	0.5 σ	0.3 σ
total	1.4 σ	0.8 σ

Table 2.6: Standard deviations of number of selected events in single top production measurements at D0 and CDF. We normalized SM contributions to reported $t\bar{t}$ number of events.

In all, we saw that small diagonal coupling can alleviate LSDL signal, $t\bar{t} + 0/t\bar{t} + j$ ratio and invariant mass distributions. Actually, diagonal coupling was essential for them to be consistent with measurements. In addition, asymmetry increases as negative contributions from Z' was reduced. $8 \sim 10\%$ (or more positively $\sim 12\%$) asymmetry can be obtained. However, diagonal coupling was constrained by resonance searches, and heavy Z' still had mild trouble with LSDL 95% CL bound. This can be made further consistent by opening up the new decay channels which are not constrained by measurements severely. One of this possibility is invisible decay of Z'.

2.5.1 Summary and the best point

For light $Z'(M_{Z'} \lesssim m_t)$, even very small diagonal coupling dramatically changes situation. LSDL signal now becomes completely consistent with 95% bound, and $t\bar{t} + 0/t\bar{t} + j$ ratio also falls within 2σ bound. Moreover, $m_{t\bar{t}}$ distribution becomes much better as well because huge Z' contributions are (almost completely) gotten rid of. Small diagonal couplings were essential for these consistencies. Asymmetry is also expected to significantly increase to about $12 \sim 15\%$. The only issue with light Z' is that total $t\bar{t}$ production cross section in dilepton channel shown in Table 2.4 is quite small. Thus we try to increase coupling constant α_X. As shown in Table 2.7 below, not only cross sections become better but also LSDL signal is safe with 95% bound. Asymmetry now can be as large as 18%.

$t\bar{t} + 0/t\bar{t} + j$ ratio also becomes better. This is our best parameter choice that is also presented in Section 2.2.

best case ($c > 0$)	l+j	dilepton	A_{FB}^{tot}	LSDL events	$t\bar{t} + 0$	$t\bar{t} + j$
160 GeV, $\alpha_X = 0.024$	7.50pb	5.83pb	18.0%	6.1	-0.6σ	-0.7σ

Table 2.7: Stronger coupling can make $M_{Z'} = 160$ GeV case much better. Measurable quantities are shown. Single top study is already shown in Table 2.6.

The light Z' physics may be potentially discovered through more precise measurement of cross sections at the Tevatron. As shown in Table 2.4 and 2.5, the lighter Z', the more different cross sections in semi-leptonic and dilepton channels. Also, the ratio $t\bar{t} + 0$ versus $t\bar{t} + j$, or similarly the ratio of single b-tagging versus double b-tagging become more sensitive to lighter Z'. More accurate measurements of these would be able to probe light Z' physics.

For heavy Z' of $M_{Z'} \gtrsim m_t$, those change in cross sections as a function of c are not as dramatic as the light Z' case because branching ratio $Z' \to t\bar{u}$ now is a less dramatic function of c. Diagonal coupling c is constrained by many pheno observations, especially by resonance searches. With allowed small couplings, there are still mild trouble with LSDL 95% bound as shown in Fig. 2.6. Cross section measurements and $t\bar{t} + 0/t\bar{t} + j$ ratio can be consistent for proper value of c. Asymmetry is also expected to increase a little bit to $A_{FB}^{tot} = 9 \sim 11\%$. In all, $c \sim 0.3$ for $M_{Z'} \lesssim 300$ GeV (possibly trouble with 95% bound of LSDL), or $c \sim 0.5$ for $M_{Z'} \lesssim 230$ GeV might be the best among heavy Z' cases.

2.6 Extension with invisible decay modes of Z'

As discussed in previous sections, importantly, the flavor-diagonal coupling opens up new decay modes of Z' which does not involve any top quarks. This property helps the model avoid too much exotic contributions to top cross sections. Another way to introduce new decay channels of Z' is to assume the existence of invisible decays of Z'. In this section,

we repeat the similar studies presented in the previous section Section 2.5 but by varying the invisible branching fraction of Z'.

The interaction Lagrangian is the same as eq.(II.4), but with $\epsilon_U = 0$

$$\mathcal{L} = g_X \bar{u} \gamma^\mu P_R t Z'_\mu + h.c. \qquad (\text{II.28})$$

The invisible branching ratio of Z' is denoted by Br_{inv} in this section, and is regarded as a free parameter. The invisible decay of Z' might be constrained by some measurements requiring a large missing energy. For the purpose of our study to generally understand the phenomenology with invisible decay modes, we simply assume that invisible decay is not constrained. We detail phenomenology of the model as a function of Br_{inv} in this section.

There have been many clues that we need some sort of new physics sectors quite hidden from our visible world now but effectively in a contact with the visible world at early universe or higher energy process. If Z' plays a role in communicating two sectors, Z' can substantially decay invisibly.

It is not difficult to understand what Br_{inv} plays a role in phenomenology. If branching ratio of invisible decay is 100%, every Z' productions are lost (acceptances are zero). Some portion of final state top quarks would decay to Z' (if Z' is lighter than the top), and are also lost. This portion is purely determined by Br_{inv}, a free parameter in our consideration. As invisible decay width decreases, more Z' events will contribute to various top quark cross section measurements.

In this section, we also approximate dependence on Br_{inv} as in eq.(II.27) in Section 2.5. The direct Z' productions linearly scale with Br_{inv} (not square of this). Various cross section observables such as asymmetry, $t\bar{t}$ total cross section and LSDL all become linear with Br_{inv} as shown in Fig. 2.11. Results are quite similar to diagonal coupling case considered in Section 2.5. However, Br_{inv} is a free parameter and is more versatile than ϵ_U because ϵ_U was constrained by several other measurements.
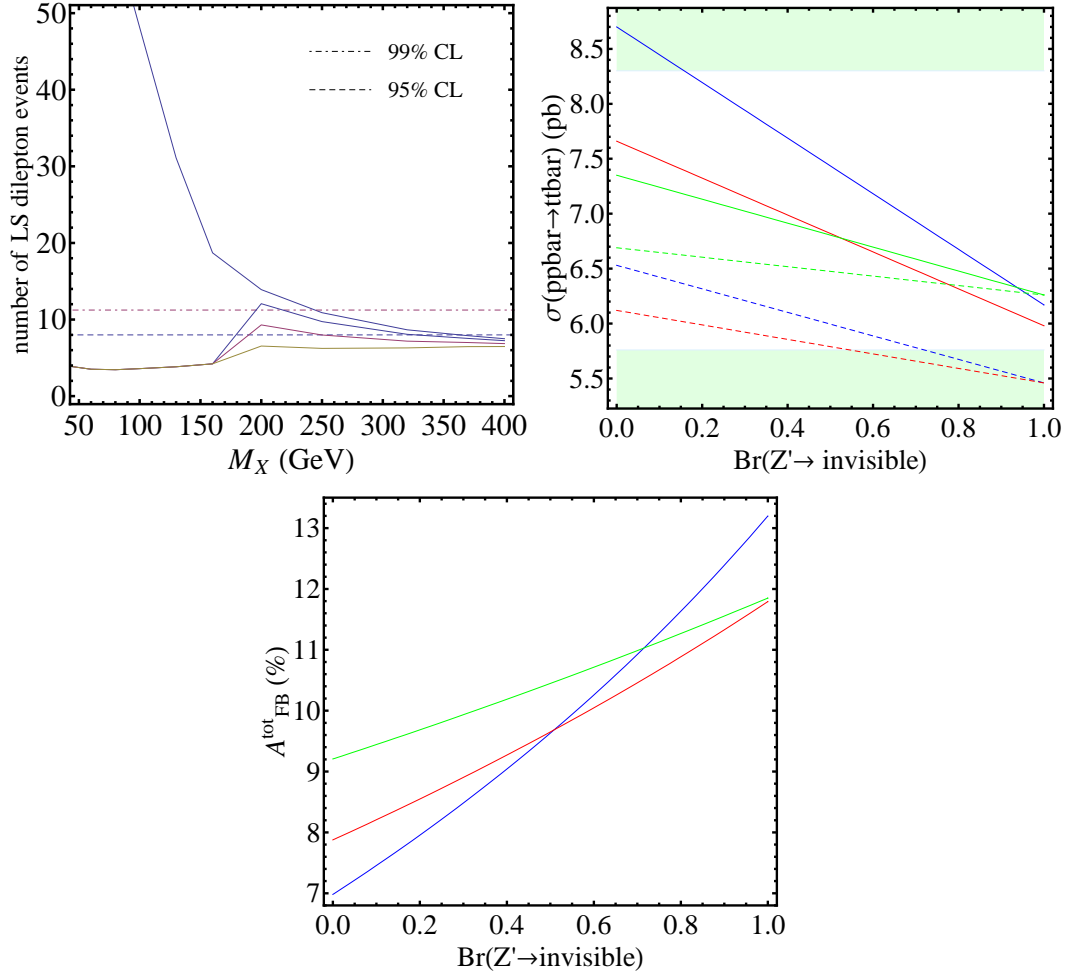
Figure 2.11: Measurable quantities with invisible decays of Z'. (a) LSDL signal for $Br_{inv} = 0, 0.2, 0.5, 0.8$ from top. (b) $t\bar{t}$ production cross section as a function of Br_{inv} in the lepton plus jet channel(solid) and the dilepton channel(dashed). Blue 200 GeV, red 250 GeV, green 300 GeV. (c) Total asymmetry is also plotted.

Fig. 2.11 shows that the larger invisible decay, the better situation except for too small total cross sections. For example, $Br_{inv} = 0.8$ makes Z' consistent with LSDL signal while some of the cross sections are too small. Maybe we can increase coupling constant α_X without distorting other measurements as we did for $M_{Z'} = 160\,\text{GeV}$ case above. Then, probably asymmetry can be as high as $11 \sim 15\%$. If we want to cure pure t-channel physics by invisible decay, then $Br_{inv} \gtrsim 0.6$ and stronger α_X might be needed for heavy Z' case.

We have considered invisible decay mode of Z' as an alternative way to make t-channel Abelian physics more consistent with data. General theory behaviors are presented as a function of invisible decay branching ratio which we simply regard as a free parameter. The result is a positive. However, by considering other measurements with a large missing energy, this conclusion might be somewhat changed. We do not pursue study in this direction any more. If the model with the flavor-diagonal coupling is in difficulty in the future, we may revisit the study in this section as an alternative model building option.

2.7 Conclusion

It has been thoroughly discussed how t-channel physics induced by a flavor-changing interaction between right-handed up and top quarks yield a large positive asymmetry while being consistent with other cross section measurements. An Abelian gauge symmetry is considered as a new physics model.

If the true asymmetry at the Tevatron is greater than 15% and is caused by our Z' theory, the LHC will also have many opportunities to discover its effects. Certainly the most important effect is again the like-sign dilepton channel. Deviations are more likely to show up there in the early years of LHC running than through the top quark asymmetry. The LHC, being a pp machine, must form the asymmetry with respect to the $t\bar{t}$ boost direction.

One can also conceive of alternative models which do not produce like-sign top quarks

(hence, like-sign dilepton events). If the particle exchanged in t-channel is complex, this will distinguish top quarks and anti-top quarks. Consequently, there is no like-sign top quarks produced. This would be the case for scalar particles as well as non-Abelian gauge bosons that have flavor-changing couplings of up and top quarks. Consideration of such models will be an interesting subject in the future.

CHAPTER III

The Four-top-quark Signature of a Low-scale Warped Extra Dimension

3.1 Introduction

The origin of heaviness of the third generation particles and its possible connection to physics responsible for electroweak symmetry breaking (EWSB) are still mysterious. Nevertheless, many candidates of new physics generically end up with either preferential couplings to the third generation or light partners of third generation. For example, top quark condensation and its mass are directly tied to electroweak scale dynamics in top-color models, and top partners are present and possibly lighter than other partners in the supersymmetry and Little Higgs models.

An extreme case is when new physics couples only to the third generation. This raises a challenge in discovering such physics at the collider because they are not produced directly from colliding partons/leptons. A gluon, not being a fermion, is an exception to this discussion, and can couple to colored new particles. However, such interaction vertices involve two or more new particles at leading order, which then are only produced in pairs in simple processes.

Meanwhile, a warped extra dimensional Randall-Sundrum (RS) model [4, 34] is a promising theory that attempts to explain the large hierarchy between Planck scale and weak scale. Exponentially warped background geometry is responsible for the huge differ-

ence of mass scales between two 4D spaces of moderate distance along the extra dimension.

The warped space in the RS model has been further feted by its ability to generate the flavor hierarchy [35, 36]. The Higgs boson, being localized on the IR brane, feels only the exponentially warped tail of the bulk wave functions of UV localized fields. By properly localizing fermions, a wide range for the fermion mass spectrum can be obtained with anarchic Yukawa couplings. However, this flavor dependence inevitably induces flavor changing neutral currents (FCNC) mediated by Kaluza-Klein (KK) gauge bosons, and the RS model of this type generically in conflict with precise measurements of flavor physics. The strongest among them, for example, are from CP violation ϵ_K of the $K - \bar{K}$ system which requires the mass of KK states to be $M_{KK} \gtrsim 20\,\text{TeV}$ [37, 38]. When the Higgs is in the bulk, bounds from ϵ_K and ϵ'/ϵ_K of the $K^0 \to 2\pi$ process can be relieved to be $M_{KK} \gtrsim 5.5\,\text{TeV}$ [39, 40] which is still well above the electroweak scale and beyond the collider reach if the anarchic Yukawa approach is pursued.

On the other hand, if one's highest priority is first and foremost to explain the Planck-weak hierarchy, the RS model can be made much more compatible with flavor measurements by assuming $c_{light} = 0.5$[1] which decouples KK gauge bosons from Standard Model (SM) fermions and by having some flavor structure. Several flavor structures of the quark [41, 42, 43] and lepton [44, 45] sectors have been discussed in the literature. Among them, flavor universality in the RH down sector is very useful to make the theory consistent with ϵ_K measurements with mildly heavy $M_{KK} \gtrsim 4\,\text{TeV}$ [46]. This is made possible by getting rid of the chiral enhanced left-right mixed current contributions to ϵ_K [37]. On the other hand, in the geometric approach to the flavor hierarchy, there still exists some tension with several flavor observables that hover around the current bounds.

Another class of flavor structure is to align bulk masses with proper combinations of

---

[1] Our definition of the bulk mass parameter c is the usual one, and matches, for example, that given in ref. [35]. By c_{light}, we mean bulk masses of both left-handed (LH) and right-handed (RH) first two generations.

anarchic Yukawa couplings [41]. The desired degree of alignment in the down-sector can be achieved by some bulk flavor symmetries [42], and the flavor bound is as low as the bound obtained from generic electroweak precision test (EWPT) $M_{KK} \gtrsim 3\,\mathrm{TeV}$ [47]. Furthermore, if the full flavor symmetry $SU(3)^5$ is gauged in the bulk and if (fully) *hierarchical* Yukawa couplings generated from the flavor breaking at the UV brane are shined to the IR brane, minimal-flavor-violation is generically obtained and fermion localization is released from the duty of generating the hierarchy [48, 49]. Consequently, universal $c_{light} \simeq c_b \simeq 0.5$ is a preferred solution for lighter KK states $M_{KK} \sim 1.5 - 2\,\mathrm{TeV}$ compatible with flavor physics as well as with EWPT [48].

Model independent global fit studies of EWPT in refs. [50, 51] have also shown that the parameter space $c_{light} \sim 0.5$ is a consistent solution allowing light KK states $M_{KK} \sim 2 - 3\,\mathrm{TeV}$ in RS models with custodial symmetry [47, 52]. Very importantly, decoupling of SM KK gauge bosons from SM fermions can render the S parameter small [47]. c_b, the bulk mass of RH bottom quark, is also somewhat consistently allowed to be around $c_b \sim 0.5$. Although the absolute minimum of the fit may be obtained with c_{light} and c_b slightly away from 0.5, this slight deviation is inconsequential if KK states are slightly heavier.

We also remark that by utilizing this special property of the $c_{light} \sim 0.5$ region with regard to EWPT, warped models of Higgless theory are made more successful [53, 54]. In this type of theory, light KK states are essential to recover unitarity around the TeV scale.

Whatever the underlying reason may be for it, if $c_{light} = 0.5$ is realized in nature, it could be difficult to discover RS physics in the standard channel $q\bar{q} \to g^{(1)} \to t\bar{t}$. In this paper, we study alternative collider signatures of the RS model with $c_{light} = 0.5$. *Four* top quarks can be abundantly produced via

- $q\bar{q}, gg \to t\bar{t}g^{(1)}$ associate production

- $gg \to g^{(1)}g^{(1)}$ pair production

followed by $g^{(1)} \to t\bar{t}$ decays. Four top quarks can then give rise to exciting collider signatures involving many leptons, bottom quarks as well as sizable missing energy. We categorize final states by the number of leptons (by "leptons" we mean electrons or muons here):

- single lepton (of any charge)

- like-sign dilepton (two and only two leptons of the same charge)

- trilepton (three leptons of any charges).

We will aim to estimate the discovery reach of the above multi-lepton channels, but not to reconstruct four top events nor a heavy resonance. That is for a later study. Also, regarding the single lepton category, in the case of nonzero left-handed top/bottom coupling, $t\bar{t}b\bar{b}$ events can also contribute to single lepton final states. This process will be considered as well.

In this paper, we will somewhat model independently assume the parameter space of $c_{light} = 0.5$ for the first two generations to decouple KK-gluon from SM light fermions, and assume the flavor universal structure at least in the RH down-sector, i.e. $c_b = 0.5$ universal to c_{light}. As discussed, this parameter space can approximately represent the attractive solution of light $M_{KK} \sim 1.5 - 3\,\mathrm{TeV}$ obtained from the EWPT point of view [47, 50, 51] as well as from the shining model of ref.[48]. Relevant theoretical issues with such parameter choices will be reviewed and discussed in section 3.2.2.

Four top events have been discussed in several different contexts. Associate production ($t\bar{t}g^{(1)}$) in RS models have been studied without emphasis on $c_{light} \simeq 0.5$ in ref.[55, 56]. These references used kinematic cuts on top quarks themselves which do not take into account topological characteristics of events such as overlap of objects, missing energy, number of objects, etc. Compositeness of the top quark can also be probed in the four

top events [57, 58, 59, 60]; results with the like-sign dilepton (LSDL) observable in ref.[57] agree with ours. Pair of gluinos in supersymmetry models [61, 62], exotic fermions mixing with top quark strongly [63], and Z' coupling preferentially to top quark [64] can also give rise to four top events.

We first set the model framework and input parameters in section 2. Some theoretical thoughts on issues regarding $c_{light} = 0.5\,(= c_b)$ will be reviewed. Then we present our Monte Carlo simulation results of discovery potential in sections 3 to 6. One can find the discussions on boosted leptonic top in section 3.5.2. Section 7 is devoted to discussing other possible collider signatures competing with four top events and sorting out parameter space where four top events are most important.

3.2 Model setup

3.2.1 Randall-Sundrum model with custodial symmetries

The Randall-Sundrum model is a five-dimensional theory in the AdS background geometry [4]. The metric is given by

$$ds^2 = e^{-2ky}\eta_{\mu\nu}dx^\mu dx^\nu - dy^2 \tag{III.1}$$

where x^μ $(\mu = 0, 1, 2, 3)$ are 4D coordinates, and y is the coordinate of the extra dimension. The extra dimension is compactified to the finite interval $0 \le y \le \pi r_c$. The curvature scale k is assumed to be $k = M_{pl}$ in numerical computation. Exponential warping generates weak scale M_{IR} from the Planck scale

$$\frac{M_{IR}}{k} = e^{-\pi k r_c} = 10^{-16}, \qquad M_{IR} \sim \mathcal{O}(1\,\text{TeV}). \tag{III.2}$$

The Higgs boson is assumed to be localized on the IR brane, but the main discussion in this paper may be applicable to bulk Higgs case as well.

We assume that electoweak gauge symmetry in the bulk is enhanced with a custodial symmetry to be $SU(2)_L \times SU(2)_R \times U(1)_X$ [47] with a discrete parity P_{LR} exchanging

$SU(2)_L$ and $SU(2)_R$ [52]. Custodial symmetry is essential to be consistent with electroweak precision tests (EWPT), and to protect the accurately measured $Zb\bar{b}$ coupling [52, 50, 65, 66]. We emphasize that since Higgs-gauge contributions to the T parameter has to be suppressed, custodial symmetry is required regardless of fermion couplings [47]. There are extra KK particles in order to embed SM particles into extended symmetry representation. These extra particles will not be needed for our main discussion on four top events, but they may contribute to additional collider signatures. More discussion on these aspects can be found in section 3.6.2.

Our focus will be on the KK excitation of the gluon $g^{(1)}$ because this feels strong coupling. $g^{(1)}$ satisfies $(+, +)$ orbifold boundary condition[2] because its zero mode is identified as SM gluon. Its mass is then given by

$$M_{KK} \simeq 2.45\, M_{IR} \tag{III.3}$$

and will be used to represent the mass scale of KK states. 5D SM fermion will also satisfy $(+, +)$ BC, and its bulk mass parameter c determines its bulk wavefunction, hence its 4D couplings. KK-gluon coupling to SM fermion is shown in Fig. 3.1 [35]. This vanishes at $c = 0.5$ due to orthogonality of wavefuntion solutions. We utilize this property and set $c_{light} = 0.5$ to decouple KK-gluons from light fermions. KK-gluons still couple to gluons via triple and quartic vector self-interactions with QCD coupling strength [67].

We comment on our notation regarding the bulk mass parameter c. Only one 4D chirality of 5D Dirac fermion will be discussed under orbifold projection. Whether it is LH or RH Weyl, $c = 0.5$ is a conformal point where the bulk wave function is flat.

---

[2]The boundary condition notation $(\pm, \pm)$ has the meaning that $+ (-)$ stands for Neumann (Dirichlet) BC of the field wave functions at a brane. The first (second) BC in the listing is at the UV (IR) brane.
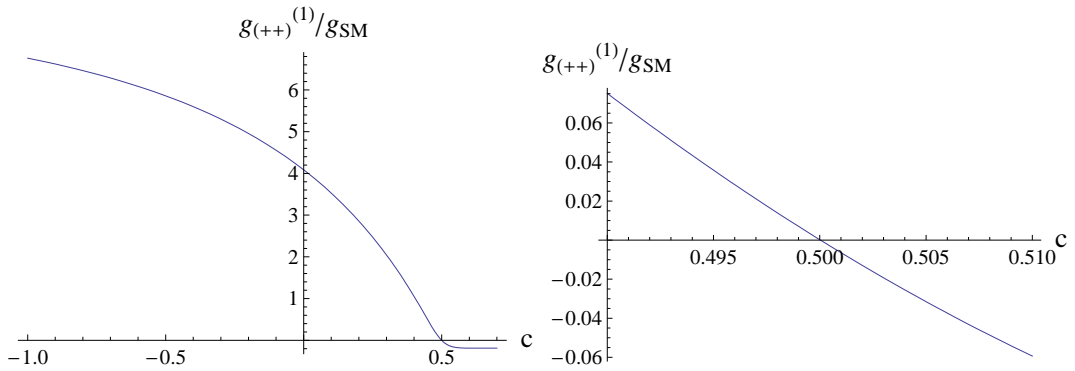
Figure 3.1: Gauge coupling of zero mode fermions with KK gluon (the first KK gauge boson with $(+,+)$ boundary condition). $g_{KK} = 0$ for $c = 0.5$, and reaches its asymptotic value $g_{KK} \simeq -0.2$ for higher c.

3.2.2 $c_{light} = 0.5$ and universality

We summarize EWPT and the flavor physics of the RS models in general. Then we discuss and review why our assumed parameter space

$$c_{light} = c_b = 0.5 \qquad \text{(III.4)}$$

is attractive. In the parameter space of eq.(III.4), c_b is for RH bottom quark, and with eq.(III.4) full universality in the RH down sector is achieved.

One can categorize the sources of ΔS and ΔT: gauge-Higgs, top/KK-fermion, and contributions involving light fermions [47, 50]. A custodial symmetry [47, 52] can tame the gauge-Higgs contributions well, and dominant contributors to negative ΔT are from top/KK-fermion sector which couple strongly via large Yukawa couplings. On the other hand, a global shift of gauge couplings to fermions gives rise to ΔS ($Zb_L\bar{b}_L$ coupling is well protected by a custodial symmetry). This ΔS is positive for the commonly assumed case of $c_{light} \sim 0.6$, conflicting with negative ΔT, which together creates the EWPT tension. Thus decoupling of SM KK gauge bosons from SM fermions can render ΔS small and make light KK states more viable. $c_{light} \ll 0.5$ will couple too strongly, which may induce too large deviations, while $c_{light} \gg 0.5$ will require too large (non-perturbative) Yukawa couplings. Therefore, $c_{light} \sim 0.5$ is preferentially obtained in many EWPT studies of RS

models [50, 51, 48, 53, 54], if one allows such parameter space which is often not considered in anarchic Yukawa approach.

Universal structure of bulk masses will tame flavor contributions in the RS model. Flavor changing neutral current originating from KK-gluons is induced by generation mixing as well as mixing of zero and KK modes of fermions. The former source can be seen by writing gauge couplings in the mass basis (e.g. RH down sector)

$$\tilde{g}_{ij} = \sum_k (D_L)_{ik} \, g_k \, (D_L^*)_{jk} \simeq (D_L)_{i3} \, g_3 \, (D_L^*)_{j3} \tag{III.5}$$

where D_L is some unitary rotation matrix. In the second equation, the equality holds for $c_{light} = 0.5 \, (g_1, g_2 = 0)$, and approximate equality holds even in the usual RS models because $g_3 \gg g_1, g_2$ [68]. Thus FCNCs are generically suppressed by small mixing angles whether $c_{light} = 0.5$ or not. In other words, $c_{light} = 0.5$ alone without $c_b = 0.5$ does not improve the flavor situation significantly from usual RS models, e.g. ϵ_K still pushes $M_{KK} \gtrsim 20 \, \text{TeV}$ [37, 38].

Given the difficulty with flavor physics from third generation mixture, we essentially assume universal bulk masses of the full RH down sector, including c_b, as in eq.(III.4). This will get rid of RH down-type FCNCs at leading order since the gauge coupling commutes with the mass matrix in flavor space. Then the bound from ϵ_K is greatly reduced due to the absence of chiral enhanced LR-type four-fermion FCNC [37, 46]. This kind of universality may be achieved by a bulk flavor symmetry [43, 44, 46] motivated by the AdS/CFT correspondence [69]. We remark that the choice of eq.(III.4) actually has been obtained as an attractive solution allowing $M_{KK} \sim 1.5 - 2 \, \text{TeV}$ in the shining model of ref.[48] with respect to both EWPT and flavor physics, although in their model there is some additional alignment and it is not so important to peg c_b very close to 0.5. In a somewhat different approach, it has been recognized previously that because c_b plays a less important role than c_{light} in the global fit of EWPT, $c_b \sim 0.5$ is consistently allowed

with low KK scale [51]. It is less required from the data point of view, and perhaps less motivating from the theory point of view, to have $c_{Q,t}$ universal with eq.(III.4), and thus we generally allow it to vary. However, some of the representative cases that we are studying exploit additional universality in the LH bulk masses (case A and B in the table 3.1) or RH up-type bulk masses (case C and D).

The implications of the mixing of KK and zero mode fermions as a source of FCNC is typically smaller [38], but one may suspect that pushing light generations closer to the IR brane as in our case may enlarge dangerous mixing effects from Higgs. However, Yukawa couplings become smaller correspondingly, and therefore mixing is reduced. For example, mixing between KK mode ψ_L^n and zero mode ψ_R^0 fermions can be written as (by matching 5D Yukawa interaction with 4D effective actions of 4D decompositions $\psi^n(x)$)

$$\mathcal{L}_{yukawa} \ni \int d^4x\, yH(x)\left(f_L^n \overline{\psi}_L^n(x)\right)\left(f_R^0 \psi_R^0(x)\right) = \int d^4x\, m_f \frac{f_L^n}{f_L^0} \overline{\psi}_L^n(x)\psi_R^0(x) \quad \text{(III.6)}$$

where zero mode fermion mass $m_f = yv\, f_L^0 f_R^0$, $v = \langle H \rangle$ is used. f^n is the n-th KK mode fermion bulk profile evaluated at the IR brane. The KK mode profile is always peaked around the IR brane; hence, f^n is almost constant with respect to bulk mass while zero mode f^0 is exponentially sensitive as

$$f^0(c) = \frac{e^{(1/2-c)\pi k r_c}}{N}, \qquad \frac{1}{N^2} = \frac{(1/2-c)}{e^{(1-2c)\pi k r_c} - 1}. \quad \text{(III.7)}$$

Therefore, the $c_{light} = 0.5$ case has rather smaller mixing by a factor of $\sim f^0(c = 0.6)/f^0(c = 0.5) \sim 0.1$. Once the former source of KK-gluon FCNC is well tamed by flavor structure, mixing of KK and zero mode becomes a leading source of down-type FCNC [46]. Now the choice of $c_{light} = 0.5$ suppresses such well-measured down-type FCNC by additional factors beyond the usual RS case. We comment that smaller 5D Yukawa may increase KK-gluon FCNC in anarchic Yukawa approach. If 5D Yukawas are anarchic, $f_{Q,u,d}^0$'s determine masses, couplings as well as mixing angles, thus giving relations between them.

These are given by

$$m_{ij} \simeq v\, y^{5D} f_{Li}^0 f_{Rj}^0, \qquad g_i \simeq g^{5D}\,(f_i^0)^2 + \cdots, \qquad (D_L)_{ij} \sim \frac{f_{Li}^0}{f_{Lj}^0} \quad \text{if } j > i \qquad \text{(III.8)}$$

where $\cdots$ represents flavor independent parts of gauge couplings. y^{5D} and g^{5D} are dimensionless couplings of the 5D bulk action in proper units of $1/k$ and $1/\sqrt{k}$, respectively. Then eq.(III.5) becomes

$$\tilde{g}_{ij} \sim f_{Li}^0 f_{Lj}^0\, g^{5D} \qquad (i, j < 3) \qquad \text{(III.9)}$$

which may increase with smaller 5D Yukawa as f can be larger. However, with hierarchic Yukawa, the above relations do not hold and the size of 5D Yukawa coupling is, in general, independent of FCNC gauge couplings.

RS contributions to various dipole operators are relatively suppressed for $c_{light} = 0.5$. Dipole operators of the form $\bar{f}_L \sigma^{\mu\nu} f_R' F_{\mu\nu}$ can induce flavor *diagonal* CP violation such as the neutron electric dipole moment (EDM) as well as flavor changing processes such as $b \to s\gamma$ and ϵ'/ϵ_K of the $K^0 \to 2\pi$ process. The neutron EDM is typically estimated to be an order of magnitude larger [68], and the other two give one of the strongest bounds on M_{KK} [39, 40]. Since dipole operators are chirality flipping, dominant contributors are one-loop diagrams in which Higgs and KK fermions are running. These involve at least two (Higgs) mixing insertions of KK-zero mode fermions which give a relative suppression factor of about $\sim (f^0(c = 0.6)/f^0(c = 0.5))^2 \sim 0.01$ as similarly discussed above.

Smaller Yukawa couplings and consequent smaller KK-zero fermion mixing suppress Higgs-mediated FCNC. In addition, universal c can be capable of additional suppression. If Yukawa couplings between wrong-chirality KK fermions vanish (e.g., between LH SM singlet and RH SM doublet), Higgs FCNC is safely chiral suppressed by $(m_{light}/M_{KK})^2$ because the IR-Higgs boson couples only to 4D chiral modes satisfying the Neumann BC on the IR brane [38, 70]. However, Higgs FCNC is generically comparable to KK-gluon induced FCNC with the wrong Yukawa couplings, since wrong Yukawa are generally allowed [71].

When such wrong Yukawas are identical to corresponding SM Yukawas (which is the case for the bulk Higgs by 5D covariance), universal c eventually has minimal-flavor-violation at low-energy as hierarchical (SM) Yukawa couplings are assumed to be the only flavor spurion (up to non-universal c_Q and c_t). Then the leading flavor spurion contribution to Higgs FCNC is aligned with the mass matrices as

$$F_Q \, Y_{u,d} Y_{u,d}^\dagger Y_{u,d} \, F_{u,d} \, \sim \, (y_{t,b}^2) \, F_Q \, Y_{u,d}^\dagger \, F_{u,d} \, \propto \, M_{u,d} \qquad (\text{III.10})$$

because hierarchical $Y_{u,d}^3 \sim (y_{t,b}^2) \, Y_{u,d}$ [48, 71]. Thus, we are safer with Higgs FCNC as well. We also comment that the degeneracy in c can get rid of radion-mediated FCNC [72].

Another concern of pushing light fermions closer to the IR brane is that higher-dimensional operators composed of light fermions are not suppressed enough purely by fermion localization. The constraint on ϵ_K requires that relevant dimension-six four-fermion operators need to be suppressed by $\Lambda \gtrsim 10^5$ TeV while 10^4 TeV is required if CP-phase is absent [37]. This effective suppression scale Λ is defined by the 4D effective action matched with 5D four-fermion interaction [35, 53]

$$\mathcal{L}_{4D} \ni \int d^4x \, \frac{a}{\Lambda^2} \, \bar\psi_i^0 \psi_j^0 \bar\psi_k^0 \psi_l^0 \, = \, \int d^4x \int dy \, \sqrt{-g} \, \frac{a}{M_{pl}^3} \, \bar\Psi_i \Psi_j \bar\Psi_k \Psi_l \qquad (\text{III.11})$$

where ψ_i^0 are zero mode 4D decomposition of 5D Dirac Ψ_i. a is a model dependent coefficient. Λ is then obtained by integrating products of fermion wave functions over the extra dimension

$$\frac{a}{\Lambda^2} \, = \, \frac{a}{M_{pl}^2} \, \frac{2}{N^4} \, \frac{e^{(4-4c)\pi kr_c} - 1}{4 - 4c} \qquad (\text{III.12})$$

with universal $c = c_{light}$. Normalization N is given in eq.(III.7). Since $c_{light} = 0.5$ gives only $\Lambda \simeq 10^2$ TeV, some sort of cancellation or suppression is necessary which can be achieved by bulk flavor symmetry, for instance. For reference, $\Lambda \simeq 10^5$ TeV is obtained for $c_{light} \simeq 0.63 - 0.67$.[3]

---

[3]Values of Λ at $c = 0.5(0.65)$ have weak(strong) dependence on the choice of M_{pl} (with fixed M_{IR}), as can be seen by computing the ratios $\Lambda(M_{pl} = 10^{19} \, \text{GeV}) / \Lambda(M_{pl} = 10^{16} \, \text{GeV}) \simeq 1.2(7.9)$ for $c = 0.5(0.65)$. The range for c_{light} quoted in the text is obtained for $k = M_{pl} = 10^{19}, 10^{16}$ GeV substituted into eq.(III.2).

We express no idealogy as to a theoretical inevitability for $c_{light} = 0.5$ besides the data preferring it. We do note that this is a point of enhanced conformal symmetry and therefore could have a strong underlying theoretical motivation. One possible connection may be that when fermions arise from adjoint representations in some D-brane models they are "born" with $c = 0.5$ [73]. Strong corrections can push the third generation away from this value, but the light fermions remain there. Further thoughts on a deeper theory motivation are beyond the scope of this paper.

3.2.3 Input parameter ranges

We fix $c_{light} = 0.5$ for the first two generations as assumed, and $c_b = 0.5$ for the RH b quark to keep universality of RH down-type bulk masses as discussed.

We now have three free parameters. Two of them are remaining bulk masses of third generation. We study the following range:

$$-0.3 \lesssim c_t \leq 0.5, \quad -0.3 \lesssim c_Q \leq 0.5 \tag{III.13}$$

for RH top, LH top/bottom doublet, respectively. Both c_t and c_Q are restricted to be less than 0.5 since otherwise the top Yukawa would be non-perturbative (see Fig. 3.2). Most of the regions of $c_t, c_Q \lesssim 0.5 - 0.4$ allow a perturbative top Yukawa. If $c_Q \lesssim -0.5$, there will be a very light custodian which is excluded (see section 3.6.2), so conservatively we consider the range of c_Q in eq.(III.13). Regarding EWPT, a large negative T parameter is typically induced unless $c_t \gtrsim 0.3 - 0.4$, e.g. $\Delta T = -0.1 \sim -0.15$ for $c_t \lesssim 0.2$ [50, 51]. For general purposes, we study a rather wide range of $-0.3 \lesssim c_t$ as in eq.(III.13), but will focus on cases that are preferred by EWPT (e.g. $c_t \gtrsim 0.3 - 0.4$ in case C and D in the Table 3.1) when it is relevant. We refer the reader to section 3.6.2 for more discussions on c_Q and c_t with respect to other collider searches.

The last free parameter is the mass of KK gluon M_{KK}. We study following range of
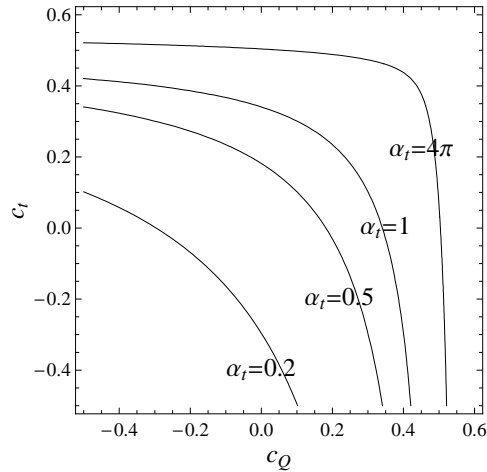
Figure 3.2: Contours of the required 5D top Yukawa $\alpha_t = (y_t^{5D}k)^2/4\pi$ to obtain top mass $\simeq v$.

M_{KK}

$$1\,\text{TeV} \lesssim M_{KK} \lesssim 3\,\text{TeV}. \tag{III.14}$$

Previous studies have focused on narrow correlated parameter sets consistent with EWPT that are within the range of such light KK states. However, we study collider phenomenology without being too much restricted a priori by these concerns, but comment on those constraints when relevant.

We choose to present results using specific choices of parameters. Four representative cases that we use are listed in Table 3.1. M_{KK} will be varied within the range above for each of the four cases. We comment that the coupling sets C and D resemble the EWPT-favored parameter space found in ref.[50, 51], and even favored by flavor physics in the shining model of ref.[48]. Coupling sets A and B have additional universality structure in LH bulk masses, and case C and D have universal RH up-type bulk masses. These additional structures are not strongly necessary, but may be useful reference points.

3.2.4 Monte Carlo pathology

We have used MadGraph/MadEvent v.4.4.42 [74] for Monte Carlo event generation. CTEQ6M PDF set [75] is used with scale choices of $\mu_R = \mu_F = \sqrt{\hat{s}}/2$, where $\hat{s}$ is the

Set A	$g_t = 4,\ g_Q = 0,\ g_b = 0$	$c_t \simeq 0.016$, $c_Q = c_b = 0.5$
Set B	$g_t = 2,\ g_Q = 0,\ g_b = 0$	$c_t \simeq 0.305$, $c_Q = c_b = 0.5$
Set C	$g_t = 0,\ g_Q = 3.5,\ g_b = 0$	$c_t = 0.5$, $c_Q \simeq 0.1,\ c_b = 0.5$
Set D	$g_t = 0,\ g_Q = 2,\ g_b = 0$	$c_t = 0.5$, $c_Q \simeq 0.305,\ c_b = 0.5$

Table 3.1: Set of parameters that we use to represent the results. Couplings are in units of g_{QCD}. Third column shows values of third family bulk masses that will give corresponding coupling strengths. The first two families are always assumed to have $c_{light} = 0.5$.

partonic center of mass energy squared. The KK gluon coupling strength is assumed to run according to the QCD beta function. NLO corrections are not included. Since a KK gluon is a broad resonance, the narrow width approximation (on-shell production and subsequent decay) is not a good approximation. For light M_{KK} MadEvent produces $5 - 20\%$ difference between cross sections from on-shell-and-decay and full matrix element computations, but a rather large difference of up to $\sim \mathcal{O}(100\%)$ for heavy KK states $M_{KK} \gtrsim 2 - 2.5\,\text{TeV}$. We have generated the full matrix elements of $t\bar{t}t\bar{t}$ and $t\bar{t}b\bar{b}$ production in MadGraph/MadEvent to take into account broad resonance effects, and we decay top quarks using BRIDGE [76]. All results are obtained for $\sqrt{s} = 14\,\text{TeV}$ LHC. We assume a luminosity $\mathcal{L} = 100\,\text{fb}^{-1}$ when a value is necessary.

Cross sections of $pp \to t\bar{t}t\bar{t}$, $t\bar{t}b\bar{b}$ via $g^{(1)}$ are plotted in Fig. 3.3. Representative cases of $g^{(1)}$ interacting only with RH top (dashed lines), and $g^{(1)}$ interacting only with LH top (solid lines) are shown. One qualitative feature that this plot shows is that cross sections in the light M_{KK} region are governed by vector self-interactions (between gluons and KK gluons). The dependence on fermion couplings is mostly in the branching ratio $Br(g^{(1)} \to t\bar{t})$. Two dashed lines (solid lines) have the same $Br(g^{(1)} \to t\bar{t}) = 100\%\,(50\%)$ [4] and thus they approach a common value in the light M_{KK} limit. However, fermion coupling dependence becomes important in the heavy M_{KK} region because vector self-interactions contribute only to pair production of $g^{(1)}$ that drops more quickly than the associated production.

---

[4] We ignore KK-gluon decays into KK-fermions because the parameter space with heavy KK-fermion is our interest.
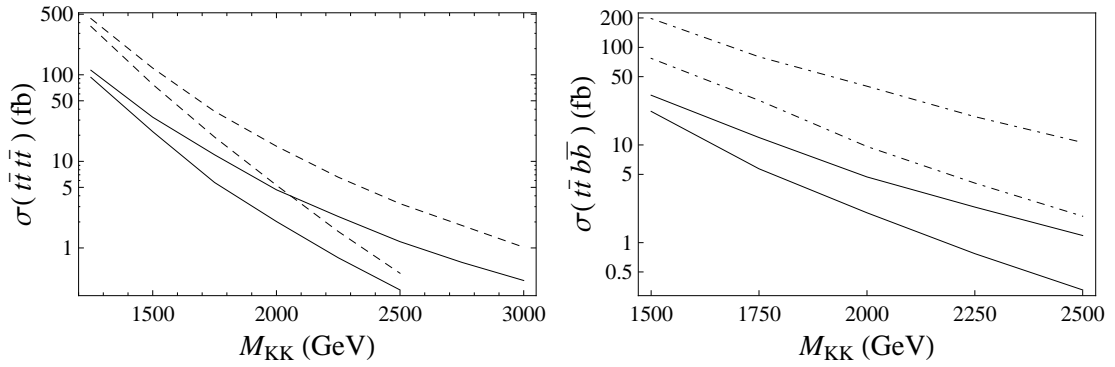
Figure 3.3: (Left): $\sigma(pp \to t\bar{t}t\bar{t})$ for coupling set A,B(dashed lines) and C,D(solid lines). (Right): $\sigma(t\bar{t}b\bar{b})$ for set C(upper dot-dashed) and set D(lower dot-dashed). Corresponding $\sigma(t\bar{t}t\bar{t})$ are also shown as solid lines for comparison. Coupling sets can be found in Table 3.1. $\sqrt{s} = 14\,\text{TeV}$ at LHC.

The other notable feature in Fig. 3.3 is the effect of the bottom coupling in $t\bar{t}t\bar{t}$ production. Bottom coupling changes the branching ratio $Br(g^{(1)} \to t\bar{t})$ which shows up in two ways: reduction of the total rate, and weaker dependence on M_{KK}. Both effects can be observed by comparing case B (lower dashed) and case D (lower solid) lines in Fig. 3.3. They have the same size of top coupling; one is LH (solid) and the other is RH (dashed). However, the LH case has a lower rate of four top due to smaller branching ratio into $t\bar{t}$. More interestingly, two lines behave differently with M_{KK}: the RH case (dashed) drops more quickly with M_{KK}. The smaller branching $Br(g^{(1)} \to t\bar{t})$ of the LH case will suppress pair production $(g^{(1)}g^{(1)} \to t\bar{t}t\bar{t})$ more relative to the associated production $(t\bar{t}g^{(1)} \to t\bar{t}t\bar{t})$. As pair production phase space quickly becomes smaller with M_{KK}, the LH case will have weaker dependence on M_{KK}.

$t\bar{t}b\bar{b}$ events are also produced if the LH top coupling is turned on (i.e. $g_Q \neq 0$). This can contribute to single lepton and opposite-sign diletpon final states. The rate is usually higher than four top production by a factor of $4 - 8$ as $b\bar{b}$ phase space is larger than $t\bar{t}$ (see Fig. 3.3). However, leptons in $t\bar{t}b\bar{b}$ generally must come from $t\bar{t}$ pair and this topology resembles that of the main SM background $t\bar{t}$. Indeed, it turns out that the majority of $t\bar{t}b\bar{b}$ events are cut out by event selections efficient for SM $t\bar{t}$ background reduction. For

the single lepton final state, the $t\bar{t}b\bar{b}$ contribution is larger than the $t\bar{t}t\bar{t}$ contributions only by a factor of $1-2$, so do not lose much discovery capability.

One concern about $t\bar{t}b\bar{b}$ is the reliability of the Monte Carlo cross section calculation. The dominant contribution to $t\bar{t}b\bar{b}$ comes from $b\bar{b}g^{(1)}$ associated production in which a large theoretical uncertainty of $b\bar{b}$ cross section may be present. Theoretical uncertainties originate from possible small scale choices, log enhanced IR contribution from collinear b production, etc. Thus this process should be studied more carefully once we can normalize the Monte Carlo simulation properly with real data. Here, we simply take minimal cuts on the $b\bar{b}$ pair to partially avoid such complications. Those are $\Delta R(b, \bar{b}) \geq 0.1$, $p_T(b) \geq 10\,\mathrm{GeV}$, $m_{b\bar{b}} \geq 10\,\mathrm{GeV}$.

We now comment on our background study.

Many dedicated studies of multi-lepton final states have been carried out in the literature. Our strategy is to use some of those available results and compare our signals with them to estimate discovery potential of the four top channel. Most background studies are aimed at heavy resonance searches as in our case. We shall see that some common features of heavy new physics enable our four top signals to beat SM backgrounds. By working with many different background studies suited for different models, we will be able to capture important qualitative features of our four top signals. We comment on some useful different features of the four top signals when it is appropriate.

Multi-lepton background results used in this paper are from several supersymmetry searches probing different parts of the parameter space [77, 78, 61], searches of exotic fermions coupling to the third generations [81, 63], search of the light Higgs in the $WH \rightarrow WWW$ channel [79, 82], and search of compositeness of top quark [57]. Among them, ref. [77, 78] are main sources that we use to analyze our results.

We do not carry out a fully detailed collider study including detector effects, optimizing

cuts, and studying fake or mis-measurement ratios. That will be done at the appropriate time by the experimental groups after understanding LHC detectors well with real data. Further optimizations of the event selection are not done here because signal cross section is already small ($\sim 10\,\mathrm{fb}$), around the upper limit of discovery reach.

3.3 Like-sign dilepton topology

Like-sign dilepton (LSDL) final states are defined as two and only two leptons (i.e., electrons or muons, but not tau leptons) with same charge accompanied by sizable missing energy. This is quite rare in the SM, which makes it one of the most promising signals of four top quark production when the goal is restricted to the first stage of just determining if there is beyond the SM processes at work in the data. We shall describe the background contributions and estimate the prospects of detecting the beyond the SM signal.

3.3.1 Comparison with background studies from supersymmetry searches

Following ref. [77], we employ the cuts:

- LSDL event selection set # 1:

  1. <u>only LSDL</u> with $p_T \geq 20\,\mathrm{GeV}$, $|\eta| \leq 2.5$, $\Delta R_{lj} \geq 0.3$

  2. <u>at least two jets</u> with $p_T \geq E_T^c$, $|\eta| \leq 3.0$, no b tagging

  3. $E_T^{miss} \geq E_T^c$

These cuts are optimized for supersymmetry searches, but we find them reasonably well optimized for the four top signatures we have in mind here. E_T^c is a useful variable that is to be varied to see the discovery reach because new physics contributions are likely to be higher p_T than SM backgrounds. Leptons are from long decay chains, and thus mild p_T cuts are used. Note that $\Delta R_{lj} \geq 0.3$ is not the standard isolation cut ($\Delta R_{lj} \geq 0.4$) that is used commonly now by ATLAS, CMS groups (e.g. see ref.[78]). This will slightly overestimate

the potential of LSDL observable as can be deduced from Table 3.8. Also, $|\eta_j| \leq 3.0$ is not likely to be the standard choice (2.5), but this modification is very insignificant since high p_T objects are generally very central.

Cross section results of signal and background (from ref. [77]) are shown in Fig. 3.4. The 5σ discovery reach of the cross section is also shown in the right panel by using

$$\frac{S}{\sqrt{B}} = \frac{\mathcal{L} \cdot \sigma_{signal}}{\sqrt{\mathcal{L} \cdot \sigma_{bkgd}}} \geq 5 \tag{III.15}$$

where the luminosity $\mathcal{L} = 100\,\mathrm{fb}^{-1}$ is assumed.

For the strong coupling case A, $M_{KK} \simeq 2200\,\mathrm{GeV}$ can be probed with optimized choice of $E_T^c \simeq 250 - 350\,\mathrm{GeV}$ while $M_{KK} \lesssim 1700\,\mathrm{GeV}$ is accessible for the weaker coupling cases B and C. Since the background drops more quickly than signal with E_T^c, discovery reach with lower E_T^c value is smaller. For higher values of E_T^c, the issue is then small number of signal events rather than suppressing background. If we require having at least 10 signal events (equivalent to $\sigma_{signal} = 0.1$ fb after cuts) to claim evidence of new physics, $E_T^c \gtrsim 300 - 350\,\mathrm{GeV}$ should not be taken for heavy $M_{KK} \sim 1.7 - 2\,\mathrm{TeV}$. However, a simple ratio of signal and background $\sigma_{signal}/\sigma_{bkgd}$ increases even for very high $E_T^c \gtrsim 350\,\mathrm{GeV}$ for all cases (see the left panel).

In the LSDL channel, either lepton must come from a $g^{(1)}$'s daughter top. This top is likely to be boosted, and its lepton is less likely to be isolated from jetty activities. We study this lepton-jet collimation issue in detail in section 3.5.2.

3.3.2 Comparison with other LSDL studies

We compare our signal with several other background studies suited for different models. Two are from gluino pair production [78, 61], one from four-top composite operator [57], and the other from pair production of heavy exotic quarks decaying to tW [63]. Kinematic cuts are varied between those references, and they seem to consider somewhat different
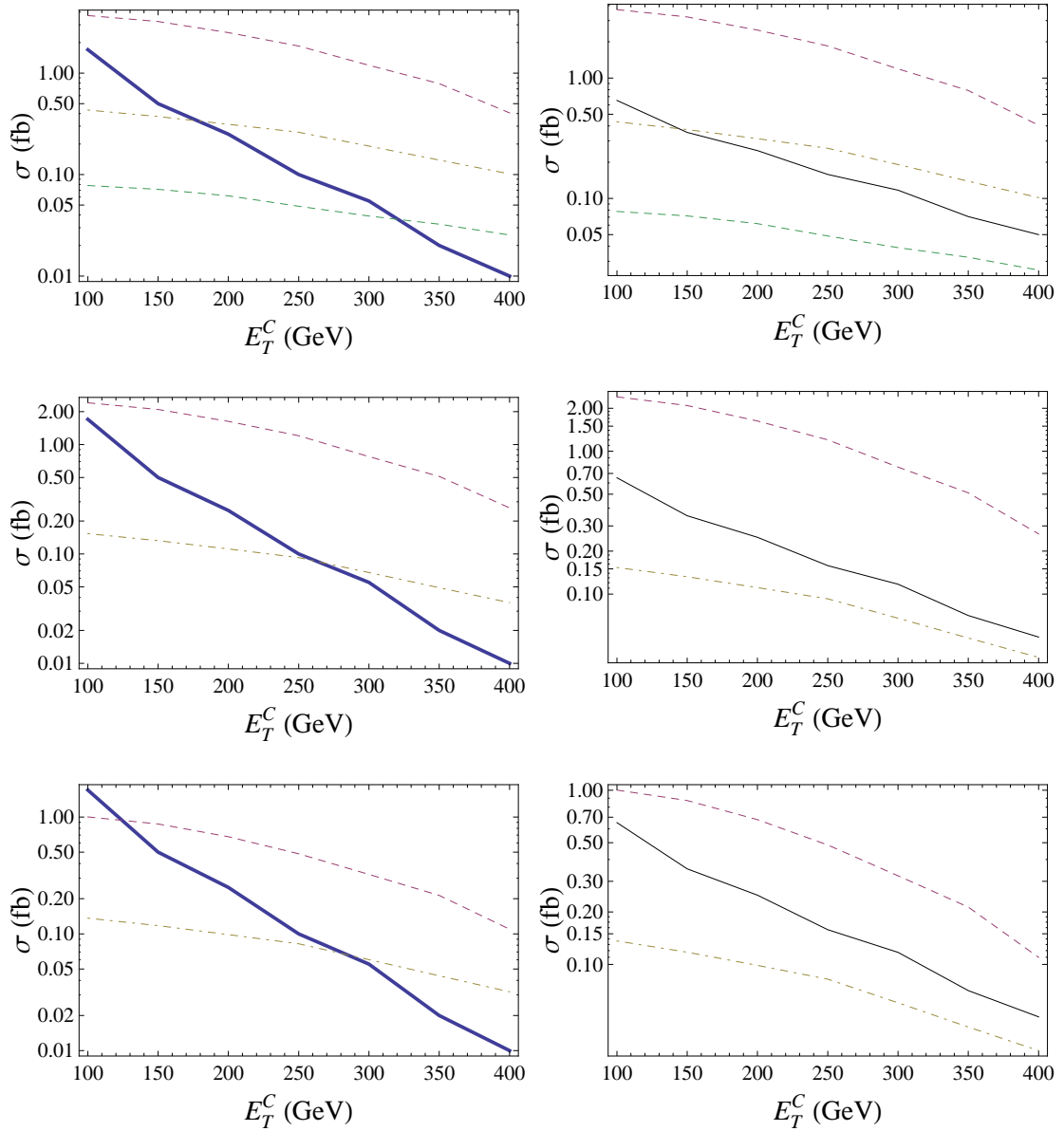
Figure 3.4: LSDL results for case A,B,C from top to bottom. (Left): LSDL cross sections after LSDL #1 cuts. Background (thick solid) from ref.[77] and signal for $M_{KK} = 2000\,\mathrm{GeV}$ (dot-dashed), 1500, 2500 GeV (dashed). (Right): Same plot as the left panel, but the corresponding 5σ reach with $100\,\mathrm{fb}^{-1}$ of data is shown as a solid line.

M_{KK} (GeV)	1000	1500	2000	2500	3000
efficiency of LSDL #2 cuts	4.3 %	2.8 %	2.3 %	1.9 %	1.3 %
$\sigma(t\bar{t}t\bar{t})_A \cdot$ efficiency (fb)	~ 90	~ 2.5	~ 0.3	~ 0.06	~ 0.01

Table 3.2: LSDL results. Efficiencies (including branching ratios) under cuts #2, and signal cross sections after cuts for case A is also shown.

sets of background processes. However, final backgrounds after cuts are all about $3 - 7\,\text{fb}$.

So we simply compare our signal cross sections with this value of background cross section.

We impose the following kinematic cuts that resemble the strongest set of cuts among

the references listed above:

- LSDL event selection set # 2:

    1. jet: leading $p_T \geq 100\,\text{GeV}$, $p_T \geq 80\,\text{GeV}$, $|\eta| \leq 5$, and $n_j \geq 4$, no b-tagging.

    2. only LSDL lepton: leading $p_T \geq 50\,\text{GeV}$, $p_T \geq 25\,\text{GeV}$, $|\eta| \leq 2.5$, $\Delta R_{lj} \geq 0.4$

    3. $E_T^{miss} \geq 20\,\text{GeV}$.

Note that multi-jet requirement may underestimate our signal sample because our sample

does not take into account initial/final state radiations. We have tried to vary number

of jet requirement and checked that selection efficiency changes by a factor of ~ 2 within

$n_j \geq 3 - 5$.

Event selection efficiency for several values of M_{KK} are given in Table 3.2. Four-top

cross sections multiplied by efficiency and branching ratios are also shown. Given the

background cross sections of about $3 - 7\,\text{fb}$, $100\,\text{fb}^{-1}$ of data can achieve 5σ significance

if the signal cross section after cuts is greater than about $0.9 - 1.3\,\text{fb}$. So it is likely that

$M_{KK} \lesssim 1600\,\text{GeV}$ for coupling set A can be probed with event selection #2 using much

milder p_T cuts than #1.

3.4 Single lepton final states

The single-lepton observable ($1l$ + high p_T jets + E_T^{miss}) is studied in this section. Later in the section, we briefly study multi b-tagging method, instead of requiring high p_T objects which seems to be more suited for supersymmery searches.

3.4.1 Discovery potential

Following ref. [77] we use following cuts:

- Single lepton event selection #1:

    1. <u>only one lepton</u> with $p_T \geq 20\,\text{GeV}$, $\Delta R_{lj} \geq 0.3$, $|\eta| \leq 2.5$

    2. <u>at least two jets</u> with $p_T \geq E_T^c$, $|\eta| \leq 3.0$

    3. $E_T^{miss} \geq E_T^c$, $M_T(l, E_T^{miss}) \geq 100\,\text{GeV}$

where the transverse mass M_T is defined using transverse four-vectors of a lepton p_T^l and transverse missing energy p_T^{miss} (treated as a light-like four vector pointing perpendicular to the beam axis). It is defined as

$$M_T^2(l, E_T^{miss}) \,=\, 2(E_T^l E_T^{miss} - p_T^l \cdot p_T^{miss}). \tag{III.16}$$

Transverse mass will be around the W boson mass if the lepton and missing energy are from a single W boson, hence effectively suppressing SM backgrounds with missing energy from $W \to l\nu$. This will also suppress the contribution from KK gluon mediated $b\bar{b}t\bar{t}$ since leptons generally must come from $t\bar{t}$ as discussed in section 3.2.4.

We comment that if we modify the old lepton isolation criteria used here to the more standard one (i.e. $\Delta R_{lj} \geq 0.3 \to 0.4$), event selection efficiency is not necessarily reduced. This is simply because many multi-lepton events ($n_l \geq 2$) will now have higher chances to contribute to the single lepton event samples with tighter lepton isolation. Refer to section 3.5.2 for discussions regarding lepton isolation and lepton-jet collimation issues.

This modification brings only about a $\mathcal{O}(0.1)\%$ efficiency change. Also, the modification $|\eta_j| \le 3.0 \to 2.5$ introduces negligible changes.

Cross section results are shown in Fig. 3.5. The strong coupling case A can be probed up to $M_{KK} \simeq 2000\,\mathrm{GeV}$ with $E_T^c \gtrsim 350\,\mathrm{GeV}$ while case B has lower discovery reach of about $M_{KK} \lesssim 1700\,\mathrm{GeV}$. Case C can reach $M_{KK} \simeq 1950\,\mathrm{GeV}$ with $E_T^c \gtrsim 350\,\mathrm{GeV}$, which is better than what can be obtained in case B. On the other hand, in the like-sign dilepton and trilepton searches, case C has a lower discovery reach than case B (see Fig. 3.4 and 3.6). This better discovery potential of case C here is due to the larger contributions from $t\bar{t}b\bar{b}$ that only exists for case C and D. By the same reason, we will see that case C has the highest discovery potential in the single lepton channel while case A and B typically do not.

It is interesting to compare the above results of cut #1 with results obtained by very similar cuts used by the ATLAS Supersymmetry group (p.1597 of ref.[78]). Those new sets of cuts are

- Single lepton event selection set #2:

    1. only one lepton with $p_T \ge 20\,\mathrm{GeV}$, $\Delta R_{lj} \ge 0.4$, $|\eta| \le 2.5$

    2. no additional leptons with $p_T \ge 10\,\mathrm{GeV}$

    3. at least 4 jets with $p_T \ge 50\,\mathrm{GeV}$, and leading $p_T \ge 100\,\mathrm{GeV}$. $|\eta| \le 2.5$

    4. $E_T^{miss} \ge max(100\,\mathrm{GeV}, 0.2H_T)$. For heavy resonances, always $0.2H_T > 100\,\mathrm{GeV}$.

    5. $M_T(l, E_T^{miss}) \ge 100\,\mathrm{GeV}$, $H_T \ge 800\,\mathrm{GeV}$, $S_T \ge 0.2$

Cross section results are shown in the Table 3.3. The 5σ discovery reach of cuts #2 is $\sigma(t\bar{t}t\bar{t}) \cdot eff \gtrsim 3.2$ fb [78] that is interpreted as $M_{KK} \lesssim 1600\,\mathrm{GeV}$ for set A from the Table 3.3. This is a lower reach than what can be obtained using cuts #1.
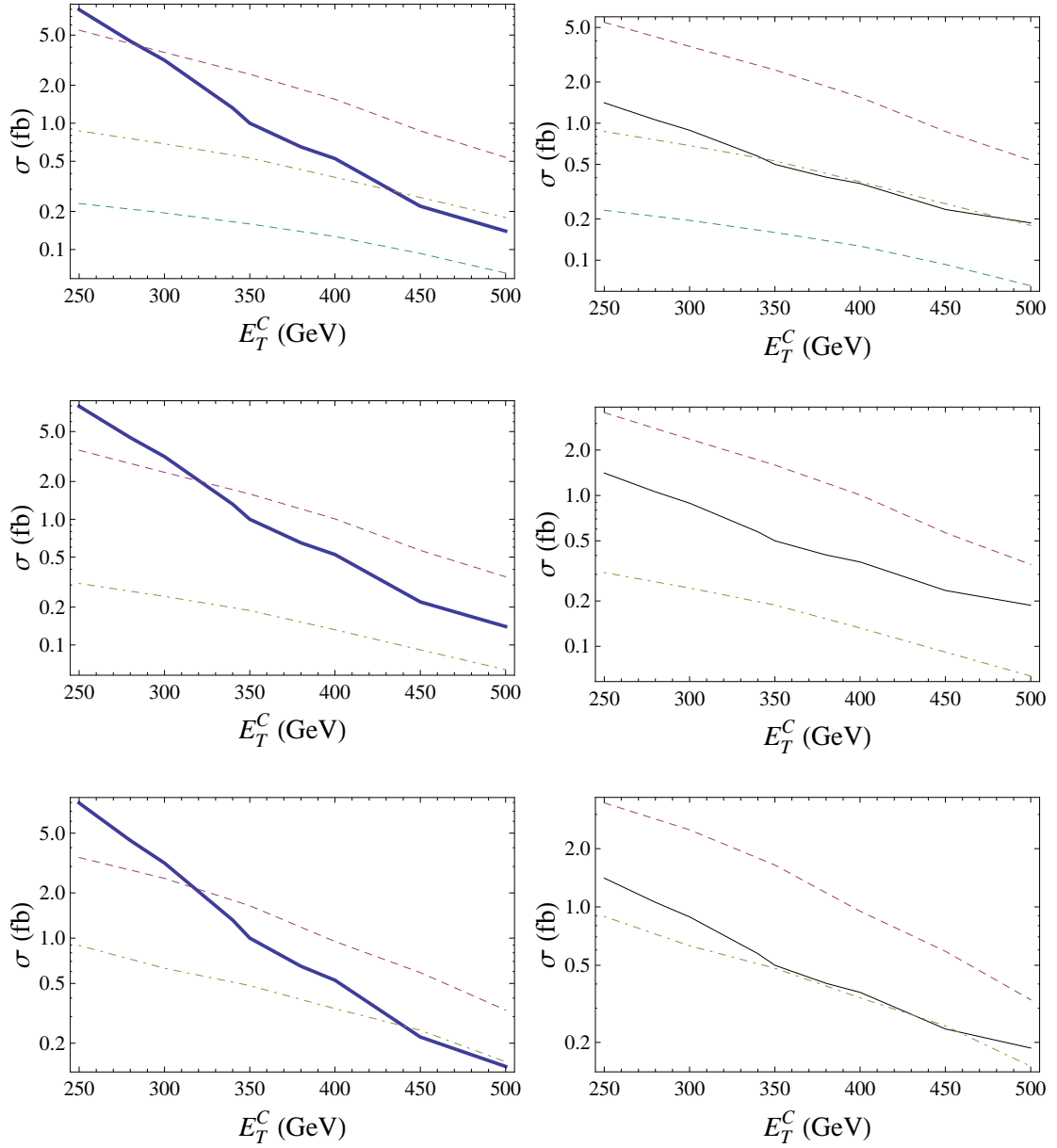
Figure 3.5: Single lepton results for case A,B,C from top. (Left) Single lepton cross sections after cut #1. Background (thick solid) from ref.[77] and $M_{KK} = 2000\,\text{GeV}$ (dot-dashed), 1500, 2500 GeV (dashed). (Right) Same plot as the left panel, but the 5σ reach with $100\,\text{fb}^{-1}$ of data is shown as a solid line.

M_{KK} (GeV)	1000	1500	2000	2500	3000
efficiency of single lepton #2 cuts	3.1 %	3.6 %	3.9 %	4.5 %	5.2 %
$\sigma(t\bar{t}t\bar{t})_A \cdot$ efficiency (fb)	68	4.3	0.58	0.15	~ 0.05

Table 3.3: Single lepton results. Efficiencies(including branching ratios) of event selection #2, and case A signal cross sections after cuts are shown.

Cuts #2 resemble cuts #1 in the sense that high E_T^{miss} and M_T cuts are used to suppress backgrounds. However, the high p_T jet requirement ($p_T \gtrsim 350\,\mathrm{GeV}$) in set #1 is replaced by high multiplicity jet topology ($n_{jet} \geq 4$) in set #2, and the former wins in our case. High p_T objects are very useful probes of new physics beyond the SM as usually expected.

3.4.2 Three b-tagging method

In the discussion above we have found to be true the expected qualitative result that utilizing high p_T jets is very useful in the search of new physics. Four top events in RS models is no except, and we can take advantage of high p_T cuts on jets and missing energy just like in supersymmetry as we saw in the previous section. However, RS four top events have qualitative differences from supersymmetry events.

RS four top events via KK-gluons have generically smaller missing energy than supersymmetry events. Cascade decays of supersymmetry particles typically end up with energetic neutrinos from heavy particle decays and/or heavy LSPs. These give rise to large missing energy. RS also predicts heavy particles decaying to neutrinos (e.g. KK excited W boson). However, decay chains of KK particles in our scenario quickly ends up only with SM particles, thus the majority of neutrinos are from W boson decay, with ultimately somewhat softer missing energy spectrum. Moreover, most leptons in RS four-top events are from W boson decays (not from heavy particle decays such as gauginos). Although the W bosons could be boosted somewhat by being daughter particles of heavier KK state production, the M_T between a lepton and missing energy will nevertheless be more likely to be around the W boson mass than in the supersymmetry case.

Given these observations, we study an alternative single lepton observable. We impose rather milder cuts of E_T^{miss} and M_T, and additionally a three b-tagging requirement (to suppress backgrounds):

$$1l + \geq 3 \text{ b-tagged jets} + \text{mild } p_T \text{ jets}, \ E_T^{miss} \qquad \text{(III.17)}$$

The simultaneous existence of a single isolated lepton and three b-jets are rare in the SM. We comment that a b-tagged jet does not have to be in reality a b-jets, but can also be a (boosted) top-jet which can increase discriminating power. Similar observable has indeed been used to search supersymmetry in ref.[80] based on the default ATLAS b-tagging algorithm (suited for non-boosted b-jets), and it has resulted in SM background of $\mathcal{O}(100)$fb which might still be too large for our four-top signal [80]. We use following event selections of the alternative observable

- Single lepton event selection cuts #3:

  1. Definitions of jet, lepton from cuts 1,2,3 of event selection #2.

  2. At least 3 b-tagged jets, and b-tagging efficiency ϵ_b will be varied.

  3. $E_T^{miss} \geq 100\,\text{GeV}$, No M_T cuts, $H_T \geq 1000\,\text{GeV}$.

Optimization of this alternative observable using three b-taggings, and consequent comparison with the previous results using high p_T objects shown in Fig. 3.5 are interesting, but will be a future project. High cuts on H_T, scalar sum of p_T of all objects in the event, is almost harmless for signal [57, 84].

Major backgrounds are categorized in Table 3.4. Category (a) have ≥ 1 lepton + no b-jets, category (b) have ≥ 1 lepton + 2 b-jets, and category (c) are none of these. Due to small number of b-jets in category (a), highly efficient b-tagging of rejection about $\sim 200 - 400$ can suppress backgrounds (a) below ~ 0.1 fb (where 10 events are obtained with $100\,\text{fb}^{-1}$) with a reasonable value of event selection efficiency times branching ratio

	Backgrounds	Cross sections
(a)	$W/Z+$ jets, $WZ+$ jets	$\sigma \simeq 8 \times 10^7$ fb with $p_T(j) \geq 10\,\text{GeV}$
(b)	$t\bar{t}+$ jets, $W/Z + b\bar{b}$	$\sigma \simeq 9 \times 10^5$ fb
(c)	$b\bar{b}$, $t\bar{t}b\bar{b}$	$\sigma(b\bar{b}) \simeq 2 \times 10^8$ fb with $p_T(b) \geq 40\,\text{GeV}$

Table 3.4: Categorization of major backgrounds to single lepton observable in eq.(III.17). Background numbers are taken from ref.[79] (see also refs.[80, 81]).

$\sim \mathcal{O}(1\%)$. To suppress (b), which already have several true b-jets, one may need to require a certain number of *boosted* objects (e.g. top) because b-jets from SM top quarks may resemble QCD background jet characteristics more than a boosted object. If a boosted jet-tagging algorithm can obtain a powerful rejection factor of $\sim 200 - 700$ and if tagging of two boosted objects is required, category (b) can be negligible. For $b\bar{b}$ in (c), by assuming jet-lepton faking rate of $\sim 10^{-4} - 10^{-5}$ and the probability of isolated leptons from leptonic decay of a b-jet about $\sim 10^{-5}$ (e.g., see ref.[78, 79]), expected additional rejection (from lack of three b taggings) of greater than ~ 100 is enough to get rid of $b\bar{b}$ backgrounds. The small cross section $\sim 1\,\text{pb}$ of SM $t\bar{t}b\bar{b}$ may render this background negligible even though its event topology resembles some of our signal. We note that such a highly efficient (boosted) jet-tagging algorithm desired has been discussed in ref.[83] in the context of boosted leptonic top tagging. Rather than estimating these backgrounds more accurately, which are subject to large uncertainties (fakes, mis-measurements, etc.), we simply study the discovery reach as a function of b-tagging efficiency ϵ_b with our reasonably assumed small backgrounds of $\lesssim 0.1\,\text{fb}$.

Results are shown in Table 3.5 for several values of b-tagging efficiency ϵ_b. With our given estimate of backgrounds, which may be optimistic compared to what a full experimental study would conclude, discovery reach is quite high around $3\,\text{TeV}$. Given that this may be one of the best signatures, it would be interesting for experiments to carry out a full simulation to compute precisely the rejection factor from lepton isolation and also the true b-tagging efficiency for $M_{KK} \gtrsim 2\,\text{TeV}$.

Single lepton	$\epsilon_b = 40\%$	$\epsilon_b = 50\%$	$\epsilon_b = 60\%$	$\epsilon_b = 100\%$
$M_{KK} = 1500$ GeV	2.7% (1.4%)	4.8 (2.5)	7.5 (3.9)	20.3 (11.3)
2000 GeV	2.6 (1.3)	4.7 (2.3)	7.3 (3.7)	19.9 (11.5)
2500 GeV	2.5 (1.0)	4.4 (1.8)	6.9 (2.9)	18.9 (8.8)
3000 GeV	2.4 (0.8)	4.3 (1.5)	6.8 (2.4)	18.8 (7.5)
10 signal A events	2400 GeV	2600	2800	~ 3200
10 signal C events	2500 GeV	2700	2900	~ 3200

Table 3.5: Efficiencies with single lepton selection #3 utilizing three b-tagging. b-tagging efficiency ϵ_b is varied. Results of $t\bar{t}t\bar{t}$ ($t\bar{t}b\bar{b}$) event samples are shown, respectively. Maximum M_{KK} giving rise to 10 signal events at $\mathcal{L} = 100\,\text{fb}^{-1}$ is also shown for points A and C.

3.5 Trilepton search

The trilepton observable is three charged leptons of any charges plus either E_T^{miss} or high p_T jets. All events have either $(+ + -)$ or $(- - +)$ charge combinations in our case since the total charge of two colliding partons do not exceed ± 1. We include both charge combinations.

3.5.1 Discovery potential

First, we use cuts in ref.[77], which were originally employed to reduce backgrounds for supersymmetry searches:

- Tri-lepton event selection set #1:

  1. Only 3 leptons with $p_T \geq 20\,\text{GeV}$, $|\eta| \leq 2.5$, $\Delta R_{lj} \geq 0.3$

  2. At least 2 jets with $p_T \geq E_T^c$, $|\eta| \leq 3.0$, no b-tagging

  3. $E_T^{miss} \geq E_T^c$

The cross section result as a function of E_T^c is shown in Fig. 3.6. Heavy resonance searches in the trilepton channel suffer from the small branching ratio into three leptons. For 2-TeV resonance, the cross section is well below ~ 0.1fb (which gives 10 number of signal events) in most of parameter space. For case B and C, $M_{KK} \simeq 1600 - 1700\,\text{GeV}$ is within reach with a mild $E_T^c \simeq 150 - 200\,\text{GeV}$ cut. However, $E_T^c \simeq 200 - 250\,\text{GeV}$ can probe strong

M_{KK}	1000 GeV	1500 GeV	2000 GeV	2500 GeV	3000 GeV
efficiency of cut #2	1.66 %	1.11 %	0.75 %	0.65 %	0.47 %
$\sigma(t\bar{t}t\bar{t})_A \cdot$ eff	36 fb	1.2 fb	0.08 fb	0.01 fb	0.001 fb

Table 3.6: Tri-lepton results with trilepton cut #2. Case A signal cross section is shown.

coupling case A still up to about $M_{KK} \simeq 1900 \, \text{GeV}$.

Second, we consider more relaxed event selections following an ATLAS report (see page 1603 of ref. [78]).

- Tri-lepton event selection set #2:

  1. <u>At least</u> 3 leptons with $p_T \geq 10 \, \text{GeV}$, $|\eta| \leq 2.5$, $\Delta R_{lj} \geq 0.4$

  2. <u>At least</u> 1 jet with $p_T \geq 200 \, \text{GeV}$, $|\eta| \leq 2.5$, no b-tagging.

  3. <u>No</u> E_T^{miss} cuts

After cuts, $\sigma(t\bar{t}) \simeq 11 \, \text{fb}$ and $\sigma(ZW) \simeq 1 \, \text{fb}$ remain dominant backgrounds. The signal cross section of 1.7 fb is required after cuts for 5σ discovery with $100 \, \text{fb}^{-1}$ of data. Signal efficiencies are given in the Table 3.6. 5σ discovery is possible for $M_{KK} \lesssim 1450 \, \text{GeV}$, which is lower than what can be obtained using the set #1 cuts above.

ref. [78] (pages 1604-1605) has studied another set of cuts using E_T^{miss} but without any jet requirements. This might be more efficient for some supersymmetry scenarios. However, a large background of $\sim 70 \, \text{fb}$ remains. Due to the small four-top cross sections, this approach is not suitable for us.

3.5.2 Identification of boosted leptonic top quark

Some leptons come from a top quark which is a daughter of $g^{(1)}$. This $g^{(1)}$'s daughter top quark is likely to be boosted with high $p_T \sim M_{KK}/2 \sim 1 \, \text{TeV}$, and its decay products are likely to be collimated. In the detector, a lepton is typically well-defined when it is well isolated from jetty activities (e.g., see ref.[78]). So many leptons might be lost. In this section, we study how serious the lepton-jet collimation issue is in our multi-lepton
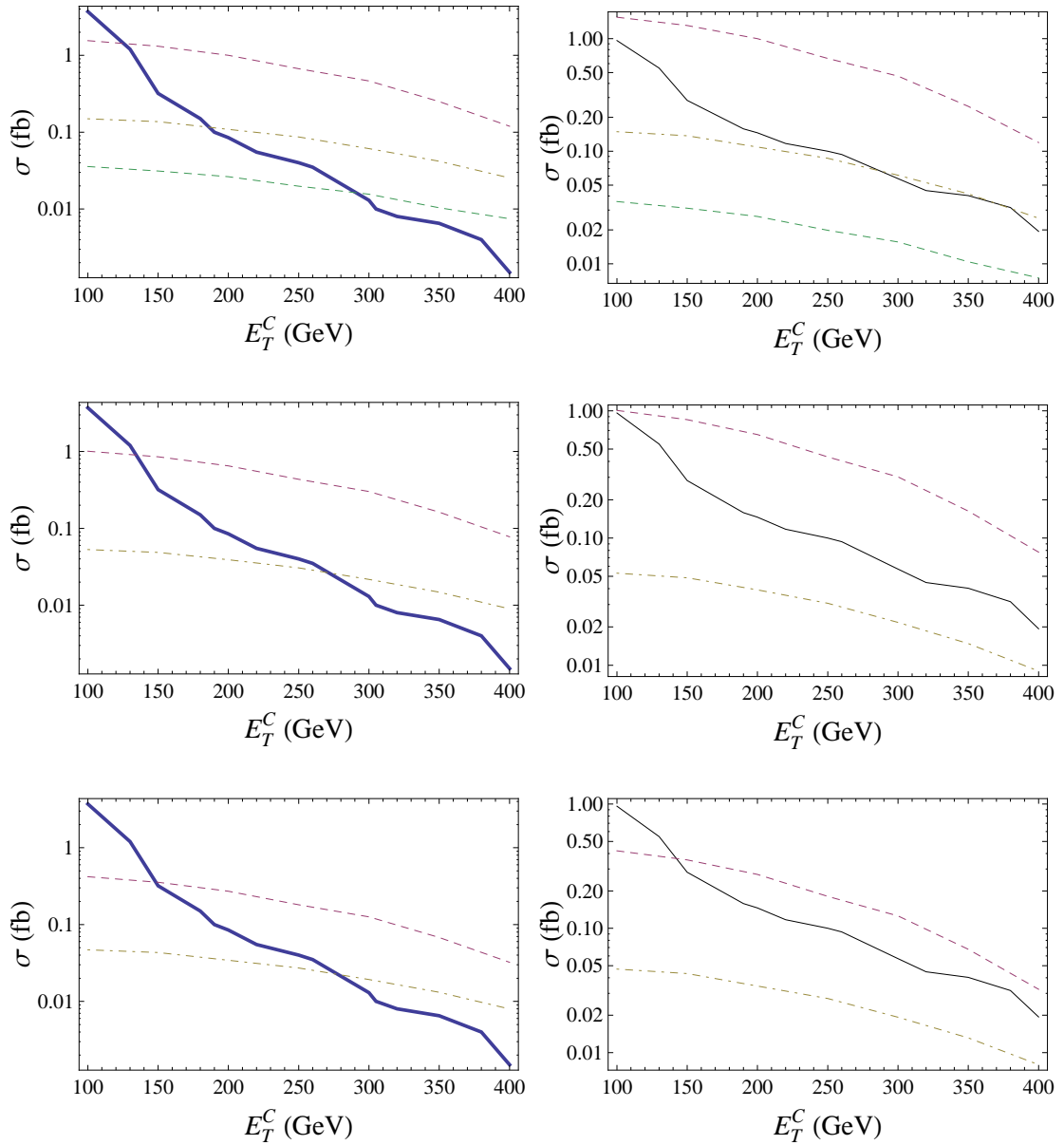
Figure 3.6: Tri-lepton results for case A,B,C from top to bottom. (Left) Tri-lepton cross sections after Tri-lepton cuts #1. Background (thick solid) from ref.[77] and $M_{KK} = 2000\,\mathrm{GeV}$ (dot-dashed), 1500, 2500 GeV (dashed). (Right) Same plot as the left panel, but the 5σ reach with $100\,\mathrm{fb}^{-1}$ of data is shown as a solid line.

LSDL	$E_T^c = 100\,\mathrm{GeV}$	300 GeV
$M_{KK} = 1500\,\mathrm{GeV}$	$2.3\% \to 3.7\%$	$0.75\% \to 1.3\%$
$M_{KK} = 2000\,\mathrm{GeV}$	$2.0\% \to 3.7\%$	$0.85\% \to 1.7\%$
$M_{KK} = 2500\,\mathrm{GeV}$	$1.7\% \to 3.5\%$	$0.79\% \to 1.8\%$
trilepton	$E_T^c = 100\,\mathrm{GeV}$	300 GeV
$M_{KK} = 1500\,\mathrm{GeV}$	$0.81\% \to 1.8\%$	$0.21\% \to 0.59\%$
$M_{KK} = 2000\,\mathrm{GeV}$	$0.51\% \to 1.7\%$	$0.15\% \to 0.72\%$
$M_{KK} = 2500\,\mathrm{GeV}$	$0.52\% \to 1.8\%$	$0.19\% \to 0.89\%$

Table 3.7: Efficiency changes by $\Delta R_{lj} \geq 0.4 \to 0.2$ to see lepton-jet collimation. LSDL, trilepton event selection #1's are used, respectively.

observables, and discuss possible improvements based on leptonic top tagging. Since the single lepton channel has a quantitatively different answer, we discuss them separately at the end of the section.

First, we compute how much leptons overlap with some jets in the LSDL and trilepton final states. Table 3.7 shows how event selection efficiency changes when lepton isolation criteria is loosened $\Delta R_{lj} \geq 0.4 \to 0.2$ (with event selection #1's). We see that in many LSDL events and the majority of trilepton events there are non-isolated leptons with the standard isolation criteria. Moreover, collimation becomes more important for a heavier resonance as its daughter top will be more boosted.

Second, we estimate how much lepton-jet collimation is really due to boosted top quark decays (not by random overlapping). If it is, lepton will be collimated with the b-jet from the same top quark (without parton showering). Table 3.8 shows the change of efficiency when such a lepton is also counted as an isolated lepton. If a boosted leptonic top can be efficiently identified, we can count such a leptonic top as an isolated lepton. ref. [83] has recently discussed such efficient leptonic top tagging where tagging efficiency of $\sim 80\%$ is obtained with a rejection $\sim 10^3 - 10^4$.

Results with standard isolation $\Delta R_{lj} \geq 0.4$ is shown in Table 3.8 to see the importance of the collimation problem in the future measurements based on such standard isolation criteria. Efficient id of leptonic top can then enhance the trilepton signal events by a large

LSDL	$E_T^c = 100\,\mathrm{GeV}$	300 GeV
$M_{KK} = 1500\,\mathrm{GeV}$	$2.3\%(3.1) \to 3.5\%$	$0.75\%(1.0) \to 1.2\%$
$M_{KK} = 2000\,\mathrm{GeV}$	$2.0\%(2.9) \to 3.9\%$	$0.85\%(1.3) \to 1.9\%$
$M_{KK} = 2500\,\mathrm{GeV}$	$1.7\%(2.4) \to 3.8\%$	$0.79\%(1.3) \to 2.1\%$
trilepton	$E_T^c = 100\,\mathrm{GeV}$	300 GeV
$M_{KK} = 1500\,\mathrm{GeV}$	$0.81\%(1.3) \to 1.8\%$	$0.21\%(0.39) \to 0.65\%$
$M_{KK} = 2000\,\mathrm{GeV}$	$0.51\%(1.0) \to 1.9\%$	$0.15\%(0.41) \to 0.93\%$
$M_{KK} = 2500\,\mathrm{GeV}$	$0.52\%(1.1) \to 2.2\%$	$0.19\%(0.48) \to 1.1\%$

Table 3.8: Efficiency changes by leptonic top quark id (refer to text) to see lepton-b collimation inside a top jet. $\Delta R_{lj} \geq 0.4(0.3)$ with event selection #1's are used. Final efficiency is almost the same for both lepton isolations.

factor of $2.5 - 6$, and the LSDL signal by about $1.5 - 2.5$ with standard $\Delta R_{lj} \geq 0.4$. Leptonic top id will be more useful for heavier $g^{(1)}$ with higher E_T^c as can be seen by the higher rate of increase in the table. It is clearly because collimation is due to high p_T boosted objects; the heavier $g^{(1)}$, the more boosted top, and high E_T^c makes us focus more on such high p_T objects. In addition, signal-to-background ratio is smaller with higher E_T^c (see Fig. 3.4 and Fig. 3.6). By comparing $\Delta R_{lj} \geq 0.3$ values in Table 3.8 with Fig. 3.4 and 3.6 (recall that event selection #1's use this lepton isolation), we estimate that 5σ reach can be extended by about $100 - 200\,\mathrm{GeV}$. By comparing Tables 3.7 and 3.8, we also see that most lepton-jet collimation happens inside a leptonic top jet. Given this potential improvements, it would be interesting to do more detailed study of id of boosted leptonic objects.

The single lepton observable, on the other hand, would not take advantage of leptonic top tagging. From Table 3.9, we see that single lepton event samples become rather smaller with the looser lepton isolation condition $\Delta R_{lj} \geq 0.4 \to 0.2$, or with efficient leptonic top tagging shown in the last column (in the last column, as we did before, we include lepton if it is collimated with the b-jet from the same top quark). This is because many single lepton events are actually contributed from multi-lepton events ($n_l \geq 2$) by losing some of their leptons. So including more leptons would take these contributions out of the single

Single lepton $M_{KK} = 2\,\text{TeV}$	$\Delta R_{lj} \geq 0.4 \rightarrow 0.2$	$\Delta R_{lj} \geq 0.4 \rightarrow 0.6$	lepton-b jet inclusion
$E_T^c = 200\,\text{GeV}$	$7.04\% \rightarrow 6.56\%$	$7.04\% \rightarrow 6.02\%$	$7.04\% \rightarrow 5.82\%$
$E_T^c = 400\,\text{GeV}$	$2.43\% \rightarrow 2.39\%$	$2.43\% \rightarrow 2.01\%$	$2.43\% \rightarrow 2.04\%$

Table 3.9: Efficiency changes due to several modifications described in the first row for two choices of E_T^c. Single lepton event selection #1 is used with $M_{KK} = 2000\,\text{GeV}$ to produce this table.

lepton sample pool. Given this observation, we try to tighten the lepton isolation criteria $\Delta R_{lj} \geq 0.4 \rightarrow 0.6$ to see if we can have larger single lepton samples. The answer is no as shown in Table 3.9. Thus, we find that the standard lepton isolation criteria is suited for the single lepton observable that we employ.

3.6 When is the quadruple top production most important?

We discuss other possible collider signatures in the present model. One type of signature is based on the prospect that $g^{(1)}$ couplings to light quarks might be somehow induced. Also, there are many other KK particles that can be very light or can interact with light fermions. Our goal is to describe the parameter space where the four top production is the most important.

3.6.1 Light quark couplings to $g^{(1)}$

The standard search channel $q\bar{q} \rightarrow g^{(1)} \rightarrow t\bar{t}$ at the LHC will be dominant over four top production even for small light quark couplings. How close should c_{light} be to 0.5 to suppress the standard channel enough? It is usually claimed that $M_{KK} \lesssim 4 - 5\,\text{TeV}$ with $g_{light}^{old} \simeq 0.2 g_{QCD}$ can be accessible around the resonance $m_{t\bar{t}} \simeq M_{KK} \pm \Gamma_{KK}$ [85]. The $t\bar{t}$ production ratio of a 2-TeV and 5-TeV $g^{(1)}$ is approximately $\sigma_{S2}/\sigma_{S5} \simeq 100 - 200$ with similar signal to background ratios $S_2/B_2 \sim S_5/B_5$ after signal kinematic cuts (with hard jet cuts or mildly efficient top-tagging rejecting QCD dijet by a factor of ~ 10) [85]. We find the required suppression factor $\epsilon = (g_{light}^{our}/g_{light}^{old})^2$ (g_{light}^{our} is our smaller couplings) of

the 2-TeV cross section to have statistical significance similar to that of 5-TeV signal is

$$\frac{(\epsilon\sigma_{S2})\,\mathcal{L}}{\sqrt{\sigma_{B2}\mathcal{L}}} \simeq \frac{\sigma_{S5}\mathcal{L}}{\sqrt{\sigma_{B5}\mathcal{L}}}. \tag{III.18}$$

Using signal to background ratios quoted above, we obtain

$$\epsilon\sqrt{\sigma_{S2}\mathcal{L}} \simeq \sqrt{\sigma_{S5}\mathcal{L}} \tag{III.19}$$

which gives

$$\epsilon \simeq \sqrt{\frac{\sigma_{S5}}{\sigma_{S2}}} \sim \frac{1}{10} - \frac{1}{20}. \tag{III.20}$$

Thus $g_{light}^{our} \lesssim 0.04 - 0.06 g_{QCD}$ will suppress the 2-TeV $g^{(1)}$ signal in the $t\bar{t}$ channel below the discovery reach. Thus, from Fig. 3.1, $0.49 \lesssim c_{light} \lesssim 0.51$ is the region where the four-top production is the primary (at least useful complimentary) channel of the RS discovery, which is our region of interest.

Another source of light quark couplings is through the mixing of gauge eigenstates. CKM matrix elements between the third and the first two generations are nonzero. From the above estimation of the range $g_{light} \lesssim 0.04 - 0.06 g_{QCD}$ with typical coupling strength of third generation $g_{top} \sim \mathcal{O}(1)g_{QCD}$, the mixture of third generation in the first generation should be of $\lesssim \mathcal{O}(1)\%$ which is fine with small CKM element $V_{td} \sim \mathcal{O}(0.001)$ although precise numbers might be model dependent.

Higher order corrections exist. The effective interaction vertex of $g - g - g^{(1)}$ can be induced by strongly coupled top quark loop. As the theory is chiral, an anomaly cancellation mechanism should be specified to estimate the finite triangle loop contribution. This has been estimated to be negligible with Chern-Simons term [56]. Another effect of loop corrections to bulk masses of a few percent may exist [86]. This correction may be quite small, but if it is larger than the characteristic range of c that we need for four top production, it merely shifts the original value of c_{light} such that after corrections the tuned value is near $c_{light} = 0.5$.

3.6.2 Targeting other KK particles

Successful custodial protection of the T parameter and $Zb_L\bar{b}_L$ coupling is based on the custodial symmetries $SU(2)_R \times P_{LR}$. Extra KK gauge bosons therefore exist. Also, SM particles should be embedded in a full representation of the custodial symmetries. This implies that there are exotic fermions (custodians) as well. We review collider searches of such KK particles and find the region of parameter space in which four top production is primarily important.

In order to protect the $SU(2)_L$ coupling part of the bottom quark (which has been measured with most precision among third generation couplings), the SM doublet should be a bi-doublet under $SU(2)_L \times SU(2)_R$ [52]

$$\begin{pmatrix} t_L \\ b_L \end{pmatrix} \quad \Rightarrow \quad \begin{pmatrix} t_L\,(+,+) & T_L\,(-,+) \\ b_L\,(+,+) & B_L\,(-,+) \end{pmatrix} \tag{III.21}$$

where $SU(2)_{L(R)}$ acts vertically (horizontally). Orbifold boundary conditions are chosen in such a way that the $SU(2)_R$ is conserved on the IR brane and only SM particles have zero modes. On the other hand, the RH top should be embedded into a singlet or triplet under $SU(2)_R$ in order to have a Yukawa coupling (Higgs is residing in $(2,2)$ representation) [52]. If t_R is embedded into a triplet, another triplet is required by P_{LR}. We will simply assume a singlet t_R.

$$t_R \quad \Rightarrow \quad (t_R(+,+)). \tag{III.22}$$

Effects of the new particles in triplets (if t_R were in a triplet) on EWPT is not that significant [50].

Collider searches of exotic fermions have been carried out in many places. Electroweak singlet t_R^1 mixing with the top quark can be probed in its pair production followed by subsequent decays to bW. 5σ discovery reach is estimated to be about $M_{t_R^1} \simeq 1\,\mathrm{TeV}$

$$M_{\mathrm{KK}} / (\mathrm{k}\, e^{-\pi \mathrm{k} r_c})$$

(++) fermion

(++) gauge
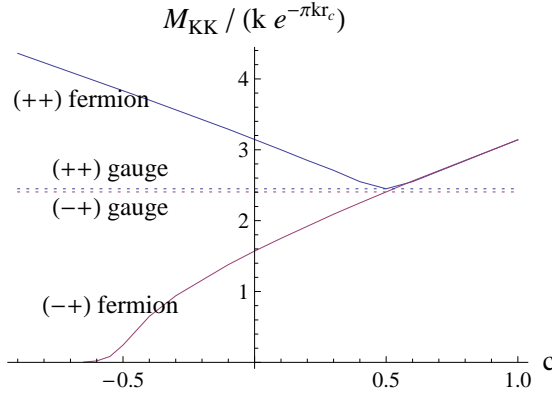
(−+) gauge

(−+) fermion

Figure 3.7: Masses of the first KK gauge boson and (LH) fermions in units of $M_{IR} = ke^{-\pi kr_c}$. Two types of orbifold boundary conditions $(+,+)$ and $(-,+)$ are shown. KK gauge masses are $M_{KK} \simeq 2.45(++),\ 2.405(-+)M_{IR}$. EWSB mixing effect is ignored.

[87]. b_L^1 and T can also be pair produced and decay to tW via mixing of their $SU(2)_L$ partners with top quark. Strategy based on jet mass can achieve $M_{b_L^1} \simeq 1\,\mathrm{TeV}\ 5\sigma$ discovery reach [88] while usage of the LSDL observable can raise the potential $M_{b_L^1,T} \simeq 1.2\,\mathrm{TeV}$ [63] which can also be augmented by combining single production of exotic fermions [84].

The KK spectrum of KK fermion is shown in Fig. 3.7 as a function of bulk mass by ignoring KK-zero mode mixing. Singlet t_R^1 will not be light enough for the entire range of c_t considered in eq.(III.13) with $M_{KK} \gtrsim 1.5\,\mathrm{TeV}$ because $t_R^1\,(+,+)$ is always heavier than $g^{(1)}$. On the other hand, for small c_Q, there will be very light $(-,+)$ fermions such as T and B. For 2-TeV $g^{(1)}$ (1.5-TeV $g^{(1)}$), T is heavy enough if $c_Q \gtrsim 0\,(0.25)$. In all, our four top production with cases A,B and D becomes a favored discovery channel for $M_{KK} \gtrsim 1.5\,\mathrm{TeV}$, while for case C four tops will be most important for a slightly heavier $M_{KK} \gtrsim 1.7$.

We comment that if t_R is a part of a triplet $(\,T_R(-,+),\ t_R(+,+),\ B_R(-,+)\,)$ (and its P_{LR} partner triplet with all fermions satisfying $(-,+)$ BC), c_t will have similar preferred range as c_Q above. This is because the expected discovery potentials of electroweak singlet and doublet fermions are similar. For all cases A-D with $M_{KK} \gtrsim 1.7\,\mathrm{TeV}$, our four top production again will be a promising channel.
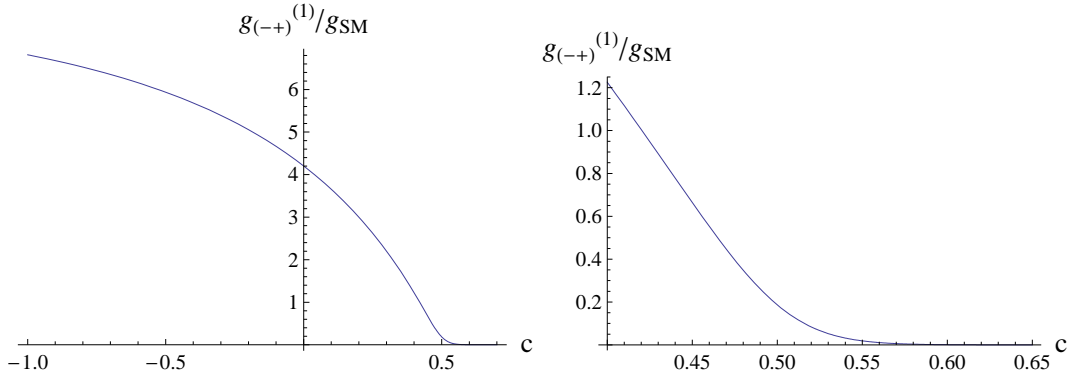
Figure 3.8: Gauge coupling of zero mode fermions with the lowest KK gauge boson with $(-,+)$ boundary condition. $g_{KK} \simeq 0.19\,(0.02)$ for $c = 0.5\,(0.6)$, and approaches zero with higher c.

There are also KK excited gauge bosons. Gauge symmetry of a model is given by

$$G_{bulk} = SU(3)_c \times SU(2)_L \times SU(2)_R \times U(1)_{B-L} \rightarrow G_{SM} = SU(3)_c \times SU(2)_L \times U(1)_Y$$

$$\text{(III.23)}$$

where symmetry breaking $SU(2)_R \times U(1)_X \rightarrow U(1)_Y$ is through orbifold boundary condition $(-,+)$. Gauge bosons associated to broken parts do not have zero modes and the lightest KK modes are denoted by $\widetilde{W}^{1,2}, Z'$ [47]. Due to this boundary condition, $\widetilde{W}, Z'$ are not orthogonal to flat wave functions. Consequently, they couple to light fermions even for $c_{light} = 0.5$. See Fig. 3.8 for their couplings to zero mode fermions: its coupling strength is $g_{KK} \sim 0.2 g_{weak}$ for $c = 0.5$, where g_{weak} is a SM weak gauge coupling. Masses of $\widetilde{W}$ and Z' are shown in Fig. 3.7. We ignore any bulk breaking of these symmetries so that masses are determined by boundary conditions $(-,+)$. Additional bulk breaking may raise masses of these KK gauge bosons, and make collider search of these KK bosons unavailable.

$q\bar{q} \rightarrow Z' \rightarrow t\bar{t}$ is smaller than the usual KK gluon-mediated $t\bar{t}$ production by a factor of $\sim (1/6)^2 \cdot 0.5 \sim 0.01 - 0.02$. $1/6$ is the ratio of weak gauge and QCD couplings, and $Br(Z' \rightarrow t\bar{t}) \sim 0.45$ which is about half the usual KK gluon case giving additional suppression factor of 0.5 if $c_Q \neq 0.5$. The branching ratio is reduced because the bottom quark coupling same size of top coupling is turned on if $c_Q \neq 0.5$. Then the 2-TeV Z'

mediated $t\bar{t}$ cross section is similar in magnitude as the usual 5-TeV KK-gluon mediated one. Given that $m_{t\bar{t}}$ around 2 TeV will be submerged into a larger QCD background than the 5 TeV case, we conclude that Z' mediated $t\bar{t}$ production may not be a promising channel. $\widetilde{W}$ may contribute to single top production as the W boson does in the SM. For instance, the process $u\bar{d} \to \widetilde{W} \to t\bar{b}$ is smaller than SM W-mediated process by $\sim (4 \cdot 0.2)^2 \cdot M_W^2/M_{KK}^2 \sim 0.002$ where $g_t/g_{weak} \sim 4$ and $g_u/g_{weak} \sim 0.2$. So some powerful discriminator is needed. Given this difficulty and the possibility of raising the mass of $\widetilde{W}$ by bulk breaking, we conclude that we have higher sensitivity through the four-top production process.

3.7 Conclusion

We have studied four-top signatures of Randall-Sundrum model in the case of $c_{light} \simeq 0.5$ with universal RH down sector $c_b = c_{light}$. Associate production of $g^{(1)}$ with $t\bar{t}$ as well as pair production of $g^{(1)}$ can produce four top quarks. We have estimated the discovery reach in the single-lepton, like-sign dilepton, trilepton final states of four-top events. For a strongly coupled right-handed top case, the like-sign dilepton observable has the highest potential that can probe up to $M_{KK} \sim 2 - 2.5\,\text{TeV}$. On the other hand, for a strongly coupled left-handed top case, the single-lepton observable, which is enhanced by $t\bar{t}b\bar{b}$ events via $g^{(1)}$ associated production, is the most promising channel for $M_{KK} \lesssim 2\,\text{TeV}$.

In the LSDL and trilepton channels, boosted top and its collimated lepton-jet issue arise. Efficient identification of boosted leptonic top quark can enhance the number of signal events by a factor of about 2(LSDL) and 4(trilepton) with standard isolation $\Delta R_{lj} \geq 0.4$ as illustrated in Table 3.8. This will be more effective with higher E_T^c cuts. A more detailed study of leptonic top id is well motivated. On the other hand, the implications of lepton-jet collimation is different in the case of single lepton final state. Since many multi-lepton events contribute to single lepton event samples by losing some of their leptons, efficient

id of leptonic objects can rather degrade the single lepton sample pool (to the benefit of other channels).

The strongly coupled LH case considered in this paper (coupling sets C and D) can represent the favored parameter space found in the previous literature when considering EWPT constraints and also the flavor-shining model of ref.[48]. Due to this importance and the relatively large signal cross sections, we have also studied an alternative single-lepton observable composed of three b-quark tags. Although detailed background estimation by experiment is required, we have estimated the discovery potential to be up to $\sim 2.4-2.8\,\mathrm{TeV}$ with assumed b-tagging efficiency $\epsilon_b = 0.4 - 0.6$.

We have also discussed competing signatures from custodians and KK gauge bosons of custodial symmetry $\widetilde{W}, Z'$. Unless $c_{t,Q} \lesssim 0$, custodians are not light enough and their pair productions are small. $Z', \widetilde{W}$ mediated top production is suppressed by their weak gauge coupling nature. In large parameter space near $c_{light} = 0.5$ our four-top signal dominates.

$c_{light} = c_b = 0.5$ more or less gives up the geometric approach to flavor physics in the collider-reachable sectors in the warped model. However, increasing tension with precision data and the ensuing tensions of a fine-tuned weak scale make deserving the study of $c_{light} = 0.5$, where many phenomenological issues are relieved. As we have discussed, this approach may significantly reduce the ability to find KK gluons through resonance production from light quarks, and four top quark events may in the end be the best path to discovery. Said a different direction, if a very light KK gluon $M_{KK} \sim 1.5 - 2\,\mathrm{TeV}$ is realized, $c_{light} = 0.5$ is likely to be Nature's choice and four-top production via KK-gluons may be the first beyond the SM discovery signature.

CHAPTER IV

Probing CP violation in Supersymmetry with Light Stops through Hadron Collisions and Electric Dipole Moments

CP violation from physics beyond the Standard Model may reside in triple boson vertices of the electroweak theory. We review the effective theory description and discuss how CP violating contributions to these vertices might be discerned by electric dipole moments (EDM) or diboson production at the Large Hadron Collider (LHC). Despite triple boson CP violating interactions entering EDMs only at the two-loop level, we find that EDM experiments are generally more powerful than the diboson processes. To give example to these general considerations we perform the comparison between EDMs and collider observables within supersymmetric theories that have heavy sfermions, such that substantive EDMs at the one-loop level are disallowed. EDMs generally remain more powerful probes, and next-generation EDM experiments may surpass even the most optimistic assumptions for LHC sensitivities.

4.1   Introduction

CKM phases explain all observed CP violations. However, baryogenesis apparently requires more CP-violation than is provided for by the Standard Model (SM). Thus physics beyond SM should contain new source of CP violation that is somehow small enough not to be in conflict with experiment.

CP violation from new physics can manifest itself in several ways. One way is by measuring an electric dipole moment (EDM) of a fermion. No EDM has been found to date. The current experimental electron EDM (eEDM) bound is $d_e \leq 2.14 \times 10^{-27}\,\mathrm{e\,cm}$ at 95% CL [89], which already puts a strong constraint on physics beyond the SM. In supersymmetric theories [1], the eEDM induced at one-loop is usually larger than this bound so we need several assumptions [90, 91, 92] or cancellation mechanisms [93, 94] to avoid this limit for a wide range of parameter space.

CP violation can also be seen in CP asymmetries of particle energy-momentum distributions at colliders. One such CP asymmetric collider observable was proposed recently using the interference effect between CP conserving and violating WWZ interactions in the diboson production processes at LHC [95]. This observable may be able to improve collider sensitivities on CP violating couplings such as triple boson vertices (TBV) by up to two orders of magnitude from the most recent LEP results. Since we expect that abundant diboson production will occur at LHC, and they have clean tri-lepton decay signals, this observable is useful to probe new physics at the LHC. This improvement raises the hope of discovery, and it is worthwhile studying the possible reach of both the collider observable and EDM measurements in more detail.

Intuition holds in the physics community that EDMs are the most powerful probes of new physics contributions to flavor-preserving CP violation. That intuition is largely based on the varieties of supersymmetric theories that have dipole moments induced at the one-loop level. However, given the possibility of the LHC increasing the probing sensitivity by a few orders of magnitude, we investigate how solid that intuition is within the context of theories that have suppressed one-loop contributions to EDMs. Our primary example is supersymmetry with heavy sfermion masses. Ultimately, we shall not disagree that EDMs are unlikely to be supplanted by the LHC in the search for new sources of CP violation.

We detail the path to that strengthened conclusion below.

We work on specific supersymmetric models. In trying to find scenarios where the LHC can probe better the new CP violating physics compared to eEDM measurements, we will work on models in which the eEDM is two-loop suppressed while TBV is only one-loop suppressed. As the simplest possibility we study the split supersymmetry limit where all scalars except SM-like neutral Higgs are heavy and decoupled [103, 104, 105, 106]. Another possibility is to take only first two generations of sleptons and squarks to be heavy, allow CP violating couplings in the trilinear scalar vertices of the third generation, which induces radiative breaking of CP invariance in the Higgs sector. The mixing of CP even and CP odd eigenstates in the Higgs sector gives opportunity to colliders to discover these new sources of CP violation.

4.2   CP asymmetric observables

4.2.1   Effective triple boson vertices

Diboson production channels at the LHC are described in Fig. 4.1 using the low-energy effective theory below the electroweak scale. This effective theory is obtained by integrating out heavy particles in physics beyond the SM. The modified SM interactions which now contain both CP-even and odd interactions are represented as small blobs in the figure. One can see from the figure that we should study the diboson production channels at the LHC, involving triple boson vertices (TBV) VVV, hVV and couplings with fermions Vff, hff.

We will focus only on TBV among them. One reason for this is that we can easily extend our work to include fermion couplings without changing the conclusions. Secondly, CP-odd effective couplings are mediated by particles in the BSM and are loop suppressed. Any charged particle couples to the vector bosons, whereas only a small number of particles couple to a specific fermion typically. Therefore, TBV is more generally present than more
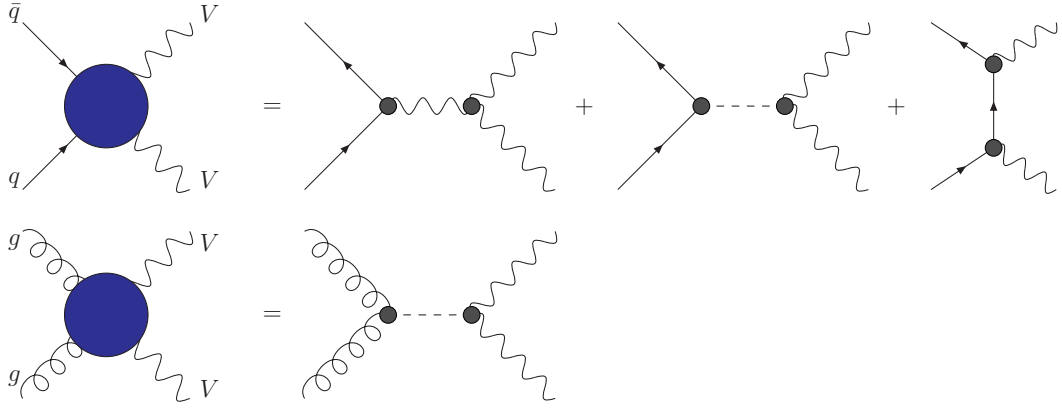
Figure 4.1: Diboson production processes at the LHC. Blobs on the right-hand side are effective interactions in the low-energy effective theory. These effective interactions contain both CP-even and odd contributions.

direct CP-violating couplings with fermions. In addition, large CP-odd Vff couplings with $V = \gamma$ can induce an EDM without loop-suppression, as is discussed in section 4.2.3. Since other Vff couplings are presumably related with the γff coupling in an underlying theory, it is difficult to avoid the experimental EDM limit with large CP-odd Vff couplings. Thus, a meaningful analysis can be carried out with TBV only.

The effective Lagrangian of CP-odd TBV is [96]

$$\mathcal{L}_{\text{CP-odd TBV}} = ig_{WWV} \left(\widetilde{\kappa}_V W_\mu^+ W_\nu \widetilde{V}^{\mu\nu} + \frac{\widetilde{\lambda}_V}{m_W^2} W_\nu^{+\mu} W_\rho^\nu \widetilde{V}_\mu^\rho + g_4^V W_\mu^+ W_\nu (\partial^\mu V^\nu + \partial^\nu V^\mu) \right)$$
$$+ \frac{g\,M_W}{4} \left(g_{H_iWW}\, \widetilde{\eta}_i^W\, \widetilde{W}^{\mu\nu} W_{\mu\nu}^+ + g_{H_iZZ}\, \frac{\widetilde{\eta}_i^Z}{2c_W^2}\, \widetilde{Z}^{\mu\nu} Z_{\mu\nu} \right) H_i \qquad \text{(IV.1)}$$

where $g_{WW\gamma} = -e$, $g_{WWZ} = -e\cot\theta_W$, and g_{H_iVV} is the ratio of CP-even H_iVV coupling to SM H_iVV coupling. V can be γ or Z. $V^{\mu\nu} = \partial^\mu V^\nu - \partial^\nu V^\mu$ and likewise for $W^{\mu\nu}$. Index i runs for two light (CP-even) Higgses. g_4^V is C-odd while others are P-odd, so g_4^V is not relevant for our work as discussed in section 4.2.2. Higher dimensional operators are suppressed by the electroweak scale M_W. Higgs couplings to photons and gluons can also be written in the same way. These effective couplings are actually momentum dependent. However, we can reasonably choose to study constant on-shell couplings as argued in Appendix A.

It is useful to know the $SU(2) \times U(1)$ invariant dimension-six operators that generate the effective triple gauge couplings in eq.(IV.1) after electroweak symmetry breaking. $H^\dagger H V^{\mu\nu} \tilde{V}_{\mu\nu}$ and $D_\mu H^\dagger T^a D_\nu H \tilde{V}^{a\mu\nu}$ generate $\tilde{\kappa}_V$. $\tilde{\lambda}_V$ is generated by $\epsilon_{abc} \widetilde{W}^{a\mu}_\nu W^{b\nu}_\rho W^{c\rho}_\mu$ which does not involve Higgs fields. $V_{\mu\nu}$ and $W_{\mu\nu}$ here are full field strengths. CP-odd neutral VVV couplings are not generated by these operators. As couplings with photons and couplings with Z bosons are presumably related in an underlying theory, we shall reduce redundancy and give results in terms of the Z boson coupling only.

4.2.2 CP asymmetric collider observables

CP asymmetries at colliders are observables well-known to probe CP violating interactions [97]. It has been shown that if absorptive SM backgrounds are known well the LHC may be sensitive to $\tilde{\lambda}_Z$ coupling perhaps as low as the $\tilde{\lambda}_Z \lesssim 0.001$ with $100\,\text{fb}^{-1}$, which would be a significant improvement over LEP2 capabilities, for example [95]. This sensitivity was achieved based on the fact that the cross section proportional to the $\epsilon_{\mu\nu\rho\sigma}$ tensor is a signal of the CP violation since the tensor is odd under time reversal. Thus, only P and CP odd couplings in Eq. (IV.1) are potentially able to be probed with this precision. Although no equivalent small value has been estimated for $\tilde{\kappa}_Z$, we shall suggest by analogy to $\tilde{\lambda}_Z$ that it may be possible. The C-odd coupling g_4^V can be probed in other ways and will not be treated in this paper.

CP violating Higgs couplings can also be probed at the LHC in the same way, in principle. Several other collider observables sensitive to Higgs couplings have been studied as well based on the angular distributions of final leptons. The sensitivities on the CP violating hZZ coupling are usually expected to be around $\tilde{\eta}^Z \lesssim O(0.1)$ with $100 - 300\,\text{fb}^{-1}$ of data from the process $h \to ZZ \to 4l$ at LHC, and possibly $O(0.01)$ from Higgsstrahlung at a future e^+e^- linear collider [98]. As we study EDM sensitivities to the CP violating couplings involving the Higgs boson, we compare results to the $\tilde{\eta}^Z \lesssim O(0.1)$ LHC expected
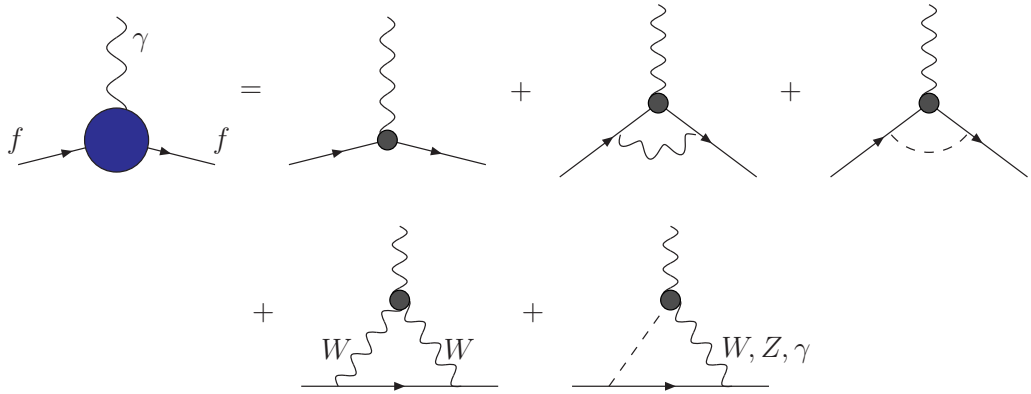
Figure 4.2: EDM diagrams at one and two-loop orders with the effective CP-odd couplings represented as small blobs. Since effective couplings are radiatively generated, the first diagram on the right-hand side is a one-loop contribution and others are two-loop.

sensitivity.

4.2.3 Electric dipole moments measurements

One and two-loop order generation of EDMs are shown in Fig. 4.2 using the effective theory. CP-odd effective couplings in the effective theory are represented as small blobs in the figure. Since effective CP-odd couplings are generated at loop order, the tree-level diagram on the right-hand side implies a one-loop contribution to the EDM and others are two-loop contributions.

We want to avoid one-loop induced EDM in our study. The first reason for this is that a one-loop induced EDM is usually larger than experimental bounds in many models. Secondly, we want to give a "one loop advantage" to collider observables – we expect that TBVs are generated at one-loop order, which only then enables EDMs at two-loop order. As can be seen from the figure, one-loop EDM (first diagram) corresponds to CP-odd Vff couplings with $V = \gamma$ and on-shell external particles. The suppression of the one-loop induced EDM roughly implies the smallness of CP-odd Vff couplings, and vice versa. Then the two-loop diagrams in the first line of Fig. 4.2 are also suppressed.

We will consider only two-loop contributions in the second line of Fig. 4.2 with specified

insertions of effective couplings. We note that these effective interactions are CP violating TBVs that were necessary for the diboson production process as discussed in sec 4.2.1. At two-loop order, WW and scalar-vector can transmit CP violation to SM fermions, whereas scalar-scalar mediation is very small due to small Yukawa couplings. Only WW can mediate CP-violation without Higgs bosons because there is no CP-odd triple neutral electroweak boson couplings. EDMs are generated only through these CP violating TBVs as long as we ignore quartic and higher effective couplings. It can also be inferred that EDMs and CP violating TBVs depend on the same CP phases as will be discussed in sec 4.2.4.

The electric dipole operator should be RG evolved from high scale down to the fermion mass scale at which the fermion EDM is defined. Renormalization group flow mixes this operator with other operators with the same quantum numbers such as chromo-electric dipole, three-gluon Weinberg operator [99] and $SU(2)$ analogies of these. For electron EDM (eEDM), not all are relevant since the electron is colorless. The remaining $SU(2)$ operators are relatively suppressed by multiple powers of g/g_S and the QED renormalization effects are smaller than QCD. We will not consider renormalization effects for eEDM.

In this paper we focus on the electron EDM since the experimental measurements are excellent and improving, and the theory computation has minimal theoretical uncertainty. Of course, one expects a high degree of correlation of one EDM to other EDMs in most theories of physics beyond the SM, and later we shall briefly study the correlation of electron EDM and neutron EDM. As stated earlier, the current sensitivity limit on the eEDM is $d_e \leq 2.14 \times 10^{-27}\,\mathrm{e\,cm}$ at 95% CL [89]. Upon surveying the literature, one expects that the future eEDM sensitivity of the near-term future experiments to be approximately $10^{-29}\,\mathrm{e\,cm}$ [100, 101, 102]. When appropriate, we shall use these numbers as benchmark sensitivities in the numerical discussion ahead.

Muon EDM (μEDM) is also measured. As fermion EDM is proportional to fermion mass, eEDM and μEDM are usually tightly correlated

$$\frac{d_\mu}{d_e} \cong \frac{m_\mu}{m_e} \approx 205. \tag{IV.2}$$

Meanwhile, eEDM sensitivity is much better than current μEDM sensitivity [127]

$$|d_\mu| < (3.7 \pm 3.4) \times 10^{-19}\,\mathrm{e\,cm}. \tag{IV.3}$$

Even proposed future sensitivity $d_\mu \lesssim 10^{-24}\,\mathrm{e\,cm}$ [128] is about three orders of magnitude below eEDM one.

Mercury EDM (d_{Hg}) is usually below the experimental sensitivity once eEDM and nEDM bounds are imposed. In addition, this also involves lots of QCD uncertainties and model-dependent factors [119, 113, 125].

Thallium EDM (d_{Tl}) might be a good complementary measurement of eEDM. CP violation in the Higgs sector can mediate CP violating four fermion operators which are enhanced by $\tan^3\beta$ so that this can have different behavior from eEDM in the intermediate $\tan\beta$ region. However, more accurate analysis requires resummation of vertex and self-energy [119, 126]. It would be good to consider d_{Tl}, but requires more complicated works.

4.2.4 Physical CP-phases in supersymmetry

One can see the relevance of TBVs in supersymmetric models in a more useful way using the physical CP-phases. Using R and Peccei-Quinn (PQ) symmetries, it is shown that in any phase conventions there are two sets of physical CP-phases in the universality ansatz [107, 108]: $\arg(A\mu b^*)$, $\arg(M_{1,2,3}\mu b^*)$, where parameters are the usual soft supersymmetry parameters and higgsino mass μ. The $\arg(M_i M_j^*)$ are also allowed by the same argument. Since we impose GUT-like relations on gaugino masses these phases are not relevant to consider. As low-energy effective operators composed of SM Dirac fermions

and vector fields are neutral under R and PQ symmetries, we can argue that low-energy physical observables should depend on the above combinations, which are the only R and PQ invariants. Indeed, both R and PQ are needed and enough for us to do that because all complex soft phases are charged under at least one of them. This argument does not restrict soft squark/slepton masses.

Since the b term appears only in the Higgs sector, CP violation in the soft supersymmetry breaking sector can be transferred to low-energy effective operators consisting of Higgs bosons at one-loop order. Possible CP violating interactions with one SM Higgs field are Higgs-vector-vector, Higgs-fermion-fermion and Higgs-scalar-scalar couplings. Higgs-Higgs-vector coupling is usually related to the Higgs-vector-vector via the underlying theory. As sizable tree-level processes at LHC involve at most two Higgs bosons, the scalar quartic coupling is not relevant.

As discussed in section 4.2.1, there are also $SU(2) \times U(1)$ invariant dimension-six operators composed of Higgs bosons and vectors. After the Higgs bosons get vacuum expectation values, these operators can induce effective triple gauge couplings WWV, where V is a neutral vector boson. Thus CP violating TBVs are not only relevant but also can indeed be generated at one-loop order in supersymmetric models. It is also clear that CP violating TBVs and EDMs depend on the same CP phases.

4.3 Supersymmetry with the light stop

The split sfermion/ino limit of supersymmetry (split supersymmetry) does not naturally induce large EDMs. In this limit, charginos and neutralinos are not decoupled, and they carry CP phases in the soft supersymmetry breaking sectors. These ino sectors couple to SM fermions at tree-level only via ino-fermion-sfermion couplings which lead to suppressed amplitudes in split supersymmetry due to the heavy sfermions. So CP violation in the SM fermion sector, e.g. EDM, are induced beginning at two-loop order. Recent studies
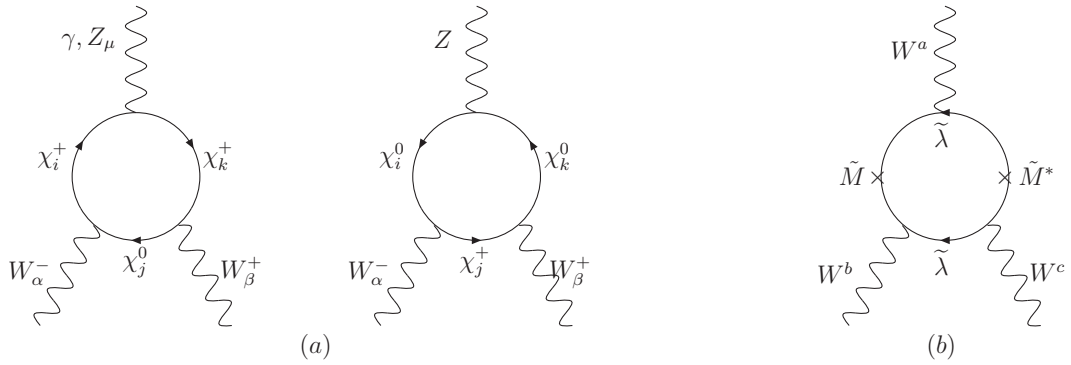
Figure 4.3: (a) CP-odd TBV diagrams mediated by charginos χ_i^+ ($i = 1, 2$) and neutralinos χ_i^0 ($i = 1, 4$). Similar diagrams generating hVV couplings can also be drawn. (b) Diagram that is responsible for the $\tilde{\lambda}_V$ coupling is shown in terms of current eigenstates. Gaugino $\tilde{\lambda}$ is running in the loop, and its complex soft mass insertion is denoted as a cross. A similar diagram in which higgsinos are running with mass μ insertions can also be drawn.

have shown that the electron EDM turns out to be generically smaller than or around the current limit in most of parameter space even with maximum CP-phases [109, 110].

To compute the effects, the input parameters are $\mu, \tilde{M}_{1,2}$ and their phases, $\tan\beta$ and SM-like neutral Higgs mass M_h. The sign of μ is not relevant as it just shifts the CP-phase by π. Since we are interested in electron electric dipole moments, the gluino mass M_3 is not relevant. Once we assume GUT-like relation between gaugino masses, only one CP-phase $\arg(\tilde{M}\mu b^*)$ is physical. The phase of b is related to the relative phase of H_u and H_d via the minimization condition of the Higgs potential; $b/(v_u v_d)$ is real at tree-level. We will work in the basis in which b is real, then the two Higgs bosons have opposite phases. $U(1)_Y$ rotations of H_u and H_d can remove this relative phase, and the Higgs boson vevs are real in the same basis [1]. The only physical combination of CP-phases remaining is $\arg(\tilde{M}\mu)$. It is clear that these CP-phases reside in the chargino and neutralino sectors.

EDMs in split supersymmetry have been computed in previous works [109, 110, 111]. We also compute the effective CP-odd TBVs generated by diagrams shown in Fig. 4.3(a), and apply them to the eEDM and collider observables. We give supporting analytic results in the Appendix.

One interesting result to notice is that the $\tilde{\lambda}_V$ coupling is not generated at one loop. It is simply because this coupling is generated by a dimension-six operator that does not involve Higgs fields as discussed in section 4.2.1, whereas the physical CP phase depends on the b term. We can see this more explicitly in terms of current eigenstates depicted in Fig. 4.3(b). As Higgs-higgsino-gaugino coupling couples gaugino and higgsino, either a gaugino or a higgsino runs in the loop without Higgs. Then μ, as an interaction between $\tilde{H}_u$ and $\tilde{H}_d$, and $\tilde{M}_{1,2}$ cannot appear together, and hence no CP-phase. (Recall that the physical phases are $\mu M_{1,2}$ in our basis.) Indeed, the diagram with only gaugino (or higgsino) is proportional to $|\tilde{M}|^2$ (or $|\mu|^2$) because of the charge flow direction as shown in the figure. These are real, i.e., no CP violation.

Both CP-violating TBVs and eEDM are approximately proportional to $\sin 2\beta$ by essentially the same reason. To see this it is again easiest to think in terms of current eigenstates. Relevant diagrams are then Fig. 4.3(b) with the W boson on top replaced by a neutral gauge boson, and with mass insertions replaced by external H_u, H_d legs and their vevs. Note that we need one H_u and one H_d in order to insert both $\tilde{M}$ and μ. As we take neutral Higgs fields other than SM-like Higgs boson to be very heavy, we obtain a simple relation between Higgs mixing angle α and vev ratio β: $\tan \alpha = \tan \beta$ at leading order. Therefore, each vev of H_u and H_d carries $\sin \beta$ and $\cos \beta$ respectively, hence $\sin 2\beta$ overall. eEDM is generated by inserting these effective interactions in Fig. 4.2, thus having the same $\sin 2\beta$ dependence.

We now look at some numerical results for this scenario. eEDM and CP violating TBVs depend on input parameters quite similarly. $\tan \beta$ dependence cancels when we study the relative importance of eEDM and collider observables as we saw above. Heavy M_h can suppress the eEDM since Higgs boson mediated two-loop eEDM dominates numerically in this scenario, while TBVs are independent of M_h. However, due to the narrow consistent

Higgs mass range $115 \, \text{GeV} \leq M_h \lesssim 150 \, \text{GeV}$ of the light SM-like Higgs boson in supersymmetry, this suppression is not very significant. M_1 dependence is weak since the bino does not couple to gauge bosons at tree-level. Dependence on the remaining gaugino/higgsino mass parameters can be different because the eEDM is two-loop while TBVs are one-loop physics.

We choose to draw plots in $M_2 - \mu$ plane. In Fig. 4.4, we show eEDM and CP violating TBVs in this plane. We set $\tan \beta = 1$ which is not allowed because this small $\tan \beta$ induces too large Yukawa coupling, but one can extrapolate the results linearly with $\sin 2\beta$ as discussed above. In almost all of the parameter space, the current eEDM limit and the expected collider observable are not sensitive enough to probe CP violations in split supersymmetry even with maximum CP-phases.

Then the next question is if there exists parameter space in which eEDM is well below the future sensitivity while TBVs are around the future reach. The answer is (almost) no. In order to see this we scatter input parameters randomly within the following range:

$$100 \, \text{GeV} \leq M_{1,2}, \mu \leq 1000 \, \text{GeV} \,, \quad 115 \, \text{GeV} \leq M_h \leq 180 \, \text{GeV} \,, \quad 2 \leq \tan \beta \leq 50. \quad \text{(IV.4)}$$

If M_2, μ are a few TeV, then both eEDM and collider observable are well below the current sensitivities as can be seen in Fig. 4.4, so we now focus on the sub-TeV gaugino/higgsinos. In addition, as stated earlier, we identify the future eEDM sensitivity to be $10^{-29} \, \text{e cm}$ for reference [100, 101, 102].

In Fig. 4.5, we see that the eEDM and TBVs are closely related so that there is a narrow allowed region of eEDM for each specific TBV value, and vice versa. The Higgs boson coupling shows stronger correlation with the eEDM due to dominance of the Higgs-mediated eEDM over WW-mediated eEDM. This correlation is what we expected based on the observation that any CP-violating TBV can induce an eEDM discussed in section 4.2.3.

For $d_e < 10^{-29} \, \text{e cm}$, which is just below the reference point of future eEDM measure-
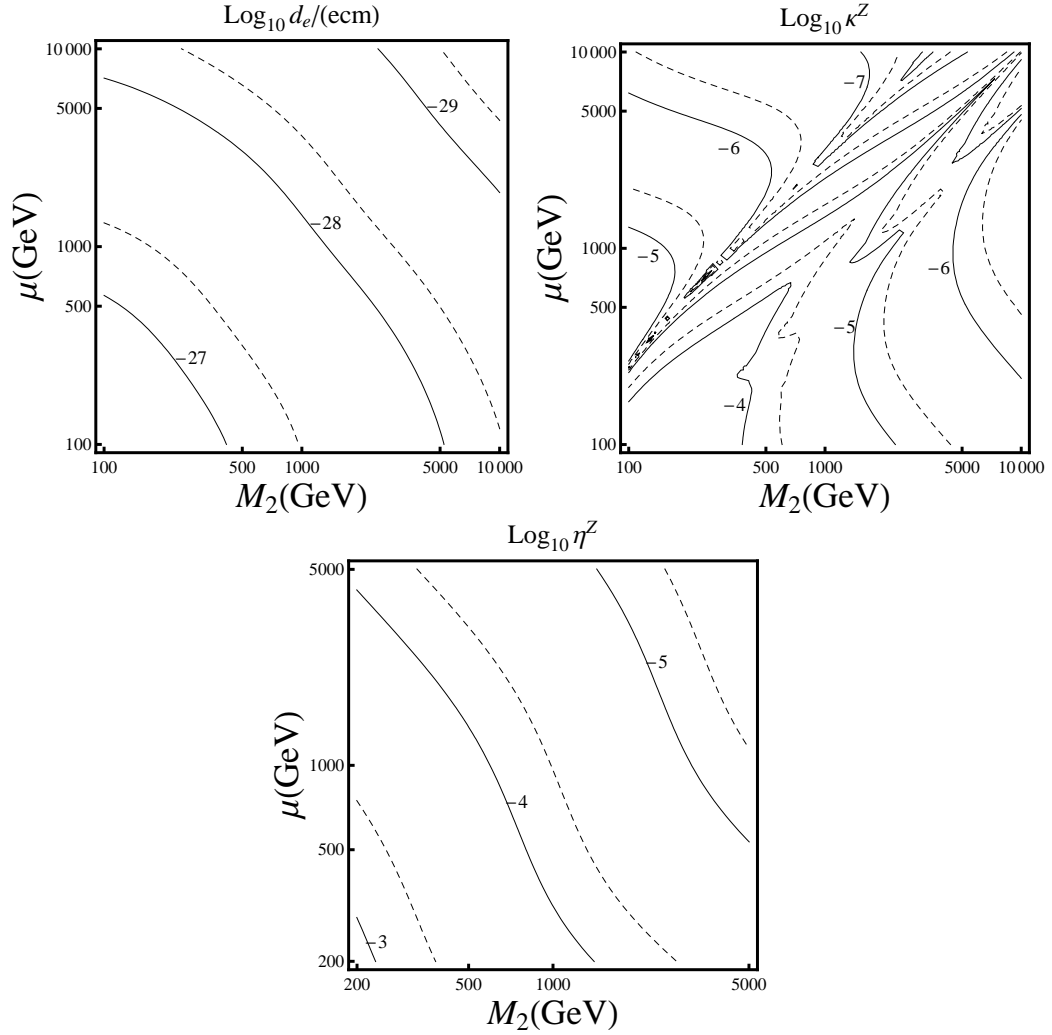
Figure 4.4: Contour plots of eEDM, triple vector coupling $\tilde{\kappa}^Z$ and the Higgs coupling $\tilde{\eta}^Z$ to the Z boson in the $M_2 - \mu$ plane. $\log_{10}$ values are written on the solid contour lines. To facilitate rescaling by the reader, contours are made for $\tan\beta = 1$ with maximum CP phases. $M_h = 120\,\text{GeV}$ is used. Abrupt changes of $\tilde{\kappa}^Z$ in the diagonal region are partially due to a change of sign.
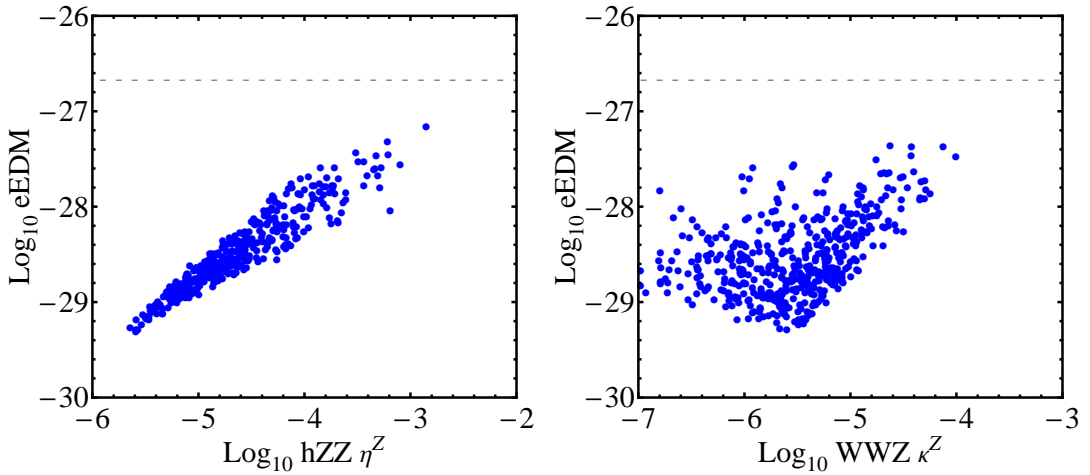
Figure 4.5: CP violating Higgs (left) coupling $\tilde{\eta}^Z$ and triple vector (right) couplings $\tilde{\kappa}^Z$ to the Z boson are plotted against eEDM in split supersymmetry. Input parameters are randomly scattered within the range Eq.(IV.4). The dashed horizontal line represents the current experimental eEDM bound $d_e < 2.14 \times 10^{-27}$ e cm.

ment sensitivity, CP violating TBV values correspond to $\tilde{\eta}^Z$, $\tilde{\kappa}^Z \lesssim 8 \times 10^{-6}$. Although it remains to be seen how well dedicated LHC experiments can do, if other CP violating observable expectations are a rough guide it is unlikely that these couplings can be probed at the one part per mil level at the LHC. If LHC fails to reach that very high sensitivity, the proposed eEDM sensitivity of $\sim 10^{-29}$ e cm would be a more powerful probe of CP violation from new physics.

The neutron EDM is also precisely measured with the current sensitivity [112] $d_n < 6.3 \times 10^{-26}$ e cm, and can be improved in the future. This can be a competitor to the eEDM measurement depending on the future improvement and the theory prediction of the neutron EDM. In split supersymmetry, we compare computed eEDM and neutron EDM in Fig. 4.6. The neutron EDM is generated by constituent quark EDMs induced by the same types of diagrams generating eEDM because heavy squarks suppress chromo-electric dipole and three-gluon Weinberg operators. Thus, the neutron EDM depends on the same CP phases as eEDM does, and is closely related to eEDM as can be seen in Fig. 4.6 [113].
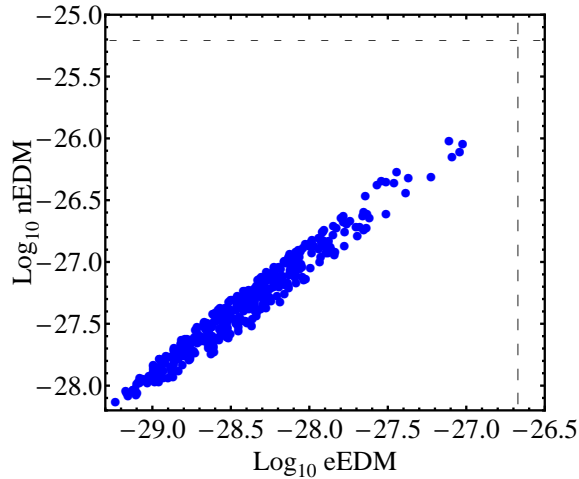
Figure 4.6: Scatter plot of electron EDM and neutron EDM in split supersymmetry. Input parameters are scattered within the range eq.(IV.4). Dashed lines represent the current experimental sensitivities.

4.4 MSSM with the radiative breaking of the Higgs sector CP invariance

We relax the split limit but keep the first two generations of squarks and sleptons to be very heavy to avoid large FCNC and one-loop induced EDM [90, 114]. There are now not only additional physical CP phases, but the CP invariance of the Higgs sector can be radiatively broken so that there might be less correlation between eEDM and CP violating TBVs.

In the low-energy effective theory, we have two more neutral Higgs bosons, charged Higgs bosons and a third generation of squarks and sleptons in addition to split limit field contents. As a trilinear A-term interaction with stop (in large extent with sbottom) becomes relevant, the physical CP phases $\arg(A\mu b^*)$ cannot be ignored. These CP phases induce CP violation in the two-point Green's function through squark and quark loops, and mix CP-even and odd Higgs eigenstates [115, 116]. Because of these loop-induced interactions, we call this "radiative breaking" of CP invariance in the Higgs sector. One consequence of this important to us is that the pseudoscalar Higgs interactions with fermions generate CP violating TBVs at one-loop order. Of course, TBVs induce EDMs and the tension between

them still exists.

However, the radiative breaking of CP invariance can enhance the CP violating collider observables. The neutral Higgs mass mixing matrix O is defined as

$$\begin{pmatrix} H_d \\ H_u \\ A \end{pmatrix} = O \begin{pmatrix} H_1 \\ H_2 \\ H_3 \end{pmatrix} \tag{IV.5}$$

with $M_{H_1} < M_{H_2} < M_{H_3}$. H_1 (H_2) becomes the light (heavy) CP-even Higgs in the absence of CP-violation. The scalar-pseudoscalar transitions O_{Ai} induce pseudoscalar couplings between Higgs boson H_i and quarks. Therefore, CP violating $H_i VV$ couplings generated by quarks are proportional to O_{Ai} as explicitly shown in Eq.(IV.27). Other mixing elements modify CP conserving $H_i VV$ couplings. The ratio of the CP-even $H_i VV$ coupling in this scenario to the SM $H_i VV$ coupling is written as [117]

$$g_{H_i VV} \equiv c_\beta O_{H_d i} + s_\beta O_{H_u i}. \tag{IV.6}$$

As scalar-pseudoscalar mixing O_{Ai} increases, $g_{H_i VV}$ decreases because the mixing matrix is normalized. Thus the ratio of the CP-odd Higgs couplings to CP-even Higgs couplings can be relatively enhanced; i.e., the collider observable can be larger than what is expected in the case of no CP even-odd mixing. It is interesting to study if this enhancement can win over the limited amount of CP-violation allowed due to the eEDM bound.

CP even-odd mixing is large between two heavy neutral Higgs states H_2 and H_3 while the lightest Higgs H_1 remains mostly CP-even [118]. So the enhancement is larger for $H_{2,3}$ couplings than for H_1. Meanwhile, as $g_{H_i VV}$ decreases we have to worry about a decrease of the cross section of diboson production mediated by Higgs bosons in Fig. 4.1. We focus on the $gg \rightarrow H_i \rightarrow ZZ \rightarrow 4l$ diboson production channel for Higgs couplings collider observable as mentioned in section 4.2.2. In order to use a collider observable, we need to

be able to obtain at least a certain number of asymmetric events at the LHC. From this point of view, H_1 is a more important contributor than heavy Higgs bosons because H_1 is lighter and has larger couplings to the SM states. For example, the heavy Higgs H_3, which becomes a CP-odd eigenstate in the limit of no CP-violation, usually has very small CP-even H_3VV couplings so there is little hope to measure them.

We now discuss the computation and numerical results for this scenario. CP violating couplings are generated by Barr-Zee type diagrams in analogy to Fig. 4.3(a). In addition to gauginos and higgsinos, the third generation squarks and quarks can run in the loop [119]. However, complex squark mixing angles cancel between adjacent vertices so squarks contribute to TBVs only at higher order. Top and bottom quarks can now generate CP violating Higgs couplings through tree-level pseudoscalar coupling. Meanwhile, the triple vector couplings are not affected by quarks, and not very different from the split supersymmetry case. Thus we focus on Higgs couplings in this section. Analytic results of quark and -ino contributions are shown in Appendix B. The complete set of two-loop induced EDMs in supersymmetry are computed in [119, 120, 121] and references therein.

$\widetilde{\lambda}_V$ couplings are still not generated at one-loop order in our analysis. Physical CP phases $\arg(A\mu b^*)$ and $\arg(M\mu b^*)$ depend on the b term, so the same argument in split supersymmetry case that forbade $\tilde{\lambda}_V$ applies here as well. We can take another linear combination $\arg(AM^*)$, which appears at two-loop order, as squark and gaugino couple through a triple vertex with a quark. This $SU(2)$ analogy of the three-gluon Weinberg operator has little effect on the eEDM, as discussed in section 4.2.3.

We assume the universality and flavor-diagonality of soft masses and the trilinear coupling A-term for simplicity. The input parameters are then

$$M_{1,2}, \quad \mu, \quad \tan\beta, \quad M_{H^\pm},$$

$$A = A_t = A_b = A_\tau, \quad M_{SUSY} = M_{Q_3} = M_t = M_b = M_{L_3} = M_\tau \qquad \text{(IV.7)}$$

and soft CP-phases. As heavy Higgs bosons are not decoupled, the Higgs boson mixing angle α is not trivially related to vev ratio β, i.e. $\tan\alpha \neq \tan\beta$. The Higgs boson mixing angle now depends on various input parameters. Then the previous argument about $\sin 2\beta$ dependence in split supersymmetry does not apply here. Indeed, several authors have shown that the eEDM increases overall with $\tan\beta$ [119]. Here, $\tan\beta$ rather plays the role of determining the amount of enhancement through g_{H_iVV} and couplings with fermions which can also be seen in eq.(IV.27).

We have modified the CPsuperH 2.0 program [122] for numerical study. We scattered input parameters within the range

$$300\,\mathrm{GeV} \leq A, M_{SUSY} \leq 2000\,\mathrm{GeV}\,,$$

$$130\,\mathrm{GeV} \leq M_{H^\pm} \leq 250\,\mathrm{GeV}\,, \quad 150\,\mathrm{GeV} \leq M_{1,2}\mu \leq 1000\,\mathrm{GeV}\,, \quad 2 \leq t_\beta \leq 50. \quad \text{(IV.8)}$$

We also consider the following consistency condition

$$M_{H_1} \geq 115\,\mathrm{GeV}\,. \tag{IV.9}$$

The light Higgs boson H_1 coupling to the Z boson (see eq.(IV.1) for definition) versus the computed eEDM is shown in Fig. 4.7. Sample points which satisfy consistency condition in Eq.(IV.9) are represented as red circles. The eEDM measurement alone eliminates most of the sample points and restricts the Higgs coupling to be well below the experimental sensitivity $\sim O(0.1)$. Actually, in most of parameter space consistent with condition Eq.(IV.9) and eEDM bound, $g_{H_1VV} \sim 1$ and $O_{A1} \lesssim O(0.01)$. Thus, enhancement is too small to overcome the eEDM constraint. Large CP violation needed to obtain large O_{A1} and small g_{H_1VV} is still prohibited by the eEDM constraint.

For heavy Higgs boson H_2, it also turned out to be very pessimistic for collider signatures of CP violation. The required cross-section just to discover the H_2 Higgs boson itself almost
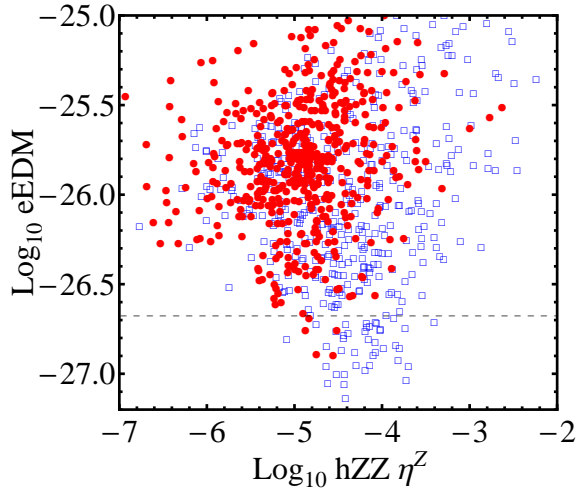
Figure 4.7: Light Higgs H_1 CP violating coupling $\tilde{\eta}^Z$ to the Z boson is plotted against eEDM with light third generation squarks. Blue $\square$ are excluded by $M_h \geq 115\,\text{GeV}$ while red $\bullet$ satisfy this condition. Dashed line represents current eEDM bound $d_e < 2.14 \times 10^{-27}\,\text{e\,cm}$. Expected sensitivity on Higgs coupling is too large to be shown. This plot is generated with maximum CP-violating phases, and all points move downward as the phase angles decrease.

eliminates the possibility for us to measure a H_2VV CP violating couplings. This cross section is at best a few hundred ab for $M_{H_2} \sim 170\,\text{GeV}$.

In this particular limit, the neutron EDM is usually predicted to be about two orders of magnitude larger than the eEDM, and hence is a stronger constraint on new physics [113]. This is mainly because the large A_t coupling generates a three-gluon Weinberg operator that dominantly contributes to the neutron EDM while the stop contribution to eEDM is subdominant. In any case, large CP violations generating CP violating TBVs eventually induce EDM, which is generally more constraining than CP-violating collider physics observables.

In concluding this section, we mention the previous work of Babu et al. [123], which had similar goals of comparison as this work. We briefly discuss that paper since it strengthens our conclusion. They found that one-loop lepton EDM mediated by slepton and gaugino/higgsino puts severe constraint on one-loop generated CP violating Higgs-lepton-lepton couplings in the MSSM. So they sought other places where CP violating Higgs boson cou-

plings may be enhanced while the lepton EDM is relatively not. They noted that there is a tree-level CP even-odd mixing in the Higgs sector of the NMSSM. Since this CP violating coupling is not loop suppressed and has different dependence on input parameters than the one-loop lepton EDM, they suggested that this would be a good place to observe large CP violating Higgs couplings. However, once Higgs-mediated two-loop EDM contributions are considered this conclusion must be modified. The large CP violating Higgs boson couplings induce a two-loop EDM regardless of the origin of such CP violating couplings, which constrains the size of these Higgs boson couplings quite severely.

4.5 Conclusions

Our basic conclusion, which is supported by detailed investigations of various candidate theories that had a chance to contravene it, is this: Whatever the origin may be of CP violating triple boson vertices, they induce EDMs, and although the physics that induces EDMs is "one loop down" compared to collider CP asymmetries, the EDM experiments are sufficiently precise that they overcome the loop factor and are generally more powerful probes. We expect this conclusion to strengthen into the foreseeable future as EDM experiments become more sensitive.

4.6 Appendix A: Analytic discussion of CP-odd effective couplings

We present our conventions and analytic results of CP violating TBVs.

4.6.1 Conventions

Gaugino and higgsino masses are given as

$$-\mathcal{L} = \frac{1}{2}M_1\widetilde{B}\widetilde{B} + \frac{1}{2}M_2\widetilde{W}^a\widetilde{W}^a + \mu\widetilde{H}_u\epsilon\widetilde{H}_d. \tag{IV.10}$$

Chargino, neutralino mixing matrices U, V, N satisfy

$$N^*M_{\chi^0}N^\dagger = M_{D^0}, \qquad U^*M_{\chi^+}V^\dagger = M_{D^+} \tag{IV.11}$$

where M_{χ^0} and M_{χ^+} are as in Ref. [1]. The subscript D implies a diagonal matrix with positive elements.

The interaction Lagrangian of split supersymmetry in terms of mass eigenstates is

$$
\begin{aligned}
\mathcal{L} \;=\; & g\overline{\chi^0_i}\gamma^\mu\left(C^L_{ij}P_L + C^R_{ij}P_R\right)\chi^+_j W^+_\mu + h.c. \\
& + \frac{g}{c_W}\overline{\chi^+_i}\gamma^\mu\left(F^L_{ij}P_L + F^R_{ij}P_R\right)\chi^+_j Z_\mu + \frac{g}{c_W}\overline{\chi^0_i}\gamma^\mu(H^L_{ij}P_L + H^R_{ij}P_R)\chi^0_j Z_\mu \\
& + \frac{g}{\sqrt{2}}\overline{\chi^+_i}\left(D^L_{ij}P_L + D^R_{ij}P_R\right)\chi^+_j h \;+\; \frac{g}{\sqrt{2}}\overline{\chi^0_i}\left(D'^L_{ij}P_L + D'^R_{ij}P_R\right)\chi^0_j h \\
& - eQ_f\bar{f}\gamma^\mu f A_\mu + \frac{gm_f}{2M_W}\overline{f}fh
\end{aligned}
\tag{IV.12}
$$

where f is a fermion for which the EDM is calculated. C,D,F and H are give by

$$
\begin{aligned}
C^L_{ij} &= N_{i2}V^*_{j1} - \frac{1}{\sqrt{2}}N_{i4}V^*_{j2}, & C^R_{ij} &= N^*_{i2}U_{j1} + \frac{1}{\sqrt{2}}N^*_{i3}U_{j2} \\
F^L_{ij} &= -\delta_{ij}c^2_W + \frac{1}{2}V_{i2}V^*_{j2}, & F^R_{ij} &= -\delta_{ij}c^2_W + \frac{1}{2}U^*_{i2}U_{j2} \\
H^L_{ij} &= -\frac{1}{4}(N^*_{i3}N_{j3} - N^*_{i4}N_{j4}), & H^R_{ij} &= -(H^L_{ij})^* = -H^L_{ji} \\
D^L_{ij} &= s_\beta U^*_{i1}V^*_{j2} + c_\beta U^*_{i2}V^*_{j1}, & D^R_{ij} &= s_\beta V_{i2}U_{j1} + c_\beta V_{i1}U_{j2} = (D^{L\dagger})_{ij} \\
D'^L_{ij} &= \left(N^*_{j2} - t_W N^*_{j1}\right)\left(N^*_{i3}c_\beta - N^*_{i4}s_\beta\right) + (i \leftrightarrow j), & D'^R_{ij} &= (D'^L_{ij})^*
\end{aligned}
\tag{IV.13}
$$

Here, index 3(4) implies $H_d(H_u)$ following Ref. [1]. In the MSSM away from the split supersymmetry limit, Higgs boson couplings are modified as the relation $\tan\alpha = \tan\beta$ does not generally hold. For the lightest Higgs boson H_1, the couplings can be obtained by substituting $h \to H_1$ and $s_\beta(c_\beta) \to -c_\alpha(s_\alpha)$ where s_β and c_β are explicitly listed in the above equations for $D^{L,R}_{ij}$.

CP and P-odd form factors are conventionally written as below [96] for incoming $V_\mu(q)$

(or $h(q)$) and outgoing $W_\alpha^-(p_1)$ and $W_\beta^+(p_2)$ (or $V_\mu(p_1)$ and $V_\nu(p_2)$)

$$
\begin{aligned}
\Gamma_{WWV}^{\mu\alpha\beta} &= ig_{WWV}\left[f_6^V(q)\,\epsilon^{\mu\alpha\beta\nu}q_\nu + \frac{f_7^V(q)}{M_W^2}(p_1-p_2)^\mu\epsilon^{\alpha\beta\rho\sigma}q_\rho(p_1-p_2)_\sigma \right.\\
&\qquad\qquad\qquad\qquad\qquad\qquad \left. + if_4^V(q)(q^\alpha g^{\mu\beta}+q^\beta g^{\mu\alpha})\right]\\
\Gamma_{H_iVV}^{\mu\nu} &= gM_W\left[g_{H_iWW}\left(S_i^W(q)(g_{\mu\nu}-\frac{2p_{1\mu}p_{2\nu}}{M_W^2})+\frac{P_i^W(q)}{M_W^2}\epsilon_{\mu\nu\alpha\beta}p_1^\alpha p_2^\beta\right)\right.\\
&\qquad\qquad \left. + \frac{1}{2c_W^2}g_{H_iZZ}\left(S_i^Z(q)(g_{\mu\nu}-\frac{2p_{1\mu}p_{2\nu}}{M_W^2})+\frac{P_i^Z(q)}{M_W^2}\epsilon_{\mu\nu\alpha\beta}p_1^\alpha p_2^\beta\right)\right]
\end{aligned}
$$

$$\text{(IV.14)}$$

where $f_6^V = \tilde{\kappa}_V - \tilde{\lambda}_V$, $f_7^V = -\frac{1}{2}\tilde{\lambda}_V$, $f_4^V = g_4^V$, $P_i^V = \tilde{\eta}_i^V$. $g_{WW\gamma} = -e$, $g_{WWZ} = -e\cot\theta_W$ and g_{H_iVV} is the ratio of the CP-even H_iVV coupling to the SM H_iVV coupling. CP-even form factor S_i^V and C-odd form factor f_4^V are shown for reference. More information about these form factors and the effective Lagrangian eq.(IV.1) can be found in [96].

4.6.2 Analytic expressions

We represent triple gauge boson form factors first. These are generated via chargino/neutralino as shown in Fig. 4.3. The effective couplings are obtained in the limit of the on-shell center-of-mass energy $s = q^2 \to M_{V,H_i}^2$. For reference we list all three types of CP violating WWV couplings in terms of loop functions a_i^{WWV}.

$$
\begin{aligned}
f_6^{Z++} &= \frac{g^2}{16\pi^2 c_W^2}\sum_{i,j,k}\left[m_i^+ m_k^+\Im(C_{ji}^{R*}C_{jk}^R F_{ki}^L - L)a_1^{WWZ} + 2m_i^+ m_j^0\Im(C_{ji}^{L*}C_{jk}^R F_{ki}^R - L)a_2^{WWZ}\right.\\
&\quad \left. + 2\Im(C_{ji}^{R*}C_{jk}^R F_{ki}^R - L)\left\{M_W^2 a_5^{WWZ} + q^2(a_4^{WWZ}/2 - a_6^{WWZ}) + 3a_8^{WWZ}\right\}\right] \quad \text{(IV.15)}
\end{aligned}
$$

$$
\begin{aligned}
f_4^{Z++} &= \frac{g^2}{16\pi^2 c_W^2}\sum_{i,j,k}\left[m_i^+ m_k^+\Im(C_{ji}^{R*}C_{jk}^R F_{ki}^L + L)a_1^{WWZ} + 2m_i^+ m_j^0\Im(C_{ji}^{L*}C_{jk}^R F_{ki}^R + L)a_3^{WWZ}\right.\\
&\quad \left. + 2\Im(C_{ji}^{R*}C_{jk}^R F_{ki}^R + L)\left\{M_W^2 a_5^{WWZ} - q^2 a_6^{WWZ} + 3a_8^{WWZ}\right\}\right] \quad \text{(IV.16)}
\end{aligned}
$$

$$
\begin{aligned}
f_6^{Z00} &= \frac{g^2}{16\pi^2 c_W^2}\sum_{i,j,k}\left[m_i^0 m_k^0\Im(C_{ij}^{R*}C_{kj}^R H_{ik}^L - L)a_1^{WWZ} + 2m_j^+ m_k^0\Im(C_{ij}^{L*}C_{jk}^R H_{ik}^L - L)a_2^{WWZ}\right.\\
&\quad \left. + 2\Im(C_{ij}^{R*}C_{kj}^R H_{ik}^R - L)\left\{M_W^2 a_5^{WWZ} + q^2(a_4^{WWZ}/2 - a_6^{WWZ}) + 3a_8^{WWZ}\right\}\right] \quad \text{(IV.17)}
\end{aligned}
$$

$$f_4^{Z00} = \frac{g^2}{16\pi^2 c_W^2} \sum_{i,j,k} \left[-m_i^0 m_k^0 \Im(C_{ij}^{R*} C_{kj}^R H_{ik}^L + L) a_1^{WWZ} + 2m_j^+ m_k^0 \Im(C_{ij}^{L*} C_{kj}^R H_{ik}^L + L) a_3^{WWZ} \right.$$
$$\left. + 2\Im(C_{ij}^{R*} C_{kj}^R H_{ki}^R + L) \left\{ M_W^2 a_5^{WWZ} + q^2 a_6^{WWZ} - 3 a_8^{WWZ} \right\} \right] \tag{IV.18}$$

$$f_7^Z = 0 \tag{IV.19}$$

$$f_6^\gamma = \frac{e^2}{8\pi^2} \sum_{i,j} m_i^+ m_j^0 \Im(C_{ji}^{L*} C_{ji}^R - L) a_2^{WW\gamma} \tag{IV.20}$$

$$f_4^\gamma = f_7^\gamma = 0 \tag{IV.21}$$

Subscript $^{++}(^{00})$ implies the contributions from the first (second) diagram in Fig. 4.3 where two charginos (neutralinos) are running in the loop. L inside the Im part implies the same coupling combination with $L \leftrightarrow R$. f_4^γ is zero because $WW\gamma$ form factors define the electric charge of the W boson in the Coulomb limit while C-odd parts flip the electric charge.

The loop functions are given as (assuming light on-shell bosons)

$$a_i^{WWZ} = \int_0^1 dx \int_0^{1-x} dy \frac{b_i}{(m_i^2 - m_j^2)x + (m_k^2 - m_j^2)y + m_j^2 - q^2 xy} \qquad \text{for } i = 1, \cdots, 7$$
$$a_8^{WWZ} = \int_0^1 dx \int_0^{1-x} dy \, (y - x) \cdot \log \left((m_i^2 - m_j^2)x + (m_k^2 - m_j^2)y + m_j^2 - q^2 xy \right)$$
$$= (m_k^2 - m_i^2) a_7^{WWZ} \tag{IV.22}$$

where q is incoming Z boson momentum. $a_2^{WW\gamma}$ can be obtained by taking $m_k = m_i$ in a_2^{WWZ}. Coefficients b_i are given as

$$b_1 = x - y, \quad b_2 = y - x + 1, \quad b_3 = x + y - 1, \quad b_4 = (y - x)(x + y - 1)$$
$$b_5 = (y - x)(x + y - 1)^2, \qquad b_6 = (y - x) xy, \qquad b_7 = xy. \tag{IV.23}$$

These results numerically match well with previous computations [124].

In a similar way, $H_i VV$ couplings are generated via chargino/neutralino and top/bottom quarks (not in split supersymmetry). Here we represent only CP-odd hZZ and hWW couplings as these are relevant for our numerical studies. These are given in terms of loop

functions c_i.

$$
\begin{aligned}
P_h^Z \cdot g_{hVV} &= \frac{\sqrt{2}\alpha M_W}{\pi s_W^2} \sum_{i,j,k=1}^{2} \left(m_i \Im(F_{ji}^R D_{ik}^R F_{kj}^R - L) c_1(i,j,k) + m_j \Im(F_{ji}^R D_{ik}^L F_{kj}^L - L) c_2(i,j,k) \right) \\
&+ \frac{\sqrt{2}\alpha M_W}{\pi s_W^2} \sum_{i,j,k=1}^{4} \left(m_i \Im(H_{ji}^R D_{ik}'^R H_{kj}^R - L) c_1(i,j,k) + m_j \Im(H_{ji}^R D_{ik}'^L H_{kj}^L - L) c_2(i,j,k) \right) \\
&+ \frac{3\alpha M_W}{\pi s_W^2} \sum_{f=t,b} m_f \left(\Im(F_Z^R D_f^R F_Z^R - L) c_3(f) + \Im(F_Z^R D_f^L F_Z^R - L) c_4(f) \right). \qquad \text{(IV.24)}
\end{aligned}
$$

$$
\begin{aligned}
P_h^W \cdot g_{hVV} &= \frac{\sqrt{2}\alpha M_W}{\pi s_W^2} \sum_{i,j,k=1}^{2} \left(m_i \Im(C_{ji}^R D_{ik}^R C_{kj}^{*R} - L) c_1(i,j,k) + m_j \Im(C_{ji}^R D_{ik}^L C_{kj}^{*L} - L) c_2(i,j,k) \right) \\
&+ \frac{\sqrt{2}\alpha M_W}{\pi s_W^2} \sum_{i,j,k=1}^{4} \left(m_i \Im(C_{ji}^{*R} D_{ik}'^R C_{kj}^R - L) c_1(i,j,k) + m_j \Im(C_{ji}^{*R} D_{ik}'^L C_{kj}^L - L) c_2(i,j,k) \right) \\
&+ \frac{3\alpha M_W}{\pi s_W^2} \sum_{f=t,b} m_f \Im(-D_f^L) c_3(f). \qquad \text{(IV.25)}
\end{aligned}
$$

where couplings with quarks are given as

$$
F_Z^{L,R} = T_f^3 - Q_f s_W^2, \qquad D_t^L = \frac{m_t}{M_W s_\beta}(O_{H_u i} + i O_{Ai} c_\beta) \quad, \qquad D_t^R = (D_t^L)^*
$$

$$
D_b^L = \frac{m_b}{M_W c_\beta}(O_{H_d i} + i O_{Ai} s_\beta) \quad, \qquad D_b^R = (D_b^L)^*
$$

$$
\text{(IV.26)}
$$

In order to see the dependence on CP even-odd mixing better, we simplify the quark contributions in the third lines by approximately treating $s_W^2 \approx 0.25$. These quark contributions are given as

$$
\begin{aligned}
P_h^Z \cdot g_{hVV} &\cong -\frac{3\alpha O_{A1}}{\pi s_W^2} \left\{ \frac{m_t^2}{t_\beta} \left(\frac{10}{72} c_3(t) + \frac{8}{72} c_4(t) \right) + m_b^2 t_\beta \left(\frac{13}{72} c_3(b) + \frac{5}{72} c_4(b) \right) \right\} + \cdots \\
P_h^W \cdot g_{hVV} &\cong -\frac{3\alpha O_{A1}}{\pi s_W^2} \left\{ \frac{m_t^2}{t_\beta} c_3(t) + m_b^2 t_\beta c_3(b) \right\} + \cdots \qquad \text{(IV.27)}
\end{aligned}
$$

We can see that the CP-odd hZZ coupling is very sensitive to the CP even-odd mixing O_{A1} and t_β. Quantum corrections to the CP-even couplings are ignored as they are much smaller than the tree-level values.

The loop functions are (assuming on-shell vector bosons)

$$
\begin{aligned}
c_1(i,j,k) &= \int_0^1 dx \int_0^{1-x} dy \frac{x+y}{(m_i^2 - m_j^2)x + (m_k^2 - m_j^2)y + m_j^2 + M_V^2(x+y)(x+y-1) - q^2 xy} \\
c_2(i,j,k) &= \int_0^1 dx \int_0^{1-x} dy \frac{x+y-1}{(m_i^2 - m_j^2)x + (m_k^2 - m_j^2)y + m_j^2 + M_V^2(x+y)(x+y-1) - q^2 xy} \\
c_3(f) &= \int_0^1 dx \int_0^{1-x} dy \frac{x+y}{m_f^2 + M_V^2(x+y)(x+y-1) - q^2 xy} \\
c_4(f) &= \int_0^1 dx \int_0^{1-x} dy \frac{x+y-1}{m_f^2 + M_V^2(x+y)(x+y-1) - q^2 xy}.
\end{aligned}
\tag{IV.28}
$$

where q is Higgs momentum.

In this paper, we use on-shell (constant) couplings rather than considering full momentum dependence. This momentum dependence comes from integrating out dynamical degrees of freedom, and are shown in Fig. 4.8. Couplings around the threshold region are different from on-shell couplings. However, the typical energy scales of LHC processes that care applicability in the measurement of TBVs are only about $200\,\mathrm{GeV}$ as shown in Fig. 4.9. The on-shell coupling thus may contribute more to the cross-section support than the threshold behavior. Fig. 4.8 also shows that the maximum couplings in the threshold region are only $\mathcal{O}(1)$ factor larger than the on-shell couplings. Although the threshold behavior depends on input parameters, we checked that maximum couplings are larger than the on-shell couplings by at most $\mathcal{O}(10)$ factor which does not affect our conclusion. It is also convenient to use on-shell couplings since it facilitates the comparison of our result with previous collider studies of TBVs that usually assume constant couplings.

4.7 Appendix B: Analytic discussion of electric dipole moments

4.7.1 Contributions from –inos

EDM is a parity and time-reversal violating electromagnetic property of a fermion at the fermion mass scale. In field theory language, EDM comes from the CP-odd low-energy effective operator $-i\frac{1}{2}\bar{f}\sigma_{\mu\nu}\gamma_5 f F^{\mu\nu}$ with on-shell fermion f and a photon. Exact full two-loop calculations have been carried out in [109, 110, 111] for split supersymmetry, and in

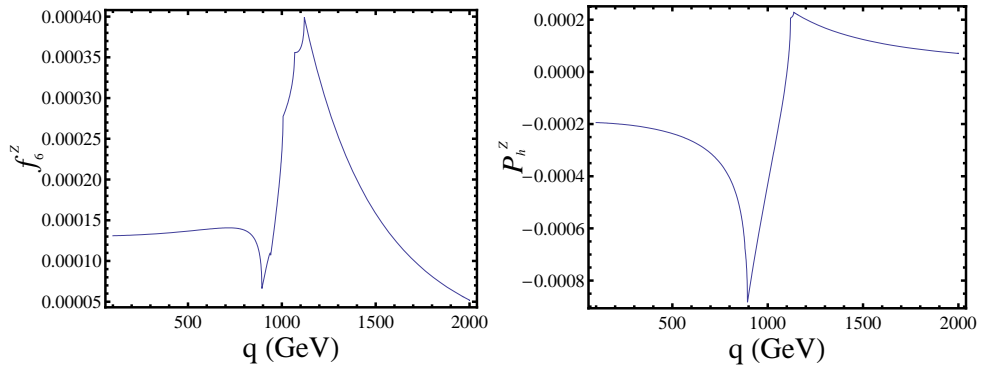Figure 4.8: Sample plots show the momentum dependence of form factors f_6^Z (left) and P_h^Z (right) in split supersymmetry. q is Z or Higgs momentum. $M_1 = M_2 = \mu = 500\,\text{GeV}$ and $t_\beta = 1$ are used.
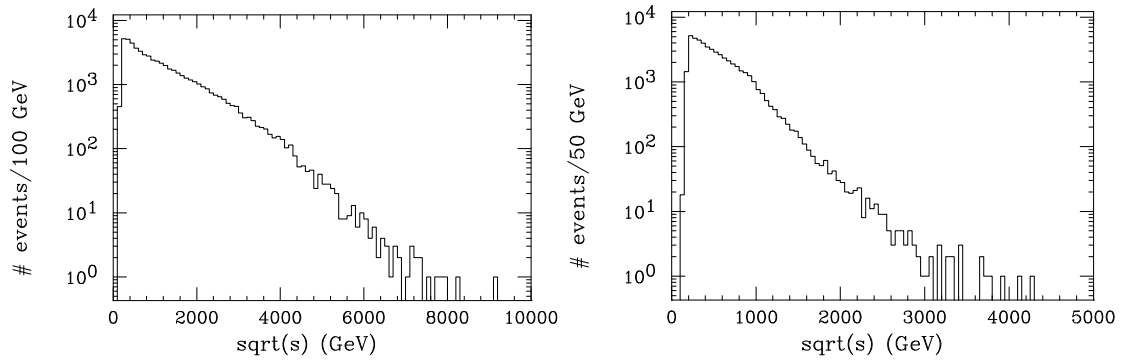

Figure 4.9: Sample center of mass energy $\sqrt{s}$ distributions of $pp \to W^* \to WZ$ (left) and $pp \to h \to ZZ$ (right) in which collider sensitivities of TBVs are usually studied in previous literatures.

[119, 120, 121] for the MSSM with one-loop EDM suppressed. In this appendix, we rather compute eEDM in split supersymmetry by inserting effective CP-odd TBVs into relevant diagrams in Fig. 4.2. We work in dimensional regularization and $\overline{MS}$-scheme. It is a good way to check the previously computed results. For more accurate numerical analysis, we use the full two-loop results.

For reference, we list the leading order EDM in split supersymmetry (in the limit $M_1, M_2, \mu \gg M_W, M_h$) calculated using effective couplings.

$$
\begin{aligned}
d_f^{WW} &= -\frac{e\alpha^2 T_f}{8\pi^2 s_W^4} \sum_{i,k} \frac{m_f m_i^+ m_k^0}{M_W^2} \Im(C_{ki}^{*L} C_{ki}^R) \\
&\quad \cdot \frac{1}{m_i^2 - m_k^2} \left(\frac{m_k^2}{m_i^2 - m_k^2} \ln \frac{m_k^2}{m_i^2} + 1 \right) \cdot \left(\log \frac{\mu^2}{M_W^2} + \frac{3}{2} \right) \quad\text{(IV.29)}
\end{aligned}
$$

$$
d_f^{\gamma h} = \frac{eQ_f \alpha^2}{4\sqrt{2}\pi^2 s_W^2} \sum_i \Im(D_{ii}^R) \frac{m_f}{M_W m_i^+} \left(\frac{1}{2} \log \frac{\mu^2}{M_h^2} + \frac{3}{4} \right) \quad\text{(IV.30)}
$$

$$
\begin{aligned}
d_f^{Zh} &= -\frac{e\alpha^2(T_f^3 - 2Q_f s_W^2)}{8\sqrt{2}c_W^2 \pi^2 s_W^4} \sum_{i,j} \frac{m_f m_i^+}{M_W} \Im(D_{ij}^R F_{ji}^R - D_{ij}^L F_{ji}^L) \\
&\quad \cdot \frac{1}{m_i^2 - m_j^2} \left(1 - \frac{m_j^2}{m_i^2 - m_j^2} \log \frac{m_i^2}{m_j^2} \right) \cdot \frac{1}{2} \left(\log \frac{\mu^2}{M_h^2} + \frac{M_Z^2}{M_h^2 - M_Z^2} \log \frac{M_Z^2}{M_h^2} \right)
\end{aligned}
$$
$$\text{(IV.31)}$$

where superscripts imply two particles that mediate CP-violation to SM fermions. When two inos running in the loop are (almost) degenerate, these formula simplify as following.

$$
d_f^{WW} = -\frac{e\alpha^2 T_f}{8\pi^2 s_W^4} \sum_{i,k} \frac{m_f m_k^0}{M_W^2 m_i^+} \Im(C_{ki}^{*L} C_{ki}^R) \cdot \left(\log \frac{\mu^2}{M_W^2} + \frac{3}{2} \right) \quad\text{(IV.32)}
$$

$$
\begin{aligned}
d_f^{Zh} &= -\frac{e\alpha^2(T_f^3 - 2Q_f s_W^2)}{8\sqrt{2}c_W^2 \pi^2 s_W^4} \sum_{i,j} \frac{m_f}{M_W m_i^+} \Im(D_{ij}^R F_{ji}^R - D_{ij}^L F_{ji}^L) \\
&\quad \cdot \frac{1}{2} \left(\log \frac{\mu^2}{M_h^2} + \frac{M_Z^2}{M_h^2 - M_Z^2} \log \frac{M_Z^2}{M_h^2} \right)
\end{aligned}
$$
$$\text{(IV.33)}$$

We checked that our results agree with the most recent calculations of [120].

Effective matching scale μ may be chosen to obtain the EDM numerically close to the

full two-loop result [105, 109]:

$$\mu^2 = m_{\chi_1^+} m_{\chi_2^+}, \quad m_{\chi_1^+} m_{\chi_2^+}, \quad m_{\chi_1^+} m_{\chi_4^0} \qquad \text{for } \gamma h, Zh, WW \text{ respectively} \qquad \text{(IV.34)}$$

We used the following relations, which follow from unitarity and the definitions of mixing matrices, to reach the final form:

$$\Im(D_{ij}^R F_{ji}^R)m_i^+ = \Im(D_{ji}^R F_{ij}^R)m_j^+ \qquad \text{no sum}$$

$$\Im(D_{ij}^R F_{ji}^L)m_j^+ = -\Im(D_{ij}^L F_{ji}^L)m_i^+ \qquad \text{and } R \leftrightarrow L. \qquad \text{(IV.35)}$$

4.7.2 Scalar contributions (suppressed with heavy scalars)

There are two types of one-loop diagrams which are mediated by scalar and chargino/neutralino(or gluino). For the following fermion-sfermion-ino interaction (in terms of mass eigenstates)

$$\mathcal{L} = \widetilde{\phi}_i \overline{\psi}(A_{ij}^L P_L + A_{ij}^R P_R)\chi_j^0 + \widetilde{\phi}_i \overline{\psi}(B_{ij}^L P_L + B_{ij}^R P_R)\chi_j^\pm - \sqrt{2} g_s T^a \widetilde{q}_i \overline{q}(J_{qi}^L P_L + J_{qi}^R P_R)\widetilde{g}^a + h.c.$$

$$\text{(IV.36)}$$

chargino, neutralino and gluino contributions are respectively

$$
\begin{aligned}
d_f^{1-loop} &= +\frac{e}{16\pi^2} \sum_i \sum_{j=1}^2 \frac{m_{\chi_j}^\pm}{m_i^2} Im(B_{ij}^R B_{ij}^{L*}) \left(-Q_i F_1\left(r_{fi}, r_{ji}\right) + Q_{\chi_j} F_2\left(r_{fi}, r_{ji}\right)\right) \\
&\quad -\frac{eQ_f}{16\pi^2} \sum_i \sum_{j=1}^4 \frac{m_{\chi_j}^0}{m_i^2} Im(A_{ij}^R A_{ij}^{L*}) F_1\left(r_{fi}, r_{ji}\right) \\
&\quad -\frac{2\alpha_s eQ_f}{3\pi} \sum_{i=1}^2 \frac{m_{\widetilde{g}}}{m_i^2} Im(J_{fi}^R J_{fi}^{L*}) F_1\left(r_{fi}, r_{\widetilde{g}i}\right) \qquad \text{(IV.37)}
\end{aligned}
$$

where $r_{ji} = m_j^2/m_i^2$, and i is a scalar index which runs from 1 to 2 except for sneutrino. The loop functions are given by

$$
\begin{aligned}
F_1(r,s) &= \int_0^1 dx \frac{x - x^2}{(1-x) + rx(x-1) + sx} \simeq \frac{1}{2(1-s)^2}\left(1 + s + \frac{2s\ln s}{1-s}\right) \\
F_2(r,s) &= \int_0^1 dx \frac{x^2}{(1-x) + rx(x-1) + sx} \simeq \frac{-1}{2(1-s)^2}\left(3 - s + \frac{2s\ln s}{1-s}\right) \qquad \text{(IV.38)}
\end{aligned}
$$

where the last approximation is for $r \ll 1$.

In universality ansatz, couplings A and B for each fermions are listed below (matches with previous literatures). For electron:

$$A_{ij}^L = -y_e N_{j4}^* U_{iL}^{e*} - \sqrt{2}g' N_{j1}^* U_{iR}^{e*} \quad , \qquad A_{ij}^R = (\sqrt{2}g N_{j2} + \frac{g'}{\sqrt{2}} N_{j1}) U_{iL}^{e*} - y_e N_{j4} U_{iR}^{e*}$$

$$B_j^L = y_e U_{j2}^* \quad , \qquad B_j^R = -gV_{j1}. \tag{IV.39}$$

For up-type quarks:

$$A_{ij}^L = -y_u N_{j3}^* U_{iL}^{u*} + \frac{2\sqrt{2}}{3} g' N_{j1}^* U_{iR}^{u*} \quad , \qquad A_{ij}^R = -(\frac{g}{\sqrt{2}} N_{j2} + \frac{\sqrt{2}g'}{6} N_{j1}) U_{iL}^{u*} - y_u N_{j3} U_{iR}^{u*}$$

$$B_{ij}^L = y_u V_{j2}^* U_{iL}^{d*} \quad , \qquad B_{ij}^R = -gU_{j1} U_{iL}^{d*} + y_d U_{j2} U_{iR}^{d*}. \tag{IV.40}$$

For down-type quarks:

$$A_{ij}^L = -y_d N_{j4}^* U_{iL}^{d*} - \frac{\sqrt{2}}{3} g' N_{j1}^* U_{iR}^{d*} \quad , \qquad A_{ij}^R = (\frac{g}{\sqrt{2}} N_{j2} - \frac{\sqrt{2}g'}{6} N_{j1}) U_{iL}^{d*} - y_d N_{j4} U_{iR}^{d*}$$

$$B_{ij}^L = y_d U_{j2}^* U_{iL}^{u*} \quad , \qquad B_{ij}^R = -gV_{j1} U_{iL}^{u*} + y_u V_{j2} U_{iR}^{u*}. \tag{IV.41}$$

For quark-squark-gluino interaction,

$$J_{qi}^L = -e^{-i\frac{\phi(M_3)}{2}} U_{iR}^{q*}, \quad J_{qi}^R = e^{+i\frac{\phi(M_3)}{2}} U_{iL}^{q*} \tag{IV.42}$$

where sfermion mixing matrix U^f is defined as $\tilde{f}_i^{mass} = U_{iA}^f \tilde{f}_A^{current}$ with $A = L, R$ and $i = 1, 2$. $\phi(M_3)$ is a phase of gluino mass soft term.

One-loop eEDM is suppressed if first two generations of sleptons are very heavy. H-A mixing induces EDM at two-loop via $a\gamma$ due to large trilinear A couplings of top and bottom quarks. Possibly, chargino can contribute as well. $H^\pm W$ and aZ contributions are suppressed in this scenario.

Scalars do not generate CP-violating effective couplings at one-loop order. In the diagram in which scalar is running, CP violation comes in through sparticle mixing. These mixing matrices at each scalar-scalar-gauge coupling are paired with its hermitian conjugate at adjacent vertex, so real.

In any phase conventions(basis), there are two sets of physical CP-phases in universality ansatz: any two of $\arg(A\mu b^*)$, $\arg(A^* M_{1,2,3})$, $\arg(M_{1,2,3}\mu b^*)$ [1]. As low-energy effective operators composed of SM Dirac fermions and vector fields are neutral under R and PQ symmetry, we can argue that low-energy physical observable should depend on the above combinations which are the only R and PQ invariants. Indeed, both R and PQ are needed and enough to do that because all complex soft phases are charged under at least one of them.

A-term comes in via sparticle mixing(tri-scalar coupling with H_u or H_d), M and μ come in chargino/neutralino mass matrices, μ also comes in sparticle mixing(supersymmetric tri-scalar coupling), and b comes in higgs mixing and higgs scalar potential. From the higgs potential minimization condition (tree level), we get the relation that $b\frac{v_d}{v_u^*}$ is real (or $\sin 2\beta \propto b$). So after higgses get vev, $\sin 2\beta$ or vevs will appear instead of b.

Working on the most general basis, we can guess the dependence on the above parameters and know why specific diagrams are not generated. In this philosophy, let us look at scalar one-loop contribution to effective couplings. Since there is no gaugino/higgsino running, only $A\mu b^*$ combination is possible. Tri-scalar coupling connects L-type(superpartner of left-handed fermion) and R-type scalars, and W boson couples only to L-type. Thus we need a pair of tri-scalar couplings and its hermitian conjugate. Thus real, and no CP-violation. (However, if W couples to both types, then there could be nonzero CP-violations due to different tri-scalar couplings according to sparticle T_3 quantum number.)

Why $f_7^V = 0$? These can be seen more easily in most general basis where b or higgs vevs are complex. Without higgs, no b term. $\mathrm{Arg}(AM_{1,2})$ are only possible CP-phases. Since there is no relevant tri-scalar couplig at one-loop, no relevant CP-phases.

---

[1] $\arg(M_i M_j^*)$ is also allowed by same argument.

BIBLIOGRAPHY

BIBLIOGRAPHY

[1] S. P. Martin, In *Kane, G.L. (ed.): Perspectives on supersymmetry* 1-98. [hep-ph/9709356].

[2] N. Arkani-Hamed, A. G. Cohen and H. Georgi, Phys. Lett. B **513**, 232 (2001) [arXiv:hep-ph/0105239].

[3] C. T. Hill, Phys. Lett. **B345**, 483-489 (1995). [hep-ph/9411426].

[4] L. Randall, R. Sundrum, Phys. Rev. Lett. **83**, 3370-3373 (1999). [hep-ph/9905221].

[5] S. Jung, H. Murayama, A. Pierce, J. D. Wells, Phys. Rev. **D81**, 015004 (2010). [arXiv:0907.4112 [hep-ph]].

[6] S. Jung, J. D. Wells, JHEP **1011**, 001 (2010). [arXiv:1008.0870 [hep-ph]].

[7] S. Jung, J. D. Wells, Phys. Rev. **D80**, 015009 (2009). [arXiv:0811.4140 [hep-ph]].

[8] T. Aaltonen *et al.* [CDF Collaboration], [arXiv:1101.0034 [hep-ex]].

[9] CDF Collaboration, CDF note 10436

[10] CDF Collaboration, CDF note 9724

[11] T. Aaltonen *et al.* [CDF Collaboration], Phys. Rev. Lett. **101**, 202001 (2008). [arXiv:0806.2472 [hep-ex]].

[12] V. M. Abazov *et al.* [D0 Collaboration], Phys. Rev. Lett. **100**, 142002 (2008). [arXiv:0712.0851 [hep-ex]].

[13] J. H. Kuhn, G. Rodrigo, Phys. Rev. Lett. **81**, 49-52 (1998). [hep-ph/9802268].

[14] J. H. Kuhn, G. Rodrigo, Phys. Rev. **D59**, 054017 (1999). [hep-ph/9807420].

[15] M. T. Bowen, S. D. Ellis, D. Rainwater, Phys. Rev. **D73**, 014008 (2006). [hep-ph/0509267].

[16] L. G. Almeida, G. F. Sterman, W. Vogelsang, Phys. Rev. **D78**, 014008 (2008). [arXiv:0805.1885 [hep-ph]].

[17] C. D. Froggatt and H. B. Nielsen, Nucl. Phys. B **147**, 277 (1979).

[18] M. Leurer, Y. Nir and N. Seiberg, Nucl. Phys. B **398**, 319 (1993) [arXiv:hep-ph/9212278]. M. Leurer, Y. Nir and N. Seiberg, Nucl. Phys. B **420**, 468 (1994) [arXiv:hep-ph/9310320].

[19] The CDF Collaboration, CDF note 9448

[20] S. Moch and P. Uwer, Nucl. Phys. Proc. Suppl. **183**, 75 (2008) [arXiv:0807.2794 [hep-ph]]. M. Cacciari, S. Frixione, M. L. Mangano, P. Nason and G. Ridolfi, JHEP **0809**, 127 (2008) [arXiv:0804.2800 [hep-ph]]. N. Kidonakis and R. Vogt, Phys. Rev. D **78**, 074005 (2008) [arXiv:0805.3844 [hep-ph]].

[21] V. M. Abazov *et al.* [D0 Collaboration], Phys. Rev. **D80**, 071102 (2009). [arXiv:0903.5525 [hep-ex]].

[22] CDF note **9462** (2009)

[23] CDF note **9399** (2009)

[24] V. M. Abazov *et al.* [D0 Collaboration], Phys. Lett. **B679**, 177-185 (2009). [arXiv:0901.2137 [hep-ex]].

[25] T. Aaltonen *et al.* [CDF Collaboration], arXiv:0903.2850 [hep-ex].

[26] S. Bar-Shalom, A. Rajaraman, D. Whiteson, F. Yu, Phys. Rev. **D78**, 033003 (2008). [arXiv:0803.3795 [hep-ph]].

[27] T. Aaltonen *et al.* [CDF Collaboration], Phys. Rev. Lett. **102**, 041801 (2009). [arXiv:0809.4903 [hep-ex]].

[28] T. Aaltonen *et al.* [CDF Collaboration], Phys. Rev. **D79**, 112002 (2009). [arXiv:0812.4036 [hep-ex]].

[29] J. Alitti *et al.* [UA2 Collaboration], Nucl. Phys. **B400**, 3-24 (1993).

[30] T. Aaltonen *et al.* [CDF Collaboration], Phys. Rev. Lett. **103**, 092002 (2009). [arXiv:0903.0885 [hep-ex]].

[31] V. M. Abazov *et al.* [D0 Collaboration], Phys. Rev. Lett. **103**, 092001 (2009). [arXiv:0903.0850 [hep-ex]].

[32] M. Gronau, J. L. Rosner, Phys. Rev. **D71**, 074019 (2005). [hep-ph/0503131].

[33] T. Aaltonen *et al.* [CDF Collaboration], Phys. Rev. Lett. **102**, 151801 (2009). [arXiv:0812.3400 [hep-ex]].

[34] L. Randall and R. Sundrum, "An alternative to compactification," Phys. Rev. Lett. **83**, 4690 (1999) [arXiv:hep-th/9906064].

[35] T. Gherghetta and A. Pomarol, "Bulk fields and supersymmetry in a slice of AdS," Nucl. Phys. B **586**, 141 (2000) [arXiv:hep-ph/0003129].

[36] Y. Grossman and M. Neubert, "Neutrino masses and mixings in non-factorizable geometry," Phys. Lett. B **474**, 361 (2000) [arXiv:hep-ph/9912408]. S. J. Huber and Q. Shafi, "Fermion Masses, Mixings and Proton Decay in a Randall-Sundrum Model," Phys. Lett. B **498**, 256 (2001) [arXiv:hep-ph/0010195].

[37] C. Csaki, A. Falkowski and A. Weiler, "The Flavor of the Composite Pseudo-Goldstone Higgs," JHEP **0809**, 008 (2008) [arXiv:0804.1954 [hep-ph]]. M. Bona *et al.* [UTfit Collaboration], "Model-independent constraints on Δ F=2 operators and the scale of new physics," JHEP **0803**, 049 (2008) [arXiv:0707.0636 [hep-ph]].

[38] M. Blanke, A. J. Buras, B. Duling, S. Gori and A. Weiler, "Δ F=2 Observables and Fine-Tuning in a Warped Extra Dimension with Custodial Protection," JHEP **0903**, 001 (2009) [arXiv:0809.1073 [hep-ph]].

[39] K. Agashe, A. Azatov and L. Zhu, "Flavor Violation Tests of Warped/Composite SM in the Two-Site Approach," Phys. Rev. D **79**, 056006 (2009) [arXiv:0810.1016 [hep-ph]].

[40] O. Gedalia, G. Isidori and G. Perez, "Combining Direct & Indirect Kaon CP Violation to Constrain the Warped KK Scale," Phys. Lett. B **682**, 200 (2009) [arXiv:0905.3264 [hep-ph]].

[41] A. L. Fitzpatrick, G. Perez and L. Randall, "Flavor from Minimal Flavor Violation & a Viable Randall-Sundrum Model," arXiv:0710.1869 [hep-ph].

[42] C. Csaki, G. Perez, Z. Surujon and A. Weiler, "Flavor Alignment via Shining in RS," Phys. Rev. D **81**, 075025 (2010) [arXiv:0907.0474 [hep-ph]].

[43] G. Cacciapaglia, C. Csaki, J. Galloway, G. Marandella, J. Terning and A. Weiler, "A GIM Mechanism from Extra Dimensions," JHEP **0804**, 006 (2008) [arXiv:0709.1714 [hep-ph]]. C. Csaki, A. Falkowski and A. Weiler, "A Simple Flavor Protection for RS," Phys. Rev. D **80**, 016001 (2009) [arXiv:0806.3757 [hep-ph]].

[44] G. Perez and L. Randall, "Natural Neutrino Masses and Mixings from Warped Geometry," JHEP **0901**, 077 (2009) [arXiv:0805.4652 [hep-ph]]. C. Csaki, C. Delaunay, C. Grojean and Y. Grossman, "A Model of Lepton Masses from a Warped Extra Dimension," JHEP **0810**, 055 (2008) [arXiv:0806.0356 [hep-ph]].

[45] M. C. Chen and H. B. Yu, "Minimal Flavor Violation in the Lepton Sector of the Randall-Sundrum Model," Phys. Lett. B **672**, 253 (2009) [arXiv:0804.2503 [hep-ph]].

[46] J. Santiago, "Minimal Flavor Protection: A New Flavor Paradigm in Warped Models," JHEP **0812**, 046 (2008) [arXiv:0806.1230 [hep-ph]].

[47] K. Agashe, A. Delgado, M. J. May and R. Sundrum, "RS1, custodial isospin and precision tests," JHEP **0308**, 050 (2003) [arXiv:hep-ph/0308036].

[48] C. Delaunay, O. Gedalia, S. J. Lee and G. Perez, "Ultra Natural Warped Model From Flavor Triviality," arXiv:1007.0243 [hep-ph].

[49] R. Rattazzi and A. Zaffaroni, "Comments on the holographic picture of the Randall-Sundrum model," JHEP **0104**, 021 (2001) [arXiv:hep-th/0012248].

[50] M. S. Carena, E. Ponton, J. Santiago and C. E. M. Wagner, "Light Kaluza-Klein states in Randall-Sundrum models with custodial SU(2)," Nucl. Phys. B **759**, 202 (2006) [arXiv:hep-ph/0607106].

[51] M. S. Carena, E. Ponton, J. Santiago and C. E. M. Wagner, "Electroweak constraints on warped models with custodial symmetry," Phys. Rev. D **76**, 035006 (2007) [arXiv:hep-ph/0701055].

[52] K. Agashe, R. Contino, L. Da Rold and A. Pomarol, "A custodial symmetry for Z b anti-b," Phys. Lett. B **641**, 62 (2006) [arXiv:hep-ph/0605341].

[53] G. Cacciapaglia, C. Csaki, C. Grojean and J. Terning, "Curing the Ills of Higgsless models: The S parameter and unitarity," Phys. Rev. D **71**, 035015 (2005) [arXiv:hep-ph/0409126].

[54] R. Foadi, S. Gopalakrishna and C. Schmidt, "Effects of fermion localization in Higgsless theories and electroweak constraints," Phys. Lett. B **606**, 157 (2005) [arXiv:hep-ph/0409266].

[55] M. Guchait, F. Mahmoudi and K. Sridhar, "Associated production of a Kaluza-Klein excitation of a gluon with a t t(bar) pair at the LHC," Phys. Lett. B **666**, 347 (2008) [arXiv:0710.2234 [hep-ph]].

[56] A. Djouadi, G. Moreau and R. K. Singh, "Kaluza–Klein excitations of gauge bosons at the LHC," Nucl. Phys. B **797**, 1 (2008) [arXiv:0706.4191 [hep-ph]].

[57] B. Lillie, J. Shu and T. M. P. Tait, "Top Compositeness at the Tevatron and LHC," JHEP **0804**, 087 (2008) [arXiv:0712.3057 [hep-ph]].

[58] K. m. Cheung, "Four top production and electroweak symmetry breaking," arXiv:hep-ph/9507411.

[59] M. Spira and J. D. Wells, "Higgs bosons strongly coupled to the top quark," Nucl. Phys. B **523**, 3 (1998) [arXiv:hep-ph/9711410].

[60] A. Pomarol and J. Serra, "Top Quark Compositeness: Feasibility and Implications," Phys. Rev. D **78**, 074026 (2008) [arXiv:0806.3247 [hep-ph]].

[61] B. S. Acharya, P. Grajek, G. L. Kane, E. Kuflik, K. Suruliz and L. T. Wang, "Identifying Multi-Top Events from Gluino Decay at the LHC," arXiv:0901.3367 [hep-ph].

[62] M. Toharia and J. D. Wells, "Gluino decays with heavier scalar superpartners," JHEP **0602**, 015 (2006) [arXiv:hep-ph/0503175].

[63] R. Contino and G. Servant, "Discovering the top partners at the LHC using same-sign dilepton final states," JHEP **0806**, 026 (2008) [arXiv:0801.1679 [hep-ph]].

[64] M. Battaglia and G. Servant, "Four-top production and t tbar + missing energy events at multi TeV e+e- colliders," arXiv:1005.4632 [hep-ex].

See also Ch.12 of G. Brooijmans *et al.*, "New Physics at the LHC. A Les Houches Report: Physics at TeV Colliders 2009 - New Physics Working Group," arXiv:1005.1229 [hep-ph].

[65] G. Cacciapaglia, C. Csaki, G. Marandella and J. Terning, "A New Custodian for a Realistic Higgsless Model," Phys. Rev. D **75**, 015003 (2007) [arXiv:hep-ph/0607146].

[66] S. Casagrande, F. Goertz, U. Haisch, M. Neubert and T. Pfoh, "The Custodial Randall-Sundrum Model: From Precision Tests to Higgs Physics," arXiv:1005.4315 [hep-ph].

[67] B. A. Dobrescu, K. Kong and R. Mahbubani, "Massive color-octet bosons and pairs of resonances at hadron colliders," Phys. Lett. B **670**, 119 (2008) [arXiv:0709.2378 [hep-ph]].

[68] K. Agashe, G. Perez and A. Soni, "Flavor structure of warped extra dimension models," Phys. Rev. D **71**, 016002 (2005) [arXiv:hep-ph/0408134].

[69] N. Arkani-Hamed, M. Porrati and L. Randall, "Holography and phenomenology," JHEP **0108**, 017 (2001) [arXiv:hep-th/0012148].

[70] S. Casagrande, F. Goertz, U. Haisch, M. Neubert and T. Pfoh, "Flavor Physics in the Randall-Sundrum Model: I. Theoretical Setup and Electroweak Precision Tests," JHEP **0810**, 094 (2008) [arXiv:0807.4937 [hep-ph]].

[71] K. Agashe and R. Contino, "Composite Higgs-Mediated FCNC," Phys. Rev. D **80**, 075016 (2009) [arXiv:0906.1542 [hep-ph]].

A. Azatov, M. Toharia and L. Zhu, "Higgs Mediated FCNC's in Warped Extra Dimensions," Phys. Rev. D **80**, 035016 (2009) [arXiv:0906.1990 [hep-ph]].

[72] A. Azatov, M. Toharia and L. Zhu, "Radion Mediated Flavor Changing Neutral Currents," Phys. Rev. D **80**, 031701 (2009) [arXiv:0812.2489 [hep-ph]].

[73] T. Gherghetta and J. Giedt, "Bulk fields in AdS(5) from probe D7 branes," Phys. Rev. D **74**, 066007 (2006) [arXiv:hep-th/0605212].

[74] J. Alwall *et al.*, "MadGraph/MadEvent v4: The New Web Generation," JHEP **0709**, 028 (2007) [arXiv:0706.2334 [hep-ph]].

[75] J. Pumplin, D. R. Stump, J. Huston, H. L. Lai, P. M. Nadolsky and W. K. Tung, "New generation of parton distributions with uncertainties from global QCD analysis," JHEP **0207**, 012 (2002) [arXiv:hep-ph/0201195].

[76] P. Meade and M. Reece, "BRIDGE: Branching ratio inquiry / decay generated events," arXiv:hep-ph/0703031.

[77] H. Baer, C. h. Chen, F. Paige and X. Tata, "Signals for Minimal Supergravity at the CERN Large Hadron Collider II: Multilepton Channels," Phys. Rev. D **53**, 6241 (1996) [arXiv:hep-ph/9512383].

[78] G. Aad *et al.* [The ATLAS Collaboration], "Expected Performance of the ATLAS Experiment - Detector, Trigger and Physics," arXiv:0901.0512 [hep-ex].

[79] V. Cavasinni, D. Costanzo, "Search for $WH \to WWW \to l^{\pm}\nu l^{\pm}\nu$jet-jet, using like-sign leptons," [ATL-PHYS-2000-013].

[80] The ATLAS Collaboration, "Discovery potential for supersymmetry with b-jet final states with the ATLAS detector," [ATL-PHYS-PUB-2009-075].

[81] J. A. Aguilar-Saavedra, "Identifying top partners at LHC," JHEP **0911**, 030 (2009) [arXiv:0907.3155 [hep-ph]].

[82] H. Baer and J. D. Wells, "Trilepton Higgs signal at hadron colliders," Phys. Rev. D **57**, 4446 (1998) [arXiv:hep-ph/9710368].

[83] K. Rehermann and B. Tweedie, "Efficient Identification of Boosted Semileptonic Top Quarks at the LHC," arXiv:1007.2221 [hep-ph].

See also for earlier work, J. Thaler and L. T. Wang, "Strategies to Identify Boosted Tops," JHEP **0807**, 092 (2008) [arXiv:0806.0023 [hep-ph]].

[84] J. Mrazek and A. Wulzer, "A Strong Sector at the LHC: Top Partners in Same-Sign Dileptons," Phys. Rev. D **81**, 075006 (2010) [arXiv:0909.3977 [hep-ph]].

[85] B. Lillie, L. Randall and L. T. Wang, "The Bulk RS KK-gluon at the LHC," JHEP **0709**, 074 (2007) [arXiv:hep-ph/0701166].

K. Agashe, A. Belyaev, T. Krupovnickas, G. Perez and J. Virzi, "LHC signals from warped extra dimensions," Phys. Rev. D **77**, 015003 (2008) [arXiv:hep-ph/0612015].

[86] H. C. Cheng, K. T. Matchev and M. Schmaltz, "Radiative corrections to Kaluza-Klein masses," Phys. Rev. D **66**, 036005 (2002) [arXiv:hep-ph/0204342].

[87] J. A. Aguilar-Saavedra, "Pair production of heavy Q = 2/3 singlets at LHC," Phys. Lett. B **625**, 234 (2005) [Erratum-ibid. B **633**, 792 (2006)] [arXiv:hep-ph/0506187].

[88] W. Skiba and D. Tucker-Smith, "Using jet mass to discover vector quarks at the LHC," Phys. Rev. D **75**, 115010 (2007) [arXiv:hep-ph/0701247].

C. Dennis, M. Karagoz Unel, G. Servant and J. Tseng, "Multi-W events at LHC from a warped extra dimension with custodial symmetry," arXiv:hep-ph/0701158.

[89] B.C. Regan et al., "New Limit on the Electron Electric Dipole Moment", Phys. Rev. Lett. **88** (2002) 071805

[90] S. Abel, S. Khalil and O. Lebedev, "EDM constraints in supersymmetric theories," Nucl. Phys. B **606**, 151 (2001) [arXiv:hep-ph/0103320].

[91] D. A. Demir, O. Lebedev, K. A. Olive, M. Pospelov and A. Ritz, "Electric dipole moments in the MSSM at large $\tan\beta$," Nucl. Phys. B **680**, 339 (2004) [arXiv:hep-ph/0311314].

[92] M. Brhlik, G. J. Good and G. L. Kane, "Electric dipole moments do not require the CP-violating phases of supersymmetry to be small," Phys. Rev. D **59**, 115004 (1999) [arXiv:hep-ph/9810457].

[93] T. Ibrahim and P. Nath, "The neutron and the electron electric dipole moment in $N = 1$ supergravity unification," Phys. Rev. D **57**, 478 (1998) [Erratum-ibid. D **58**, 019901][arXiv:hep-ph/9708456].

[94] T. Ibrahim and P. Nath, "The neutron and the lepton EDMs in MSSM, large CP violating phases, and the cancellation mechanism," Phys. Rev. D **58**, 111301 (1998) [Erratum-ibid. D **60**, 099902 (1999)] [arXiv:hep-ph/9807501].

[95] J. Kumar, A. Rajaraman and J. D. Wells, "Probing CP-violation at colliders through interference effects in diboson production and decay," arXiv:0801.2891 [hep-ph].

[96] K. Hagiwara, R. D. Peccei, D. Zeppenfeld and K. Hikasa, "Probing the Weak Boson Sector in $e^+e^- \to W^+W^-$," Nucl. Phys. B **282**, 253 (1987).

[97] B. Ananthanarayan, S. D. Rindani, R. K. Singh and A. Bartl, Phys. Lett. B **593**, 95 (2004) [Erratum-ibid. B **608**, 274 (2005)] [arXiv:hep-ph/0404106]. M. Diehl, O. Nachtmann and F. Nagel, Eur. Phys. J. C **32**, 17 (2003) [arXiv:hep-ph/0306247]. D. Choudhury, J. Kalinowski and A. Kulesza, Phys. Lett. B **457**, 193 (1999) [arXiv:hep-ph/9904215]. A. A. Likhoded, G. Valencia and O. P. Yushchenko, Phys. Rev. D **57**, 2974 (1998) [arXiv:hep-ph/9711325]. D. Choudhury and S. D. Rindani, Phys. Lett. B **335**, 198 (1994) [arXiv:hep-ph/9405242]. B. Ananthanarayan and S. D. Rindani, Phys. Rev. D **70**, 036005 (2004) [arXiv:hep-ph/0309260]. V. D. Barger, T. Falk, T. Han, J. Jiang, T. Li and T. Plehn, Phys. Rev. D **64**, 056007 (2001) [arXiv:hep-ph/0101106], P. Langacker, G. Paz, L. T. Wang and I. Yavin, JHEP **0707**, 055 (2007) [arXiv:hep-ph/0702068].

[98] R. M. Godbole, D. J. Miller and M. M. Muhlleitner, JHEP **0712**, 031 (2007) [arXiv:0708.0458 [hep-ph]]. C. P. Buszello, P. Marquard and J. J. van der Bij, arXiv:hep-ph/0406181. E. Accomando *et al.*, arXiv:hep-ph/0608079. T. Han and J. Jiang, Phys. Rev. D **63**, 096007 (2001) [arXiv:hep-ph/0011271]. S. S. Biswal, R. M. Godbole, R. K. Singh and D. Choudhury, Phys. Rev. D **73**, 035001 (2006) [Erratum-ibid. D **74**, 039904 (2006)] [arXiv:hep-ph/0509070]. R. M. Godbole, S. Kraml, S. D. Rindani and R. K. Singh, Phys. Rev. D **74**, 095006 (2006) [Erratum-ibid. D **74**, 119901 (2006)] [arXiv:hep-ph/0609113].

[99] S. Weinberg, "Larger Higgs Exchange Terms in the Neutron Electric Dipole Moment," Phys. Rev. Lett. **63**, 2333 (1989).

[100] D. Kawall, F. Bay, S. Bickman, Y. Jiang and D. DeMille, "Proof of principle for a high sensitivity search for the electric dipole moment of the electron using the metastable $a(1)[^3\Sigma^+]$ state of PbO," Phys. Rev. Lett. **92**, 133007 (2004) [arXiv:hep-ex/0309079].

[101] J.J. Hudson, B.E. Sauer, M.R. Tarbutt, E.A. Hinds, "Measurement of the Electron Electric Dipole Moment Using YbF Molecules", Phys. Rev. Lett. **89**,023003 (2002)

[102] C.Y.Liu and S.K.Lamoreaux, "A New Search for A Permanent Dipole Moment of the Electron in a Solid State System", Mod. Phys. Lett. A 19(2004) 1235

[103] N. Arkani-Hamed and S. Dimopoulos, "Supersymmetric unification without low energy supersymmetry and signatures for fine-tuning at the LHC," JHEP **0506**, 073 (2005) [arXiv:hep-th/0405159].

[104] G. F. Giudice and A. Romanino, "Split supersymmetry," Nucl. Phys. B **699**, 65 (2004) [Erratum-ibid. B **706**, 65 (2005)] [arXiv:hep-ph/0406088].

[105] N. Arkani-Hamed, S. Dimopoulos, G. F. Giudice and A. Romanino, "Aspects of split supersymmetry," Nucl. Phys. B **709**, 3 (2005) [arXiv:hep-ph/0409232].

[106] J. D. Wells, "Implications of supersymmetry breaking with a little hierarchy between gauginos and scalars," arXiv:hep-ph/0306127; Phys. Rev. D **71**, 015013 (2005) [arXiv:hep-ph/0411041].

[107] S. Dimopoulos and S. D. Thomas, "Dynamical Relaxation of the Supersymmetric CP Violating Phases," Nucl. Phys. B **465**, 23 (1996) [arXiv:hep-ph/9510220].

[108] M. Dugan, B. Grinstein and L. J. Hall, "CP Violation In The Minimal $N = 1$ Supergravity Theory," Nucl. Phys. B **255**, 413 (1985).

[109] G. F. Giudice and A. Romanino, "Electric dipole moments in split supersymmetry," Phys. Lett. B **634**, 307 (2006) [arXiv:hep-ph/0510197].

[110] D. Chang, W. F. Chang and W. Y. Keung, "Electric dipole moment in the split supersymmetry models," Phys. Rev. D **71**, 076006 (2005) [arXiv:hep-ph/0503055].

[111] T. F. Feng, L. Sun and X. Y. Yang, "The two loop supersymmetric corrections to lepton anomalous dipole moments in split supersymmetry scenarios," Phys. Rev. D **77**, 116008 (2008) [arXiv:0805.0653 [hep-ph]].

[112] P. G. Harris *et al., Phys. Rev. Lett. 82(1999) 904*

[113] S. Abel and O. Lebedev, "Neutron electron EDM correlations in supersymmetry and prospects for EDM searches," JHEP **0601**, 133 (2006) [arXiv:hep-ph/0508135].

[114] S. Dimopoulos and G. F. Giudice, "Naturalness constraints in supersymmetric theories with nonuniversal soft terms," Phys. Lett. B **357**, 573 (1995) [arXiv:hep-ph/9507282];

A. G. Cohen, D. B. Kaplan and A. E. Nelson, "The more minimal supersymmetric standard model," Phys. Lett. B **388**, 588 (1996) [arXiv:hep-ph/9607394].

[115] A. Pilaftsis, "CP-odd tadpole renormalization of Higgs scalar-pseudoscalar mixing," Phys. Rev. D **58**, 096010 (1998) [arXiv:hep-ph/9803297].

[116] A. Pilaftsis, "Higgs scalar-pseudoscalar mixing in the minimal supersymmetric standard model," Phys. Lett. B **435**, 88 (1998) [arXiv:hep-ph/9805373].

[117] A. Pilaftsis, "Radiative Higgs-sector CP violation in the MSSM" arXiv:hep-ph/0003232.

[118] D. A. Demir, "Effects of the supersymmetric phases on the neutral Higgs sector" Phys. Rev. D **60**, 055006 (1999) [arXiv:hep-ph/9901389].

[119] A. Pilaftsis, "Higgs-mediated electric dipole moments in the MSSM: An application to baryogenesis and Higgs searches," Nucl. Phys. B **644**, 263 (2002) [arXiv:hep-ph/0207277].

[120] Y. Li, S. Profumo and M. Ramsey-Musolf, "Higgs-Higgsino-Gaugino Induced Two Loop Electric Dipole Moments," arXiv:0806.2693 [hep-ph].

[121] T. H. West, "Fermion Electric Dipole Moments Induced By T And P Odd $WW\gamma$ Interactions In The Multi - Higgs And Supersymmetry Models," Phys. Rev. D **50**, 7025 (1994).

T. Kadoyoshi and N. Oshimo, "Neutron electric dipole moment from supersymmetric anomalous W-boson coupling," Phys. Rev. D **55**, 1481 (1997) [arXiv:hep-ph/9607301].

[122] J. S. Lee, M. Carena, J. Ellis, A. Pilaftsis and C. E. M. Wagner, "CPsuperH2.0: an Improved Computational Tool for Higgs Phenomenology in the MSSM with Explicit CP Violation," arXiv:0712.2360 [hep-ph].
J. S. Lee, A. Pilaftsis, M. S. Carena, S. Y. Choi, M. Drees, J. R. Ellis and C. E. M. Wagner, "CPsuperH: A computational tool for Higgs phenomenology in the minimal supersymmetric standard model with explicit CP violation," Comput. Phys. Commun. **156**, 283 (2004) [arXiv:hep-ph/0307377].
The program can be found at http://www.hep.man.ac.uk/u/jslee/CPsuperH.html.

[123] K. S. Babu, C. F. Kolda, J. March-Russell and F. Wilczek, "CP violation, Higgs couplings, and supersymmetry," Phys. Rev. D **59**, 016004 (1999) [arXiv:hep-ph/9804355].

[124] M. Kitahara, M. Marui, N. Oshimo, T. Saito and A. Sugamoto, "CP-odd anomalous W boson couplings from supersymmetry," Eur. Phys. J. C **4**, 661 (1998) [arXiv:hep-ph/9710220].

[125] T. Falk, K. A. Olive, M. Pospelov and R. Roiban, "MSSM predictions for the electric dipole moment of the Hg-199 atom," Nucl. Phys. B **560**, 3 (1999) [arXiv:hep-ph/9904393].

[126] O. Lebedev and M. Pospelov, "Electric dipole moments in the limit of heavy superpartners," Phys. Rev. Lett. **89**, 101801 (2002) [arXiv:hep-ph/0204359].

[127] J. Bailey *et al.* [CERN-Mainz-Daresbury Collaboration], Nucl. Phys. **B150**,1 (1979).

[128] Y. K. Semertzidis *et al.*, "Sensitive search for a permanent muon electric dipole moment," arXiv:hep-ph/0012087.